Parabrachial and central amygdala circuits for affective nociceptive processing

Anna Joy Bowen

A dissertation

submitted in partial fulfillment of the

requirements for the degree of

Doctor of Philosophy

University of Washington

2020

Reading Committee:

Richard Palmiter, Chair

Larry Zweifel

Jeansok Kim

Program Authorized to Offer Degree:

Neuroscience

University of Washington

Abstract

Parabrachial and central amygdala circuits for affective nociceptive processing

Anna Joy Bowen

Chair of the Supervisory Committee:

Richard Palmiter

Department of Biochemistry

The central amygdala (CeA) and parabrachial nucleus (PBN) are two crucial nodes in the nociceptive relay from the spinal cord to the forebrain. Recent work suggests that nociceptive neurons of the PBN expressing calcitonin gene-related peptide (CGRP) act as integrators, receiving multisensory aversive stimuli and relaying a scaled threat-signal to forebrain nuclei to affect defensive responses. The CeA, in contrast, is a striatum-like structure with multiple cross-inhibitory subnuclei that accomplishes hierarchical processing and action selection through antagonizing opposing stimuli. The purpose of this thesis is to delineate systems underpinning affective processing of aversive stimuli at the level of the PBN and CeA, focusing on the complementary roles played by $CGRP^{PBN}$ neurons, their various projections, and CGRP-receptor (Calcrl) neurons in the CeA. Using cell-type-specific tracing and optogenetics we identify distinctly collateralizing subpopulations of $CGRP^{PBN}$ neurons, with individual projections differentially promoting distinct unconditioned behavioral and physiological responses or associative fear learning to aversive stimuli. We also find that some responses generated by $CGRP^{PBN}$ neuron activation requires summed activity at multiple downstream nodes, suggesting that defensive

responses do not occur exclusively through labeled-line circuit structure. At the level of the CeA, we use anatomical and functional analyses of connectivity, cell activity dynamics and behavioral and physiological response characteristics to reveal that CeA Calcrl^{+} neurons have biased influence over aversive processing based in part on their spatial location. In particular, rostral and caudal Calcrl^{+} neurons exert opposing effects on active vs passive defensive response strategies, and, while both have similar response profiles to external stimuli, caudal Calcrl^{+} neurons preferentially respond to and orchestrate responses to aversive internal states and profoundly affect stimulus valence. Importantly, both populations contribute to associative fear learning, highlighting their intersectional importance in affective processing.

Table of Contents

Introduction

Approximately half of animal behavior is directed towards reducing current or predicted risk of harm, while the rest balances risk with appetitive drive. This necessary defensive behavior results from recognizing an imminent physical or environmental threat, that, when combined with other environmental cues indicating the location and type of threat, directs motivation towards reducing exposure (Gross and Canteras, 2012). Defensive behaviors can be learned or innate and are selected for based on environmental and evolutionary pressures, which determine the nature of the stimuli threatening the organism (Fanselow, 1994; Fanselow et al., 1987; Gross and Canteras, 2012; Silva et al., 2013). Perhaps it is unsurprising then that the most universally recognized threat is noxious stimulation, whose defining feature is the activation of sensory nociceptors signaling tissue damage (Basbaum et al., 2009). It also follows that affective processing of aversive stimuli layered onto these preexisting networks dedicated to sensory processing of nociceptive stimuli; hence, understanding the systems and circuits underpinning affective processing generally is best approached through the lens of primary signals differentially giving rise to appropriate behaviors (LeDoux, 2000). This endeavor has profound implications for understanding how affective processing goes awry in mental disorders ranging from anxiety (Grupe and Nitschke, 2013) to post-traumatic stress (Liberzon and Sripada, 2007) and chronic pain (Basbaum et al., 2009; Neugebauer et al., 2009).

The goal of this thesis is to contribute to our understanding of how the brain gives rise to appropriate defensive responses and affective coding when faced with diverse aversive stimuli. More specifically, this thesis focuses on the role of calcitonin gene-related peptide (CGRP)-expressing neurons in the parabrachial nucleus (PBN) and downstream neurons throughout the brain and in the central amygdala (CeA) in assembling coherent affective, behavioral, and physiological responses to threat. This Introduction describes the circuits conveying nociceptive information from the periphery to the forebrain

and how that has directed our attention to the PBN→CeA CGRP system. The Results section contains a published manuscript dissociating control of unconditioned responses and associative fear learning by discrete $CGRP^{PBN}$ neuron-projections, and a second prepared manuscript recording from and manipulating the activity of downstream neurons in the CeA with spatial precision to demonstrate that subpopulations differentially influence the salience and valence of aversive events. The last section is a summary of my findings and questions that remain unanswered, like the genetic identity of downstream neurons in the thalamus and basal forebrain that promote acquisition of conditioned fear.

Circuits for nociception

Nociception starts at the level of the primary sensory neuron, where Aδ and C-type fibers terminating in the skin and viscera are positioned to sense a variety of noxious stimuli including heat, pressure, inflammation, and direct depolarization by shock (Basbaum et al., 2009; Saper et al., 2012). Viscera-terminating neurons in dorsal root ganglia connect to deeper spinal laminae, while skin-terminating neurons primarily target lamina I (Basbaum et al., 2009); nociceptive vagal neurons innervating visceral organs project to the nucleus of the solitary tract (NTS) in the caudal hindbrain (Saper, 2002). After the first synapse, the perception of noxious stimuli diverges, forming three complementary paths to the forebrain. Spinal projection neurons from deeper laminae project primarily to internal lateral subregions of the PBN (Bernard et al., 1995; Bourgeais et al., 2001a), while lamina I projection neurons form two paths, the spinothalamic pathway to sensory thalamus that eventually terminates in primary sensory cortex (Bernard et al., 1995; Ledoux et al., 1987), and the spino-parabrachial pathway, which primarily targets dorsal and internal lateral subregions of the PBN and extends into hypothalamic and extended amygdalar structures (Bernard et al., 1995; Bourgeais et al., 2003; Choi et al., 2020; Gauriau and Bernard, 2002). The vagal nociceptive viscerosensory pathway carries through the NTS to the external lateral PBN (Roman et al., 2016), the home of $CGRP^{PBN}$ neurons, and ultimately terminates in a variety of forebrain

structures including the capsular subnucleus of the CeA (CeC) (Bernard and Besson, 1988a; Bester et al., 1997; Bourgeais et al., 2001b; Tokita et al., 2010). All of the aspects of the noxious stimulus – its identity, valence, and intensity – are built from these components. Classically, it was proposed that the thalamic pathway provided stimulus identity, while the parabrachial pathway contributed valence and intensity (Gauriau and Bernard, 2002). This view is supported by evidence that PBN neurons respond to noxious stimulation across the body without somatotopy (Bernard et al., 1994; Campos et al., 2018) but do code for stimulus intensity (Campos et al., 2018). Similarly, neurons in the CeC have broad somatotopy that tends to be noxious-stimulus specific (Bernard and Besson, 1990). The interplay of stimulus identity and valence underpins the formation of associative memories between noxious stimuli and environmental cues, to which I turn next since they provide key insights into affective processing.

Associative learning

In aversive associative learning an unconditioned stimulus (US, e.g., foot shock) is paired with a non-aversive environmental stimulus (CS, e.g., tone), and following repeated pairing, the CS presentation alone is sufficient to produce aversive responses, termed the conditioned response (CR) (LeDoux, 2000). Associative learning to noxious exteroceptive stimuli such as foot shock involves both the spino-parabrachial and spinothalamic nociceptive pathways: eliminating signaling at the level of the parabrachial nucleus attenuates association formation (Han et al., 2015), as does silencing neurons within intralaminar thalamic nuclei that receive nociceptive input (Barsy et al., 2020; Lanuza et al., 2008; Shi and Davis, 1999). The site of CS-US association is the basal lateral amygdala (BLA) principal neurons, where concomitant US activation strengthens synapses receiving CS input, driving the eventual development of auditory-threat CR (Blair et al., 2001; Kim et al., 2016; Maren, 2005). Following memory consolidation, re-exposure to the CS generates CRs through the BLA activation of downstream partners including the CeA (Ciocchi et al., 2010). Notably, while the broader locations of association formation and recall remain

consistent across conditioning stimuli (e.g., CS identity, US modality), the underlying populations adjudicating the responses vary depending on stimulus valence, biophysical salience, and potential to evoke goal-directed behavior (Fadok et al., 2017; Gozzi et al., 2010; Killcross et al., 1997). Interestingly, while signaling by the neuropeptide CGRP and the activity of Calcrl neurons within the CeA both contribute to associative memory formation to noxious stimuli, $CGRP^{PBN}$ neurons are not the primary target of the nociceptive spino-parabrachial pathway (Chiang et al., 2020; Choi et al., 2020) but are instead the target of rich excitatory input from the ascending vagal viscerosensory pathway via the nucleus of the solitary tract (NTS) (Roman et al., 2016), with indirect spinal input likely added on through intra-PBN excitatory microstructure (Chiang et al., 2020).

Parabrachial CGRP neurons

$CGRP^{PBN}$ neurons were first identified as potent suppressors of appetite in response to aversive viscerosensory agents, including administration of LiCl and lipopolysaccharide (LPS), which cause malaise (Carter et al., 2013). Later work revealed that these neurons both contribute to homeostatic satiety (Campos et al., 2016) and are broadly tuned to aversive stimuli of both somatic and visceral origin (Campos et al., 2018). This suggests that $CGRP^{PBN}$ neurons, rather than conveying a clear somatic-specific aversive signal to forebrain structures are instead relaying an integrated measure of internal state that is combined with broader sensory context to elicit appropriate response and association formation. In addition to their projections to the CeA, $CGRP^{PBN}$ neurons also project to numerous forebrain structures, including the visceral thalamus (VPMpc), parasubthalamic nucleus (PSTN), lateral hypothalamus (LH), substantia innominata (SI), and oval part of the bed nucleus of the stria terminalis (ovBNST), providing a canvas through which a simple negative valence signal can be shaped in diverse ways depending on broader connectivity to affect behavior and physiology.

CeA Calcrl^{+} neurons

The CeA is a complex striatum-like structure comprising three cross-inhibitory subnuclei that together orchestrate diverse adaptive behaviors, including defensive and appetitive responses (Fadok et al., 2018; Janak and Tye, 2015). As such, the CeA is notable for its bivalent functionality, an example being antagonistic fear$_{ON}$ somatostatin (SOM+) and fear$_{OFF}$ protein-kinase c-delta (PKCδ+) expressing neurons that both reside in the lateral CeA (CeL) and respectively are anti- and pro-nociceptive (Wilson et al., 2019) and promote or inhibit conditioned fear responses (Ciocchi et al., 2010; Haubensak et al., 2010). Their relationship highlights the crucial role filled by the CeA in affective processing and associative fear learning, as its activation by the aversive US is necessary for subsequent plasticity in the lateral amygdala (LA) that underlies conditioning stimulus CS-US association (Yu et al., 2017), and reactivation by association-storing neurons in the basal lateral amygdala (BLA) also contributes to the expression of conditioned fear (Ciocchi et al., 2010). While neuronal subpopulations within the CeA have been demonstrated to fill specific roles in shaping adaptive behaviors (Kim et al., 2017), CeA subnuclei also have recognized places within the information processing hierarchy: broadly, the capsular CeA (CeC) is slated as the primary recipient of incoming nociceptive information, while the CeL receives input from both the CeC, LA and BLA to gate output from the medial CeA (CeM) to midbrain, hindbrain, and hypothalamic structures controlling behavioral and physiological responses (Duvarci et al., 2011; Janak and Tye, 2015).

The CeC, the only substructure within the broader CeA whose activation leads to aversion (Kim et al., 2017), appears central to aversive processing as it is the primary recipient of nociceptive signals and also sends efferent projections to brain regions controlling autonomic and behavioral responses (Petrovich and Swanson, 1997). Signaling by the excitatory neuropeptide CGRP itself within the CeLC, the site of receptor expression, while entirely lacking the temporal dynamics of a nociceptive stimulus contributes both to affective-behavioral responses and associative learning to pain (van den Burg and

Stoop, 2019; Han et al., 2005; Okutsu et al., 2017; Shinohara et al., 2017), supporting the possibility that the nociceptive CeA signals valence and arousal-related affective components of pain. Interestingly, recent evidence suggests that the CeA can be parcellated along its rostrocaudal axis (Han et al., 2015; Sanford et al., 2017). Specifically, caudal CeA Calcrl+ neurons co-express PKCδ and are located in both the lateral and capsular subregions, while rostrally CeA Calcrl+ neurons are restricted to the CeC and do not co-express PKCδ (Han et al., 2015; Kim et al., 2017). Since these subregions tend to cross-inhibit each other, I hypothesized that rostral and caudal CeA Calcrl+ neurons may differentially promote distinct affective and behavioral response strategies to a single nociceptive event.

Results

I. Dissociable control of unconditioned responses and associative fear learning by parabrachial CGRP neurons

*This section was published with minor reformatting as an article with the same title in eLife. The full citation is as follows:

Bowen, A.J., Chen, J.Y., Huang, Y.W., Baertsch, N.A., Park, S. and Palmiter, R.D. Dissociable control of unconditioned responses and associative fear learning by parabrachial CGRP neurons (2020) eLife 2020;9:e59799.

Activation of CGRP^{PBN} neurons generates defensive responses

To determine whether activation of CGRP^{PBN} neurons is sufficient to induce both the behavioral and physiological correlates of the unconditioned response in addition to fostering associative fear learning (Han et al., 2015), we bilaterally injected an adeno-associated virus carrying Cre-dependent channelrhodopsin (AAV1-DIO-ChR2:YFP) and implanted fiber-optic cannulae over the PBN of *Calca*$^{Cre/+}$ mice, while control mice received AAV1-DIO-YFP (Figure 1A; figure supplement 1A). Repeated high-frequency (30 Hz) activation of CGRP^{PBN} neurons induced profound freezing behavior (Figure 1B, Figure 1—figure supplement 1B-C and Video 1), as indicated by rigid, uninterrupted immobility. In addition to eliciting robust freezing behavior, we confirmed that pairing photostimulation with an auditory CS rapidly induced conditioned freezing responses to the CS (Figure 1C) (Han et al., 2015). To test whether CGRP^{PBN} neurons can recapitulate physiological aspects of the unconditioned response, we photostimulated the neurons while monitoring heart rate with a pulse oximeter (Figure 1D). Interestingly, while modest activation (15 Hz, subthreshold for eliciting freezing behavior) resulted in moderate tachycardia (Figure

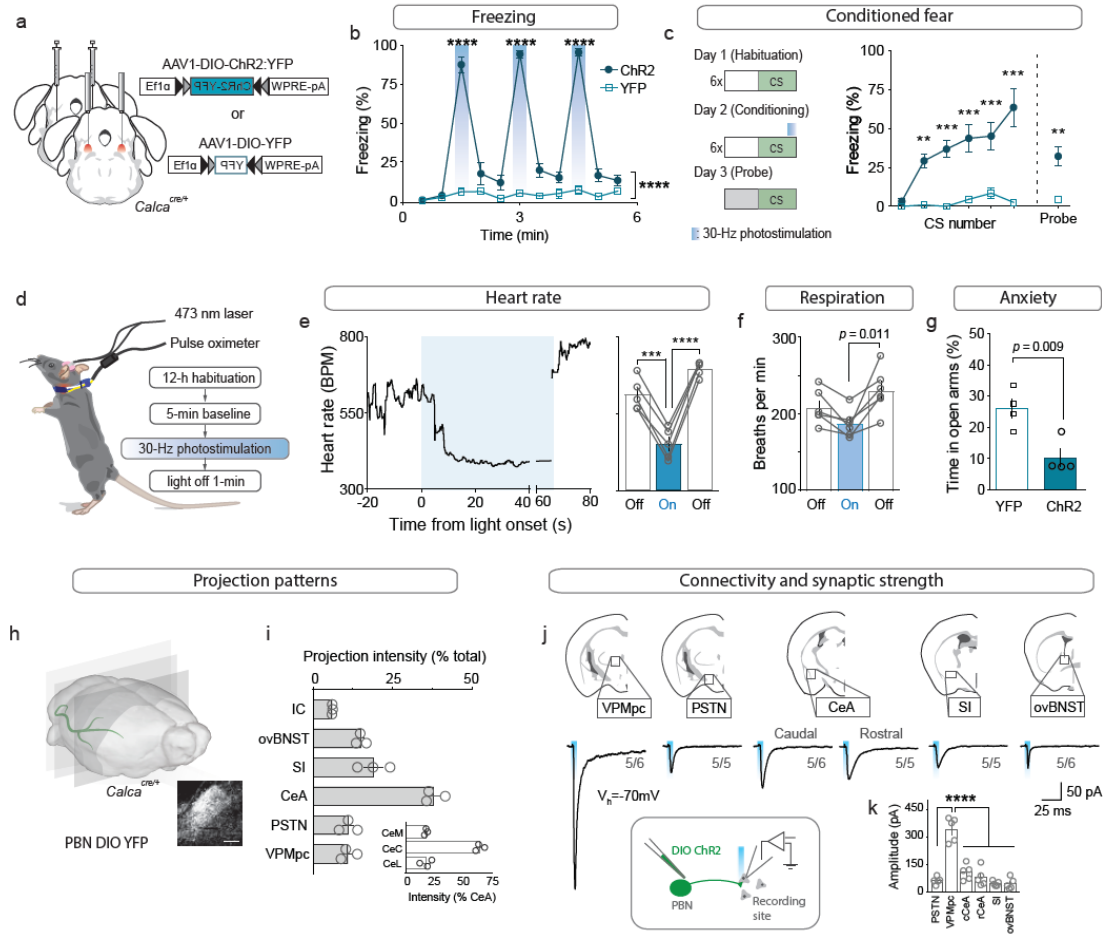

Figure 1. CGRP^{PBN} neurons potentiate fear behavior, drive associative learning and robustly activate forebrain targets

(**A**) Bilateral injections of AAV1-DIO-ChR2:YFP or AAV1-DIO-YFP and fiberoptic cannula implants above the PBN of Calca$^{Cre/+}$ mice. (**B**) Photostimulation (30 Hz) of CGRP^{PBN} neurons generated robust freezing behavior (n=8,6 (n=ChR2, YFP); significant group x time interaction in a two-way ANOVA, $F_{10,120}$ = 83.53, p < 0.0001; subsequent Sidak pairwise comparisons, ****p < 0.0001). (**C**) Optogenetic stimulation of CGRP^{PBN} neurons conditioned freezing behavior when preceded by a 10-kHz auditory CS (n=4,4 (n=ChR2, YFP); significant group x time interaction in a two-way ANOVA, $F_{5,36}$ = 5.62, p = 0.0006; subsequent Sidak pairwise comparisons, **p < 0.01; ***p < 0.001; and Welch's unpaired t-test for probe trial, $t(3.47)$ = 5.62, *p = 0.016). (**D**) Schematic and timeline for pulse-oximetry measurements of autonomic responses to optogenetic stimulation. (**E**) Representative and mean bradycardia caused by 30-Hz photostimulation of CGRP^{PBN} neurons (n=5, one-way ANOVA, $F_{2,12}$ = 39.66, p < 0.0001; subsequent Dunnett correction for multiple comparisons). (**F**) Respiratory rate was also reduced during photostimulation (n=6, one-way ANOVA, $F_{2,15}$ = 5.12, p = 0.0196; subsequent Dunnett correction for multiple comparisons, p = 0.011). (**G**) Stimulation of CGRP^{PBN} neurons was anxiogenic (n=4,4, Welch's unpaired t-test, $t(5.93)$ = 3.78, p = 0.009). (**H**) Expression of a fluorescent protein in CGRP^{PBN} neurons to identify efferent projections. Scale bar: 100 µm. (**I**) Fluorescence in downstream targets relative to cumulative projection intensity; inset is fluorescence in CeA subnuclei relative to total CeA fluorescence. (**J**) Representative light-evoked EPSCs from cells downstream of CGRP^{PBN} neurons; figures below traces (e.g. 5/6) indicate proportion of recorded cells that responded within each region. (**K**) Average amplitudes of EPSCs from responsive cells (5 cells for each site from 4 mice; 30/33 cells responded, significance for one-way ANOVA, $F_{5,24}$ = 38.75, p < 0.0001; subsequent Tukey correction for multiple comparisons). Data are represented as mean±SEM.

1—figure supplement 1E), high-frequency activation (30 Hz) led to profound bradycardia and decreased respiration followed by dramatic post-stimulation rebound tachycardia and mild hyperventilation (Figure

1E-F, respiration measured in plethysmography chamber); it also produced vasoconstriction (Figure 1—figure supplement 1H) (Vianna and Carrive, 2005). Hence, $CGRP^{PBN}$ neurons are capable of exerting opposing effects on autonomic physiology depending on their activation frequency. Comparing the latencies of somatic vs autonomic responses to 30-Hz photostimulation, we found that freezing behavior is rapidly initiated (median 0.42 s), while bradycardia takes longer to develop (median 22.15 s, Figure 1—figure supplement 1C-D), suggesting that freezing behavior does not emerge simply as a consequence of adverse autonomic effects. To test whether $CGRP^{PBN}$ neurons can also elicit behavioral alterations associated with late-phase responses to threat exposure, we subjected mice to an elevated-plus-maze test (Martin, 1961; Pellow et al., 1985) while activating $CGRP^{PBN}$ neurons; this treatment attenuated open-arm exploration consistent with an anxiogenic effect (Figure 1G).

To map the forebrain connections from $CGRP^{PBN}$ neurons that underlie their wide physiological and behavioral repertoire, we sectioned the forebrain of mice expressing a fluorescent tracer (AAV1-DIO-YFP) in $CGRP^{PBN}$ neurons and identified axon terminals in various downstream sites (Figure 1H). Comparing individual targets to cumulative projection intensity, we found major projections to the central amygdala (CeA, ~40%, primarily targeting the capsular sub-nucleus), substantia innominata (SI, ~20%), and oval sub-nucleus of the bed nucleus of stria terminalis (ovBNST, ~15%), with weaker projections to the parasubthalamic nucleus, thalamus and visceral insular cortex; PSTN and VPMpc, ~10% each, IC, ~5% (Figure 1I, for abbreviations see figure supplement 2). With the exception of the IC, $CGRP^{PBN}$ neurons also target the contralateral hemisphere for all of their downstream partners, markedly to the contralateral PSTN and VPMpc, with ~75% and 50% of the ipsilateral projection intensity, respectively (Figure 1—figure supplement 1I-J). To confirm that downstream neurons receive monosynaptic excitation from $CGRP^{PBN}$ neurons and also to compare synaptic strength across targets, we expressed channelrhodopsin (ChR2) in $CGRP^{PBN}$ neurons and photostimulated terminals in downstream regions while recording from putative postsynaptic neurons in a slice preparation (Figure 1J). Interestingly, we found that while all of the major

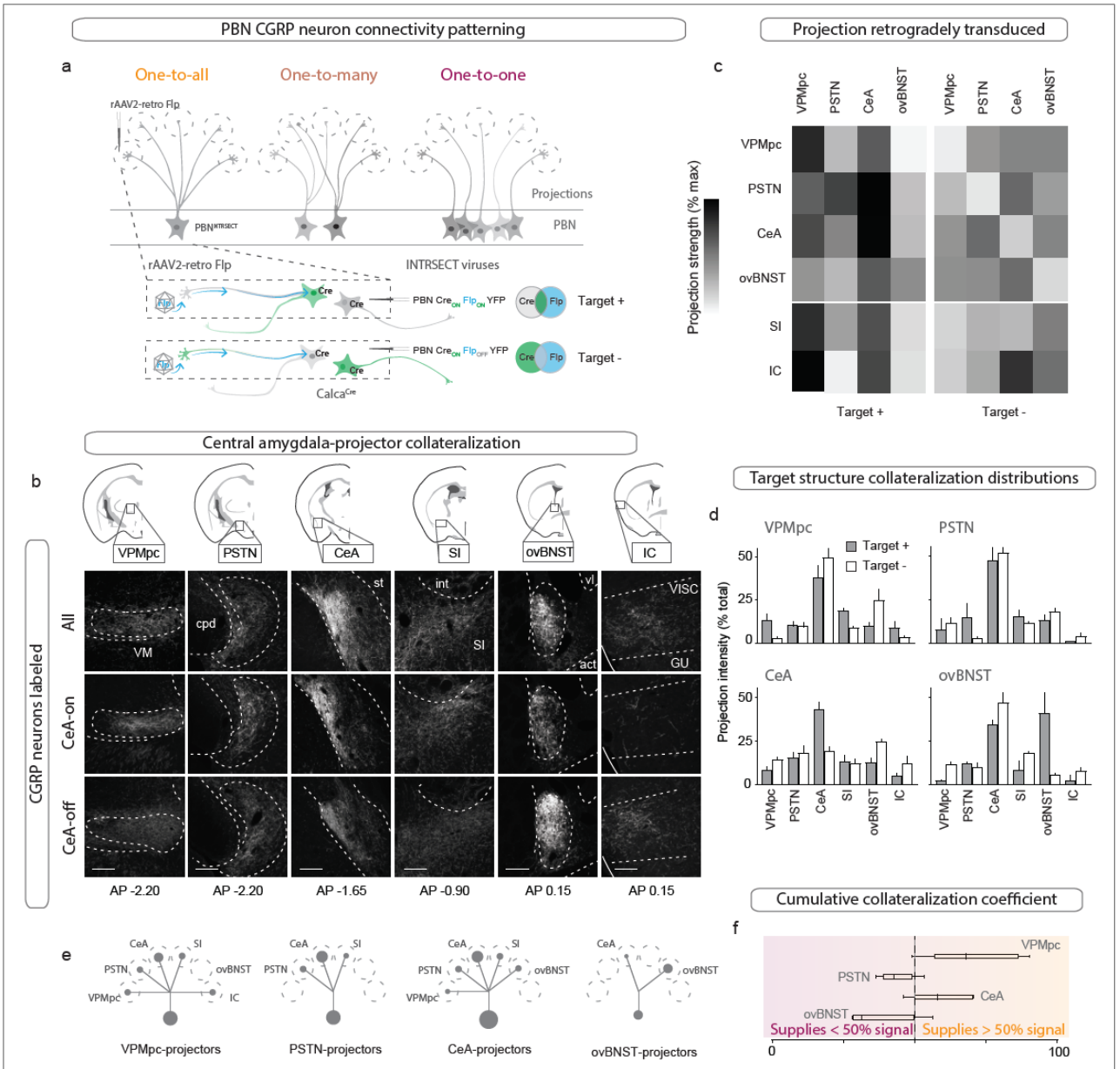

Figure 2. CGRP^{PBN} neurons broadly collateralize to forebrain targets (**A**) Injections of rAAV2-retro-Flp into projection targets and INTRSECT viruses into the PBN of Calca$^{Cre/+}$ mice to isolate target-projecting (Target +, Cre-on Flp-on) or non-projecting (Target -, Cre-on Flp-off) populations. (**B**) Fluorescent images of projection targets in mice expressing tracer in either all CGRP^{PBN} neurons, CeA-projectors (CeA-on), or non-CeA-projectors (CeA-off). Scale bar: 100 µm.(**C**) Heat maps of averaged fluorescent intensity in downstream sites for Target + or Target - viral expression conditions for the VPMpc, PSTN, CeA, and ovBNST; values normalized to maximal target projection intensity given by expression of DIO-YFP (n=3 per condition). (**D**) Overview of target-projecting projection distributions for VPMpc, PSTN, CeA, and ovBNST in Target + and Target – conditions (mean±SEM). (**E**) Schematic of relative population size and collateralization distribution from each target-projecting subset. Collaterals were indicated if collateralization coefficient was >50% (see below), *or* if structure made up >35% projection distribution in (**D**) from Target + condition. (**F**) Collateralization coefficient calculated as difference between normalized fluorescence intensity in projection site in Flp-on condition – Flp-off condition, averaged across all sites, scaled by 50% and forced through 0 for y-intercept. Example calculation for VPMpc-projector to CeA collateralization coefficient: (([CeA fluorescence]$_{VPMpc\text{-}ON}$ – [CeA fluorescence]$_{VPMpcOFF}$)/[CeA fluorescence]$_{DIOYFP}$)x 50% + 50%. Center line, mean; box limits, upper and lower quartiles; whiskers, min to max. See also Fig. 2 – figure supplement 1.

downstream targets were recipients of reliable excitatory input from CGRP^{PBN} neurons (Figure 1J, IC not tested), the VPMpc, while not receiving the strongest input based on fiber density, exhibited significantly greater excitation from terminal activation than any other recording site (Figure 1K).

The heterogeneity of behavioral and physiological outcomes elicited by activation of CGRP^{PBN} neurons raises questions about the underlying circuit organization responsible for their generation. We envisioned several potential circuit structures underlying CGRP^{PBN} neuron connectivity to the forebrain: while distributed, one-to-all connectivity involving extensive collateralization from each CGRP neuron to every target structure would be well suited for simultaneous, parallel activation of diverse regions, a one-to-one, segregated organization would better support separable generation of distinct functions via activation of designated partners. To reveal the structure underlying CGRP^{PBN}-neuron connectivity to the forebrain, we devised a method to selectively isolate subsets of CGRP^{PBN} neurons as defined by their target-projecting behavior. By injecting AAV expressing retrogradely-transported Flp-recombinase (rAAV2-retro-Flp) into a downstream site and a fluorescent tracer requiring both Cre and Flp for expression (Fenno et al., 2014) (AAV-Cre$_{on}$-Flp$_{on}$-YFP; Target +), or that is turned on by Cre but off by Flp (Fenno et al., 2014) (AAV-Cre$_{on}$-Flp$_{off}$-YFP; Target –) into the PBN of *Calca*$^{Cre/+}$ mice (Figure 2A), we were able to isolate fluorescent expression to neuronal subpopulations defined by whether or not they targeted a region of interest (Figure 2B, figure supplement 1A). Normalizing the resulting projection intensity in each downstream region under each condition to the maximal signal given by transducing all CGRP^{PBN} neurons, we determined the proportion of terminal density in each downstream partner supplied by target-projecting CGRP^{PBN} neurons for the VPMpc, PSTN, CeA, and ovBNST (Figure 2C). This analysis revealed that CeA-projectors contributed substantially to PSTN, SI, VPMpc and ovBNST projections, but not IC. VPMpc-projectors, interestingly, while also projecting to the CeA, contributed more substantially to the SI and IC, while PSTN-projectors had limited secondary output to the CeA and SI, and ovBNST-projectors had only a weak secondary projection to the CeA (Figure 2C), shown schematically in Figure 2E.

Quantifying the number and location of the different projecting subpopulations within the PBN revealed that neurons projecting to the CeA made up the largest proportion of $CGRP^{PBN}$ neurons residing within the external lateral PBN, while neurons projecting to VPMpc accounted for most of the $CGRP^{PBN}$ neurons residing in the medial and waist regions; neurons projecting to ovBNST, the smallest group, were restricted to the external lateral PBN (Figure 2—figure supplement 1B-F). Comparing projection distributions for the Target + or Target - expression conditions, we found that regardless of the downstream target used to drive expression, the CeA was the primary downstream partner in terms of projection intensity (Figure 2D). Excluding CeA-projecting $CGRP^{PBN}$ neurons flattened the distribution, with the ovBNST narrowly making up the largest projection contribution. As a summary statistic to directly compare the collateralization tendencies across subpopulations, we calculated a collateralization coefficient defined as the difference between projection strength for each downstream partner in the Target + and Target - conditions, for each target, where a value of 50% corresponds to half of the signal in the area of interest being supplied by target-site projectors (Figure 2F, figure supplement 1G). Looking at the distribution of these coefficients across secondary downstream partners for each target site, we found that VPMpc projectors had the greatest tendency to collateralize, while ovBNST projectors collateralized primarily to the CeA (Figure 2G, figure supplement 1G). In summary, there is extensive collateralization by $CGRP^{PBN}$ neurons with no one-to-one projections; rather, $CGRP^{PBN}$ neurons tend to distribute their projections among large groups of downstream targets, composing a one-to-many distributed projection arrangement (Figure 2E).

Individual $CGRP^{PBN}$ projections exert diverse effects on physiology and behavior

To assess the contribution of activating $CGRP^{PBN}$ projections to individual brain regions in eliciting behavioral and physiological processes associated with unconditioned responses to aversive stimuli, we used ChR2 to stimulate terminals within specific target regions (Figure3—figure supplement 1A-C, for fiber placement summary; fibers targeting the caudal and rostral CeA were placed in the caudal or rostral third

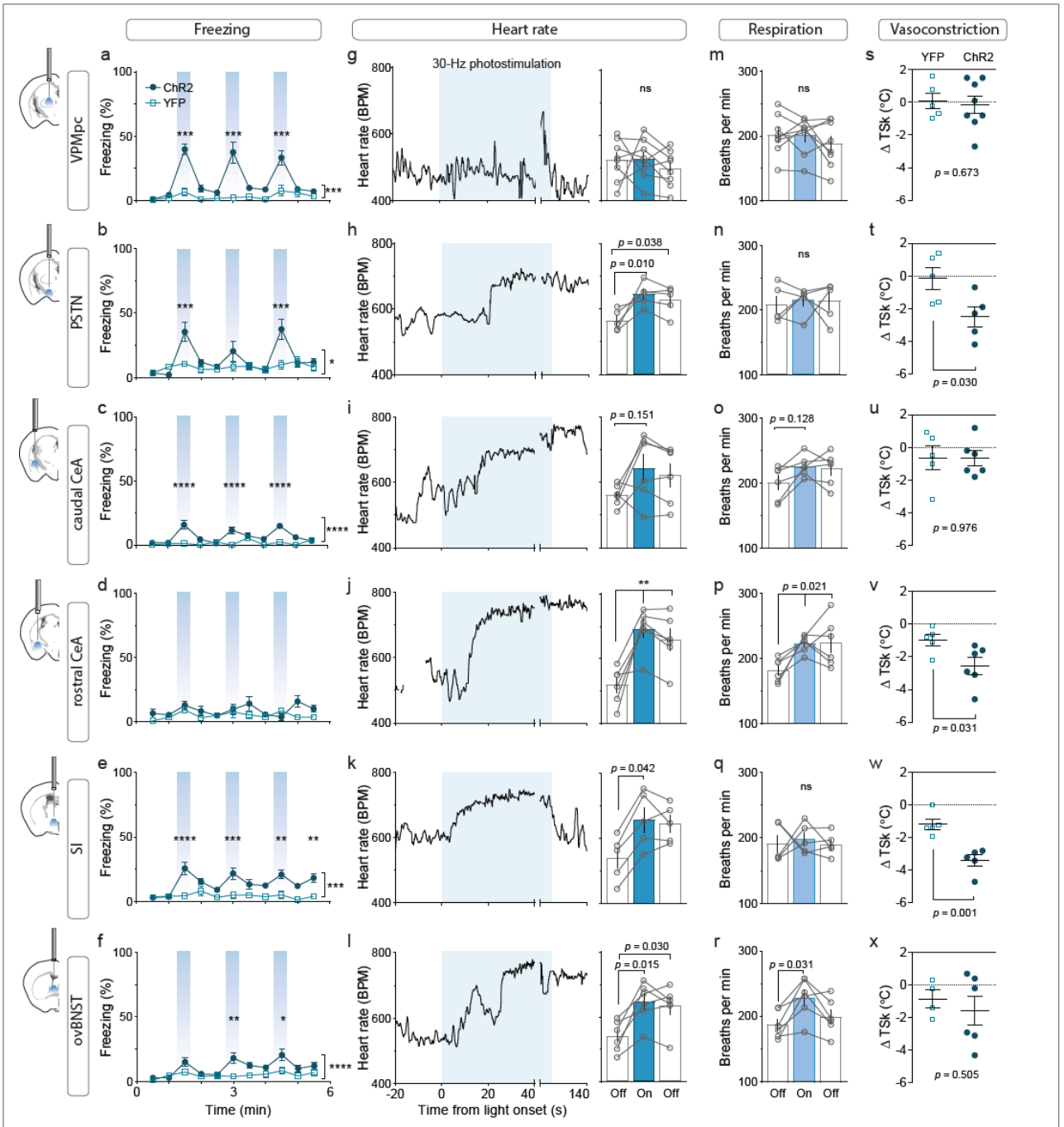

Figure 3. Photostimulation of CGRP^{PBN} neuron terminals in individual downstream targets exerts diverse effects on physiology and behavior (**A**) Activating terminals in the VPMpc (n=8,5 (ChR2, YFP) elicited freezing behavior but had no effect on (**G**) heart rate (**M**) respiration or (**S**) vasoconstriction. (**B**) Photostimulating terminals in the PSTN (n=6,5) elicited freezing behavior, (**H**) caused mild tachycardia, (**N**) had no effect on respiration but (**T**) caused vasoconstriction. (**C**) Photostimulating terminals in the cCeA (n=6,5) increased freezing behavior but had no effect on (**I**) heart rate (**O**) respiration or (**U**) vasoconstriction. (**D**) Photostimulating terminals in the rCeA (n=6,5) had no effect on freezing behavior (**J**) elicited robust tachycardia (**P**) hyperventilation and (**V**) vasoconstriction. (**E**) Photostimulating terminals in the SI (n=8,6) increased freezing behavior, (**K**) caused tachycardia (n=5), (**Q**) had no effect on respiration and (**W**) caused vasoconstriction. (**F**) Photostimulating terminals in the ovBNST (n=9,5) increased freezing behavior, (**L**) caused tachycardia and (**R**) hyperventilation but **(X)** did not affect vasoconstriction. (**A-F**) Significance for effect of group in a two-way ANOVA with subsequent Sidak pairwise comparisons. (**G-R**) Significance for one-way ANOVA with subsequent Dunnett correction for multiple comparisons. (**S-X**) Significance for Welch's unpaired t-test. Data are represented as mean±SEM. *p < 0.05; **p < 0.01; ***p < 0.001; ****p < 0.0001. See also Fig. 3 – figure supplement 1-3.

of the CeA (caudal to -1.4 AP and rostral to -1.0 AP, respectively). Because of the high degree of collateralization, it is possible that stimulating one region will result in antidromic activation and neurotransmitter release in all areas with shared innervation. If that occurred, then stimulating in one area that shares strong co-innervation with another should yield similar phenotypic outcomes. Surprisingly, given the broad collateralization of $CGRP^{PBN}$ neurons, that was not the case. Only photostimulating terminals in the VPMpc or PSTN led to reliable initiation of freezing behavior (Figure 3A-B, ~40% time-spent freezing), while photostimulating the caudal CeA (cCeA), SI, or ovBNST had more subtle effects (~25% time-spent freezing, Figure 3C-F), and stimulating the rostral CeA (rCeA) actually led to a non-significant increase in locomotion (Figure 3—figure supplement 2B; for cross-area mean freezing response comparisons see figure supplement 2A). Notably, activating no individual projection was able to match $CGRP^{PBN}$ cell-body activation in generating robust freezing behavior (Figure 3—figure supplement 2A, C). Importantly, while freezing behavior is an unconditioned response to predator incursion (Roelofs, 2017), when elicited by noxious stimulation it is instead a learned response to contextual cues because adaptive responses to ongoing noxious stimulation are always to flee or withdraw (Fanselow, 1982; Landeira-Fernandez et al., 2006). To examine whether the freezing behavior we observed was directly elicited by photostimulation or was instead driven by processes secondary to contextual conditioning, we looked at the temporal structure of the freezing responses to light onset and offset. We found that photostimulation led to short-latency freezing bout initiation (<5 s after stimulation onset) for most terminal stimulation groups except the rCeA, which instead elicited short-latency freezing bouts after stimulation offset (~2.4 s) (Figure 3—figure supplement 2C-D). Freezing-bout initiation occurred with lower latencies than control animals during the 20-s post-stimulation epoch in all stimulation groups except the VPMpc and cCeA (Figure 3—figure supplement 2C-D). When taken together with the observation that freezing behavior occurs with greater frequency during the stimulation epoch than post-stimulation epoch for all fiber-placement groups except those in the CeA and ovBNST (Figure 3—figure

supplement 2E), these findings suggest that stimulation of most $CGRP^{PBN}$ neuron projections simultaneously elicits a direct effect on freezing behavior while also generating aversive properties that promote transient contextual freezing. Interestingly, in the case of the rCeA, the direct effect on freezing is absent, while the contextual memory effects on freezing are instead the primary effect (Figure 3—figure supplement 2C-E).

By measuring the effect of photostimulating different terminal fields on multiple physiological measures, we found that activating the PSTN, rCeA, SI or ovBNST led to tachycardia, while activating the VPMpc or cCeA had no effect (Figure 3F-L). In addition to eliciting tachycardia, photostimulating terminals in the PSTN, rCeA or SI caused vasoconstriction (Figure 3S-X), while activating only the rCeA, SI, or ovBNST elicited hyperventilation (Figure 3M-R). Lower frequency stimulation (15 Hz) led to similar, less robust physiological effects across regions (Figure 3—figure supplement 3A-F), while light delivery alone in control animals had no effect on any of these measures (Figure 3—figure supplement 3G-L). Compellingly, the most co-innervated downstream regions – the VPMpc and SI, CeA and ovBNST, and PSTN and CeA, each had distinct effects on physiology and behavior, with some (VPMpc, PSTN) preferentially inducing freezing behavior, and others (SI, CeA, ovBNST) robustly eliciting autonomic responses, suggesting that terminal stimulation does not produce robust antidromic activation that homogeneously activates all co-innervated regions. In support of this conclusion, we observed that photostimulation of terminals in each downstream target did not generate antidromic activation of $CGRP^{PBN}$ cell bodies sufficiently to induce Fos expression in the PBN (Figure 3—figure supplement 2G). Taken together, these behavioral and physiological data suggest that the projections to thalamic (VPMpc) and hypothalamic (PSTN) targets elicit freezing behavior the best, while activating extended amygdalar structures (rCeA, SI, ovBNST) elicits sympathetic autonomic responses, implying a specialization in function across downstream partners.

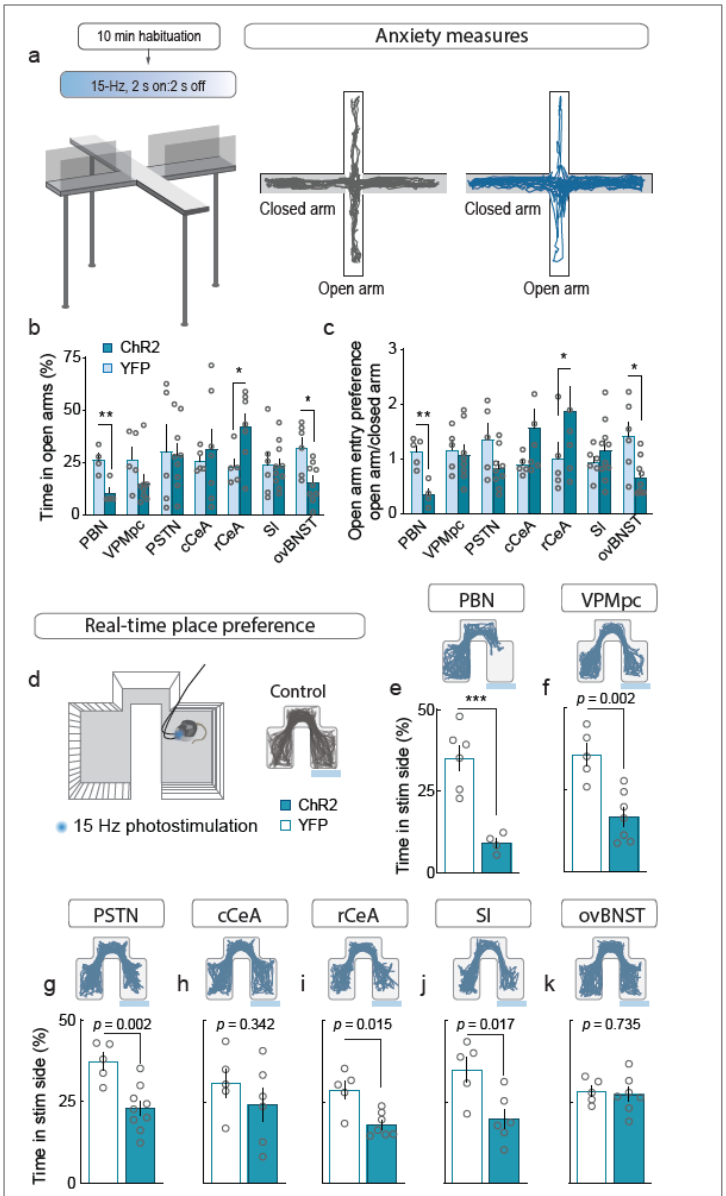

Fig. 4 | Stimulating the CGRP^{PBN} neuron terminals in ovBNST is anxiogenic while stimulating most other projections is aversive. (A) Experimental timeline and example responses to stimulation of CGRP^{PBN} neuron terminals or somata during measurements of anxiety-like behavior. **(B)** Activation of CGRP^{PBN} neurons reduced time spent in open arms, as did stimulation of their terminals in the ovBNST. Activation of terminals in the rCeA increased open-arm exploration time. **(C)** Activation of CGRP^{PBN} neurons or their projection to the ovBNST reduced open-arm entry preference; activation of the projection to the rCeA increased open-arm entries. **(D)** Illustration of RTPP paradigm and example trace of control mouse maze exploration. **(E-F)** activation of CGRP^{PBN} neurons **(E)** led to avoidance of light-paired side, as did stimulation of individual projections to **(F)** the VPMpc, **(G)** PSTN, **(I)** rCeA, and **(J)** SI, while projections to **(H)** the cCeA or **(K)** ovBNST had no effect on side-preference. Data are represented as mean±SEM. *p < 0.05; **p < 0.01; ***p < 0.001. See also Figure 4 – figure supplement 1.

CGRP^{PBN}-neuron projections differentially control learning and affect

To measure alterations in anxiety state, potentially indicative of enhanced arousal or vigilance in response to threats (Martin, 1961; Mestanik et al., 2015), we photostimulated terminals in downstream targets while mice explored an elevated-plus maze (Figure 4A). Only photostimulation of terminals in the ovBNST significantly reduced open-arm exploration, consistent with an anxiogenic effect, while photostimulating terminals in the rCeA paradoxically increased open-arm exploration (Figure 4B-C).

To further interrogate the affective state generated by activation of each downstream partner we utilized a real-time, place-preference (RTPP) assay to assess whether mice would choose to seek out or avoid terminal photostimulation (Figure 4D). Mice with photostimulation of either CGRP^{PBN} somata or their terminals in the VPMpc, PSTN, rCeA, or SI robustly

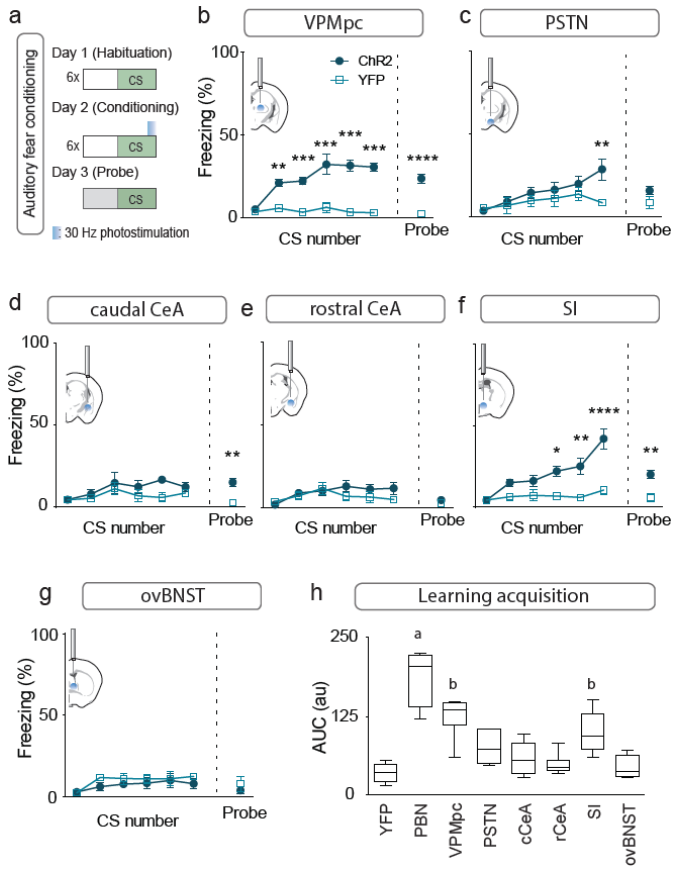

Figure 5. Photostimulating terminals in the VPMpc or SI can promote associative fear learning

(**A**) Illustration of experimental paradigm for cue-dependent optogenetic conditioning. (**B**) Conditioned-freezing responses to CS paired with $CGRP^{PBN}$ terminal stimulation in the VPMpc during training (n=8,5; ChR2, YFP; significant effect of group in two-way ANOVA, $F_{1,66}$ = 115.4, p < 0.0001; subsequent Sidak pairwise comparisons, **p < 0.01; ***p < 0.001) and in probe test 24-h following conditioning (Welch's unpaired t-test, $t(8.93)$ = 7.29, ****p < 0.0001). (**C**) Conditioned freezing responses to PSTN (n=5,4) terminal stimulation (significant effect of group in two-way ANOVA, $F_{1,42}$ = 6.99, p = 0.012; subsequent Sidak pairwise comparisons). (**D**) Conditioned freezing responses to cCeA (n=7,5) terminal stimulation (significant group effect in two-way ANOVA during training, $F_{1,60}$ = 4.69, p = 0.0343; and probe test, Welch's unpaired t-test, $t(8.15)$ = 4.40, **p = 0.0022). (**E**) Conditioned freezing responses to rCeA (n=8,5) terminal stimulation (two-way ANOVA effect of group, $F_{1,60}$ = 2.74, p = 0.1032). (**F**) Conditioned freezing responses to SI (n=8,6) terminal stimulation. Significant group effect in two-way ANOVA during training, $F_{1,60}$ = 23.45, p = 0.0004; subsequent Sidak pairwise comparisons; and in probe test 24-h following conditioning (Welch's unpaired t-test, $t(11.15)$ = 3.86, **p = 0.0026). (**G**) Conditioned freezing responses to ovBNST (n=5,4) terminal stimulation (two-way ANOVA effect of group, $F_{1,66}$ = 2.764, p = 0.1011). (**H**) Area under the curve for conditioning in each ChR2 fiber-placement group, including PBN-stimulation (n=8) and control groups (n=6, averaged for each YFP fiber-placement group). Significance for one-way ANOVA, $F_{7,40}$ = 19.44, p < 0.0001; subsequent Tukey correction for multiple comparisons, differences indicated by dissimilar letters above data columns. Bar graphs are represented as mean±SEM.

avoided photostimulation (Figure 4E-K, figure supplement 1E-K), whereas mice with photostimulation of terminals in the cCeA or ovBNST had no preference relative to control animals, which spent equal time in the 3 compartments. Considering aversive valence in combination with the observation that photostimulation of terminals in the rCeA robustly potentiated escape attempts during exposure to noxious heat (Figure 4—figure supplement 1A-C) without affecting spinal analgesia (Figure 4—figure supplement 1D), implies that activating the rCeA may not be anxiolytic *per se*, but shift behavior towards active coping strategies during threatening situations (D'amour and Smith, 1941; Espejo and Mir, 1993).

While we had observed that stimulation of multiple individual projections was able to transiently generate contextual freezing, we were interested in distinguishing between intrinsic effects of stimulation on freezing behavior versus secondary effects on associative learning. To accomplish this, we subjected

mice to an associative fear-learning paradigm where an auditory conditioning stimulus (CS) precedes and co-terminates with terminal photostimulation as an unconditioned stimulus (US) to assess the ability of activating each individual projection target to generate a fear memory, revealed by testing for conditioned responses to the CS in a novel environment (Figure 5A). Photostimulation of $CGRP^{PBN}$-neuron terminals in the VPMpc, PSTN, or SI resulted in significant freezing to the auditory CS after 6 CS-US pairings (Figure 5B-G), with only activation of terminals in the VPMpc or SI generating a significant association as indicated by area under the curve exceeding that of control animals (Figure 5H) and robust conditioned freezing to the CS in a novel context 24 h following conditioning (Figure 5B-G). While photostimulation of $CGRP^{PBN}$ neuron terminals in either the SI or VPMpc was sufficient to drive associative fear learning, the association formed is weaker than that driven by photostimulating $CGRP^{PBN}$ neuron cell bodies (Figure 5H), suggesting they play complementary roles.

Emergent properties of combined activation of downstream targets

Activation of no single projection from $CGRP^{PBN}$ neurons was sufficient to elicit profound freezing behavior or bradycardia; therefore, we devised a method to simultaneously activate multiple terminal fields by implanting 3 fiber-optic cannulae in a single hemisphere over multiple areas of interest to determine the threshold of downstream activity necessary to elicit these phenotypes (Figure 6A). We placed one cannula over the SI, one over the cCeA and one over the VPMpc. Then, we determined the strength of freezing responses capable of being generated by each individual projection field by varying the light power. Maintaining stimulation frequency at 30 Hz and increasing laser power from 10 to 40 mW, we found that activation of $CGRP^{PBN}$ neuron terminals in the cCeA or VPMpc led to a gradual increase in freezing but activating terminals in the SI was maximal at 10 mW (Figure 6B). Combining photostimulation of terminals in the VPMpc and SI (10 mW each) led to rapid entrainment of freezing behavior to an auditory CS, and the resulting association strength, though not significantly greater than either projection individually

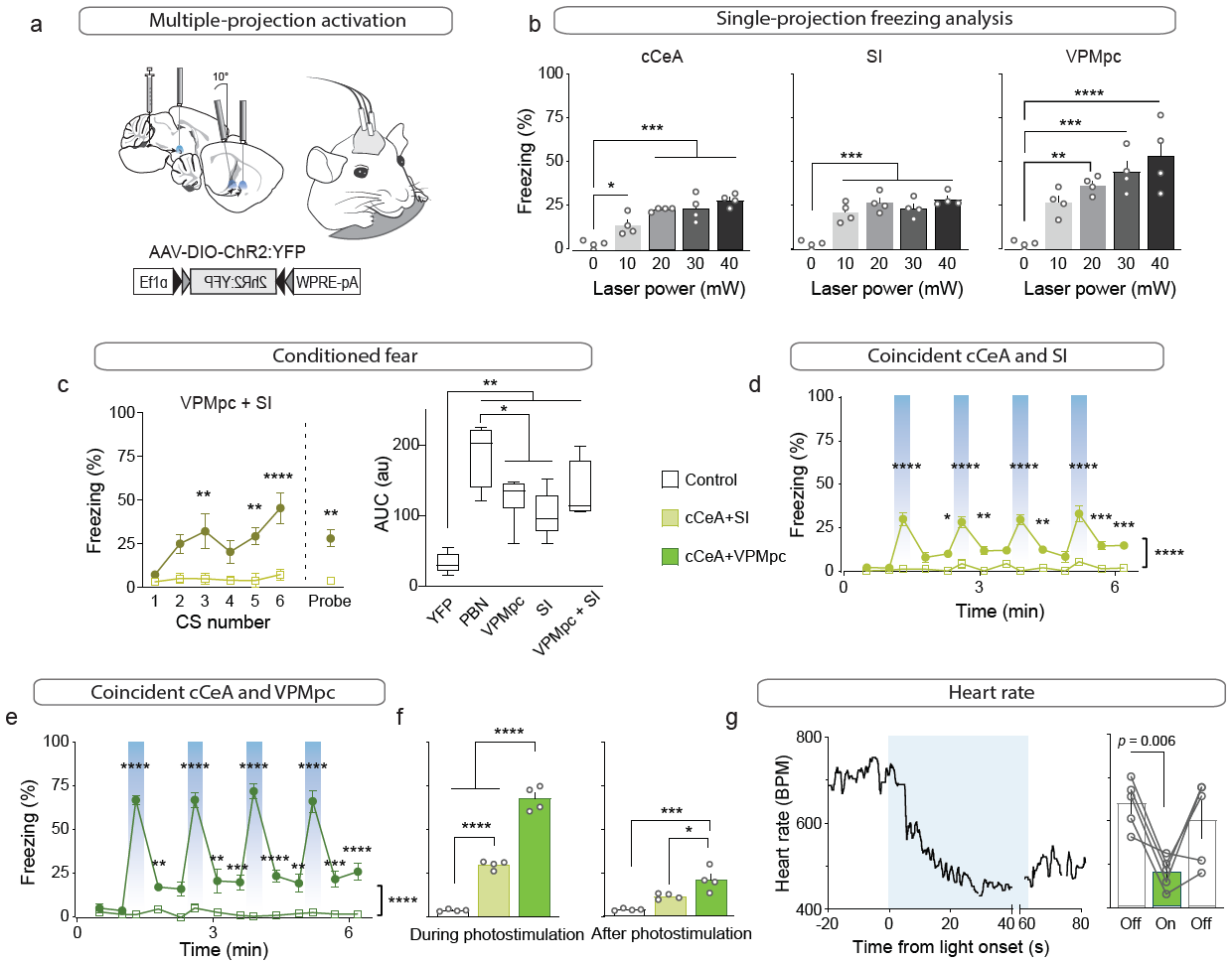

Figure 6. Combined activation of CGRP^{PBN} neuron terminals in the VPMpc and cCeA scales freezing responses and produces bradycardia

(**A**) Schematic showing configuration for implantation of 3 fiberoptic cannulae into one hemisphere allowing simultaneous photostimulation of multiple CGRP^{PBN}-neuron terminal fields. (**B**) Freezing behavior during 30-Hz photostimulation with increasing power of CGRP^{PBN} neuron terminal fields in the cCeA (n=4, one-way ANOVA, $F_{4,15}$ = 18.08, p < 0.0001), SI (n=4, $F_{4,15}$ = 19.21, p < 0.0001), or VPMpc (n=4, $F_{4,15}$ = 12.09, p = 0.0001). Subsequent Tukey correction for multiple comparisons, *p < 0.05; **p < 0.01; ***p < 0.01; ****p < 0.0001. (**C**) Freezing behavior to auditory CS co-terminating with simultaneous photostimulation of terminals in the VPMpc and SI (left) (significant group effect in two-way ANOVA, $F_{1,6}$ = 21.57, p = 0.0035; subsequent Sidak pairwise comparisons) or probe test with CS presented in novel context 24 h after conditioning (Welch's unpaired t-test, *t(3.414)* = 4.90, p = 0.012). Comparison of area-under-curve for associative learning generated by CS paired with CGRP^{PBN} neuron or terminal activation (right) (one-way ANOVA, $F_{4,27}$ = 19.73, p < 0.0001; subsequent Tukey correction for multiple comparisons. Center line, mean; box limits, upper and lower quartiles; whiskers, min to max. (**D**) Freezing behavior in response to simultaneous activation of CGRP^{PBN} neuron terminals in the cCeA and SI (n=4,4 (ChR2, control), significant group effect in two-way ANOVA, $F_{1,78}$ = 213.5, p < 0.0001; subsequent Sidak pairwise comparisons). (**E**) Freezing behavior in response to simultaneous activation of CGRP^{PBN} neuron terminals in the caudal CeA and VPMpc (n=4,4; significant group effect in two-way ANOVA, $F_{1,84}$ = 631.5, p < 0.0001; subsequent Sidak pairwise comparisons). (**F**) Comparison of averaged freezing behavior for each stimulation combination during the stimulation epoch (left) (n=4,4; one-way ANOVA, $F_{2,9}$ = 218.9, p < 0.0001), and during the post-stimulation epoch (right) (n=4,4; one-way ANOVA, $F_{2,9}$ = 17,67, p = 0.0008; subsequent Tukey correction for multiple comparisons). (**G**) Representative (left) and mean bradycardia elicited by simultaneous photostimulation of CGRP^{PBN}-neuron terminals in the cCeA and VPMpc (n=5; one-way ANOVA, $F_{2,12}$ = 7.38, p = 0.0081; subsequent Dunnett correction for multiple comparisons, p = 0.0058). Bar graphs represented as mean±SEM. See also Figure 6 – figure supplement 1.

generated, was no longer significantly weaker than that generated by the entire population even though our dual-stimulation arrangement was unilateral and all other groups were bilateral (Figure 6C).

We then combined activation of multiple projection fields using 20-mW power to determine which combination of $CGRP^{PBN}$ neuron projections could elicit profound freezing behavior. Activating the cCeA and SI projection fields resulted in moderate freezing behavior that did not appear to be additive (cCeA 23.2±0.5% freezing; SI 26.9±2.5; Combined 30.4±1.3 (mean±sem), Figure 6D; Figure 6—video 1), while simultaneous activation of terminals in the VPMpc and cCeA elicited robust freezing behavior exceeding that produced individually (VPMpc 37.1±2.3% freezing; cCeA 23.2±0.5; Combined 68.9±3.6 (mean±sem), Figure 6B and E-F; Figure 6—video 2), comparable to freezing behavior elicited by activating all $CGRP^{PBN}$ neurons bilaterally (93.0±2.9% freezing (mean±sem), Figure 1B; Figure 6—video 1). These phenotypes were enhanced by driving photostimulation with a red light-activated opsin (Yizhar et al., 2011) (VPMpc+cCeA 94.5±3.0% freezing (mean±sem), Figure 6—figure supplement 1A-I), suggesting that a combination of light-spread and faithfulness of activation underlies reliable freezing generation. Importantly, simultaneous photostimulation of terminal fields did not dramatically induce Fos in $CGRP^{PBN}$ neurons (<10% compared to 80% for soma activation sufficient to generate freezing behavior) (Figure 6—figure supplement 1J-L). We also tested whether simultaneous photostimulation of terminals in the cCeA and VPMpc would affect autonomic physiology by measuring heart rate using a pulse oximeter. While activating neither projection alone affected heart rate (Figure 3), simultaneous photostimulation robustly elicited bradycardia, which consistently took longer to develop than freezing responses (Figure 6G, Figure 6—figure supplement 1A). These results imply that when combinations of projections from $CGRP^{PBN}$ neurons are activated simultaneously their combined output is able to generate phenotypes beyond their individual ability, suggesting a mechanism by which defensive responses can be tuned depending on whether downstream partners are already in an ‘up’ or ‘down’ state as determined by broader sensory context when they receive input from $CGRP^{PBN}$ neurons.

CGRP^{PBN} projections to the VPMpc and SI contribute to associative fear learning

While previous studies that permanently silenced CGRP^{PBN} neurons demonstrated that their activity contributes to conditioned-fear responses (Han et al., 2015), we asked whether photoinhibition restricted to the peri-foot shock period during conditioning would be sufficient to attenuate conditioned responses to the CS, as post-shock recurrent activity, stress-induced activation, or recall-driven reactivation could also potentially affect association formation, memory consolidation, or recall. Using AAV-mediated expression of a red-light activated chloride pump (Chuong et al., 2014) (JAWS) to inhibit CGRP^{PBN} neurons during 0.5-mA foot-shock delivery (Figure 7A, figure supplement 1A), we found that selective inhibition of CGRP^{PBN} neurons during the foot shock significantly attenuated both conditioned responses during training and in a CS-probe trial 24 h later, while also reducing freezing behavior conditioned to the training context (Figure 7B). These findings affirm that the signal relayed by CGRP^{PBN} neurons to downstream partners during the foot shock directly contributes to associative memory formation.

To determine whether individual projections contribute to associative fear learning, we used JAWS to inhibit CGRP^{PBN}-neuron terminals in the VPMpc, CeA, or SI during the foot shock (Figure 7C). We first confirmed that JAWS-mediated inhibition of CGRP^{PBN}-neuron terminals significantly reduced EPSC frequency in post-synaptic neurons (Figure 7D) (Mahn et al., 2016). Inhibiting synaptic release during the foot shock at CGRP^{PBN}-neuron terminals in the VPMpc or SI, but not CeA, significantly attenuated both memory formation (Figure 7E-G) and association strength (Figure 7H), without affecting contextual-fear learning. While inhibiting CGRP^{PBN} neurons non-significantly reduced foot shock-induced locomotion (Figure 7I), no individual projection tested was necessary for this response. In addition, transiently inhibiting either CGRP^{PBN} cell bodies or their individual projections did not significantly affect behavioral responses to noxious heat (Espejo and Mir, 1993) (Figure 7—figure supplement 1B-E), nor did it lead to a place preference in a RTPP paradigm (Figure 7—figure supplement 1F-I), suggesting that basal activity of

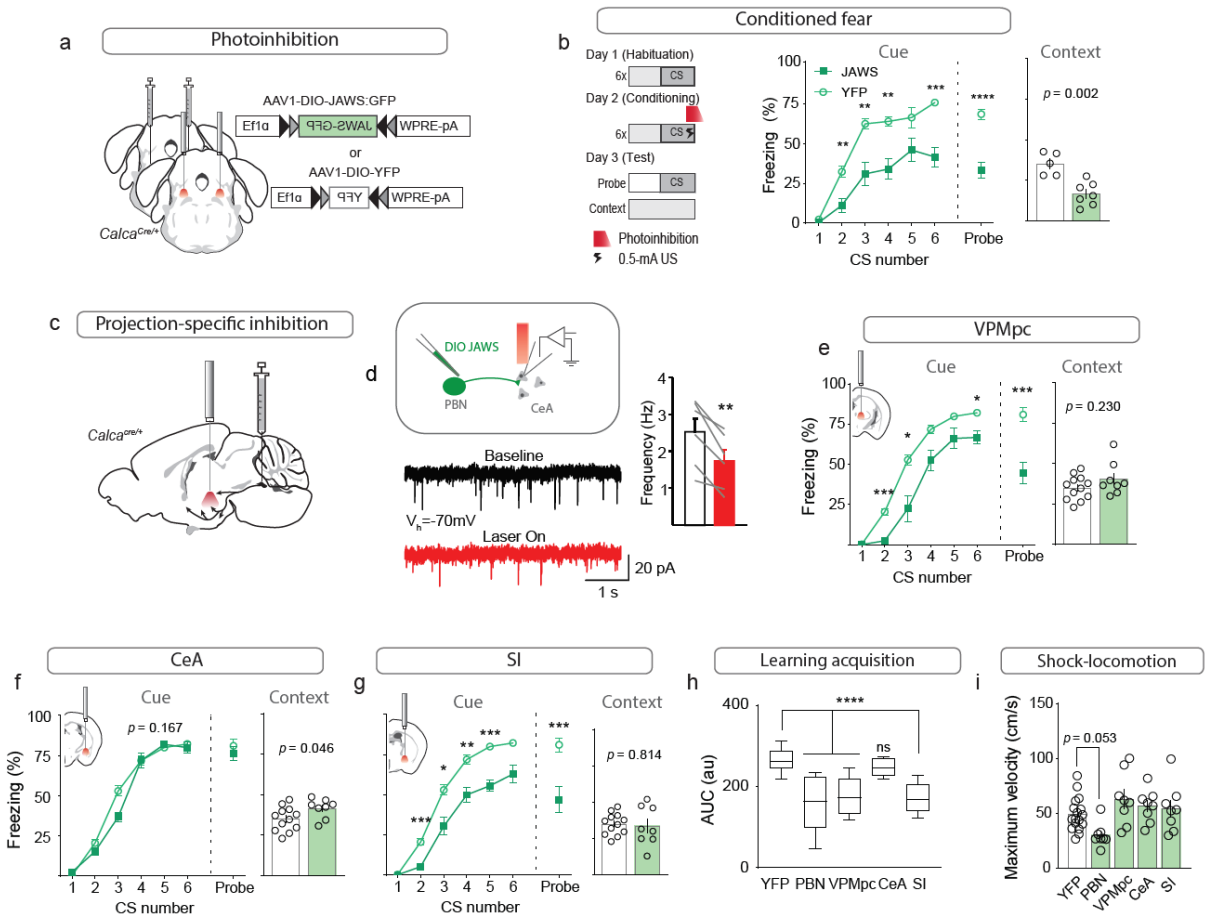

Figure 7. Foot shock-induced activation of the VPMpc and SI by CGRP^{PBN} neurons contributes to associative fear learning

(**A**) Bilateral injections of AAV1-DIO-JAWS:GFP or AAV1-DIO-YFP and fiber-optic cannula implants above the PBN of Calca$^{Cre/+}$ mice for photoinhibition of CGRP^{PBN} neurons. (**B**) Photoinhibition of CGRP^{PBN} neurons (n=8,5; JAWS, GFP) during foot shock delivery attenuated freezing responses both to CS and context (significant group effect in two-way ANOVA for training, $F_{1,55}$ = 21.66, p = 0.0007; subsequent Sidak pairwise comparisons, *p < 0.05; **p < 0.01; Welch's unpaired t-test for probe and context, probe *t(10.88)* = 6.45, ****p < 0.0001; context *t(8.93)* = 4.43, p = 0.002). (**C**) Placement of fiber-optics over projection sites for projection-specific photoinhibition. (**D**) Representative recording of EPSCs in a CeA neuron surrounded by JAWS:GFP-positive fibers from CGRP^{PBN} neurons. Red light decreased frequency of EPSCs in downstream cells (6 cells from 2 mice, paired t-test, *t(5)* = 4.84, **p = 0.0047). (**E**) Photoinhibition of CGRP^{PBN} neuron terminals in the VPMpc (n=8,12) during footshock attenuated freezing responses to CS (significant group effect in two-way ANOVA for training, $F_{1,18}$ = 28.78, p < 0.0001; subsequent Sidak pairwise comparisons; probe test Welch's unpaired t-test, *t(14.41)* = 4.58, ***p = 0.0004) but not context (Welch's unpaired t-test, *t(11.72)* = 1.27, p > 0.05). (**F**) Effect of photoinhibition of CGRP^{PBN} neuron terminals in the CeA (n=8,12) during foot shock on conditioned freezing responses to cue (two-way ANOVA for training, group effect $F_{1,18}$ = 2.08, p = 0.167; Welch's unpaired t-test for probe, *t(16.69)* = 0.76, p = 0.46) or context (Welch's unpaired t-test, *t(17.17)* = 2.15, p = 0.046). (**G**) Photoinhibition of CGRP^{PBN} neuron terminals in the SI (n=8,12) during shock attenuated freezing responses to CS (significant group effect in two-way ANOVA for training, $F_{1,18}$ = 40.52, p < 0.0001; subsequent Sidak pairwise comparisons; probe test Welch's unpaired t-test, *t(11.06)* = 3.70, **p = 0.0035) but not the context (Welch's unpaired t-test, *t(9.83)* = 0.24, p > 0.05). (**H**) Photoinhibition of CGRP^{PBN} neuron projections to either the VPMpc or SI during footshock attenuated associative learning (area under learning curve) as efficiently as silencing the entire population. Center line, mean; box limits, upper and lower quartiles; whiskers, min to max. Significance for one-way ANOVA, $F_{4,45}$ = 15.35, p < 0.0001; subsequent Sidak pairwise comparisons found no difference between PBN, VPMpc, and SI fiber-placement groups. (**I**) Locomotion during foot shock was not significantly affected by photoinhibition of CGRP^{PBN} neurons (one-way ANOVA, $F_{4,44}$ = 4.13, p = 0.0063; subsequent Dunnett pairwise comparisons p > 0.05). See also Figure 7 – figure supplement 1.

CGRP^{PBN} neurons is insufficient for their inhibition to generate a salient shift in affective state. Taken together, these data reveal an unexpected role for the SI and VPMpc, two regions respectively implicated

in arousal (Kaur et al., 2017; Mogenson et al., 1985) and taste processing (Liu and Fontanini, 2015), in contributing to an affective pain signal that drives associative fear learning.

Discussion

Disentangling the interacting neural substrates responsible for generating affective, behavioral, and physiological responses to environmental threats is a necessary endeavor for understanding and eventually treating the alterations in threat processing that underlie affective disorders such as PTSD (Flandreau and Toth, 2018; Mikics et al., 2008) and anxiety (Davis and Whalen, 2001; Lissek et al., 2014). Leveraging what is known about the circuits ascending from the spinal cord to drive affective, motivational responses to pain (Bernard and Besson, 1988b; Campos et al., 2018; Gauriau and Bernard, 2002; Han et al., 2015), we aimed to dissect at the level of the PBN the multi-faceted system that simultaneously generates diverse innate unconditioned responses and drives learned associations to aversive stimuli.

Generation of unconditioned behavioral and physiological responses

Previous studies silencing $CGRP^{PBN}$ neurons implicated them in contributing to both affective responses to somatic pain, including nocifensive behavior, post-shock freezing behavior (Han et al., 2015), and illness-induced increases in anxiety state (Campos et al., 2017). We found that photostimulation of $CGRP^{PBN}$ neurons, in addition to driving profound freezing behavior, can also generate either tachycardia or parasympathetic responses depending on stimulation frequency, and elicit anxiety-like behavior. These findings collectively suggest that activation of $CGRP^{PBN}$ neurons during somatic pain has the potential to contribute to many aspects of the unconditioned response cascade, from shock-induced locomotion to post-shock freezing behavior, autonomic responses including simultaneous enhancement of parasympathetic and sympathetic outflow, and post-insult anxiogenesis. A complication of this arrangement is that neither freezing behavior (Blanchard and Blanchard, 1969), parasympathetic responses (Iwata and LeDoux, 1988), nor anxiety occur during the shock. Hence, the role played by

$CGRP^{PBN}$ neurons in these phenotypes would necessarily result from recurrent reactivation, rather than a direct ascending signal.

By selectively activating $CGRP^{PBN}$-neuron terminals in their various downstream targets, we distinguished the potential of individual downstream partners to contribute to distinct components of the behavioral and physiological alterations that comprise the unconditioned- response cascade. We found that with the exception of the rCeA, all projections generated some amount of freezing behavior, with the most robust responses elicited by the PSTN and VPMpc, two projections that were overlooked in previous work. We also found a marked disparity in function across the CeA, with activation of terminals in the cCeA eliciting only mild freezing behavior, while activating the rCeA had no effect on freezing behavior during photostimulation but did produce robust sympathetic responses, brief contextual freezing following stimulation offset, avoidance, and nocifensive behaviors on a hot plate, all phenotypes reminiscent of responses to noxious stimulation. In general, our results suggest that $CGRP^{PBN}$-neuron connections to extended amygdalar structures (i.e., the CeA, SI, and ovBNST) influence freezing behavior, affective processing including negative valence and anxiety state, and physiological responses, while thalamic and hypothalamic connections transmit a negative-valence signal and elicit freezing behavior. These results are supported by the fact that, in rats, extended amygdalar structures are richly interconnected with hindbrain nuclei controlling autonomic outflow (Dong and Swanson, 2004; Rizvi et al., 1991; Veening et al., 1984), while the VPMpc is not (Cechetto and Saper, 1987). Our findings complement recent work that distinguished between PBN populations that target the extended amygdala and hypothalamus/periaqueductal grey and differentially drive affective and nocifensive responses, respectively (Chiang et al., 2020). However, by distinguishing between conditioned freezing responses and avoidance behavior, we were able to specifically implicate two novel targets, the VPMpc and SI, in generating associative fear learning, whereas Chiang et al. (2020) studies were limited to learned valence and they only tested the CeA and ovBNST. We found that the PSTN, SI, and VPMpc also relay a negative

valence signal. Hence, populations contributing to the negative valence of noxious or aversive stimuli may not necessarily contribute to associative fear learning, which has important implications for understanding the neural underpinnings of affective disorders such as PTSD.

Our collateral-tracing experiments revealed that, in contrast to the distinct phenotypes generated by terminal photostimulation, $CGRP^{PBN}$ neurons form a broadly distributed network with their downstream partners in which no forebrain target receives solitary innervation. There was some bias in the connectivity groupings, with neurons projecting to the CeA tending to also strongly innervate the PSTN, neurons projecting to the VPMpc also innervating the SI and IC and avoiding the ovBNST, and neurons projecting to the ovBNST also targeting the CeA. Our findings are broadly in agreement with previous experiments that delineated sub-region- specific output and collateralization in rats (Sarhan et al., 2005)and mice (Chiang et al., 2020), neither of which, however, reported connections or collateralization with the VPMpc, suggesting that cell-type specific expression more efficiently reveals this connection. Of interest, Sarhan et al. (2005) beautifully outlined rostral and caudal capsular CeA branching patterns across all extended amygdalar structures using single-axonal reconstructions, finding collateralization between the rCeA and lateral hypothalamus (PSTN), and cCeA and ventral BNST. Taken as a whole, the distributed, collateralization organization of $CGRP^{PBN}$ neurons may be important for generating highly coordinated actions and associations by simultaneously driving activity in downstream sites that have related or complementary functions. An example in support of this arrangement is that stimulation of terminals in the SI and VPMpc generated disparate effects on physiology, but collaboratively supported associative fear learning.

While activating some individual terminal fields from $CGRP^{PBN}$ neurons in different downstream sites recapitulated – in a scaled-down fashion – most of the phenotypes driven by photostimulating the cell bodies, we found that profound freezing behavior and bradycardia were not produced by stimulation of any individual projection, suggesting they instead arise from additive interactions between

downstream structures and their respective circuits. We tested this hypothesis by simultaneously activating terminals in the VPMpc and cCeA, two targets that generated reliable freezing behavior, and observed not only a robust potentiation of the freezing behavior but also profound bradycardia. Interestingly, neither of these populations generated autonomic responses when activated individually. One possible arrangement that explains this phenotype is that their concurrent activation gates activity in secondary structures that drive parasympathetic responses.

An important consideration in implicating individual downstream partners in generating distinct aspects of behavioral and physiological response is the inherent limitation of terminal photostimulation. It is difficult, if not impossible, to ensure that antidromic activity does not activate secondary targets, an especially important possibility given the broad collateralization of $CGRP^{PBN}$ neurons. However, secondary techniques aimed at accounting for this situation also have their shortcomings: axons may bifurcate near the sites of interest rather than at the cell body, hence silencing cell bodies may not prevent antidromic activation. Moreover, since many of the forebrain structures contributing to threat processing are interconnected, silencing other portions of the downstream circuit to attempt to isolate the effect of the target of interest on the measured phenotype may affect phenotype generation if the populations are interconnected. We argue that the very fact that terminal stimulation in different downstream targets generates distinct phenotypes supports the fact that at minimum, preferential activation of the site of interest is occurring. If photostimulation of terminals was efficiently activating cell bodies within the PBN then the same phenotypes should be observed regardless of fiber location. Perhaps most compelling is that CeA-projecting $CGRP^{PBN}$ neurons make up the bulk of the population yet photostimulation of terminals in the CeA does not efficiently produce either freezing behavior or anxiety, two of the distinct phenotypes produced by activating other downstream targets that receive collateral innervation with the CeA.

Another necessary caveat of using artificial stimulation to probe the intrinsic functionality of different projection partners is that variation in transport rate and axon length across downstream partners could profoundly influence ChR2 levels at terminals and thus terminal stimulation efficacy, which in turn would confound the observed differences in function and connection strength across the circuit. We attempted to account for this by allowing 4 weeks after virus injection for ChR2 expression and transport before beginning experiments, having observed that 2-3 weeks was sufficient to observe robust labelling in the most distant terminal fields. While our electrophysiological measures revealed the greatest synaptic strength in $CGRP^{PBN}$ neuron connections to one of their more proximal downstream partners, the VPMpc, the fact that the PSTN, which is equally close to the PBN but has a connection strength that is similar to what we observed with all other targets suggests that ChR2 transport cannot be the primary reason for the strength of the connection to the VPMpc. Moreover, we did not see a declination of synaptic strength across the proximal-distal axis – synapses in the ovBNST, the most distal target, exhibited similar synaptic strength to those 2 mm more proximal, in the PSTN. What underlies the large differences in synaptic strength we observed across downstream targets that was independent of projection strength as measured by terminal labelling density? Differences in release probability, convergence (the VPMpc is a much smaller structure than the CeA, for example, hence each neuron might receive more contacts), postsynaptic receptor number or dendrite structure could all contribute to the observed differences in synaptic strength. One particularly interesting possibility is that the VPMpc, which does not express receptors for CGRP, may primarily rely on glutamatergic input from the PBN and hence exhibits large-amplitude EPSCs in response to $CGRP^{PBN}$ neuron terminal photostimulation, while extended amygdala targets may rely more on CGRP release for activation (Okutsu et al., 2017), which our experiment would not have been able to reveal. A more detailed analysis of the electrophysiological properties of $CGRP^{PBN}$ neuron to forebrain connections is necessary to understand the temporal and chemical underpinnings that help give rise to the different functions of each downstream connection.

Associative fear learning

Associative learning is a highly tractable and informative process because it reliably depends on the salience of the CS and US, and the innate associability of these stimuli (Garcia et al., 1968; Sigmundi et al., 1980). The interplay of these factors on the association is indicated by the learning rate and asymptote – the maximal conditioned response for a particular CS-US pair (Rescorla, 1972; Sigmundi et al., 1980). Here, we maintained a constant CS and varied the US by activating specific projections from $CGRP^{PBN}$ neurons to condition predictive freezing to an auditory CS, or by silencing either $CGRP^{PBN}$ neurons or individual projections during foot-shock delivery. Activation of $CGRP^{PBN}$ neurons elicited the most robust association, followed by stimulation of terminals in the VPMpc or SI. No individual projection was sufficient to recapitulate the learning asymptote generated by stimulating all $CGRP^{PBN}$ neurons; hence, some combination of projections relays salient aspects of the US, generating complementary signals that eventually reach the basolateral amygdala (BLA) to potentiate synapses receiving coincident CS information (Blair et al., 2001; Maren, 2001; Romanski et al., 1993). In support of this hypothesis, inhibiting $CGRP^{PBN}$-neuron terminals in either the VPMpc or SI during the US attenuated the association strength to the same degree as inhibiting the entire population, suggesting that preventing activation of either downstream partner impairs associative learning. We also observed that a substantial degree (~50%) of the conditioned response was maintained when inhibiting $CGRP^{PBN}$ neurons, indicating that they are part of a distributed network that collectively relays the affective, motivational signal to forebrain neurons that form and store the associative memory (Lanuza et al., 2004, 2008; Shi and Davis, 1999). Interestingly, work examining the ability of the $CGRP^{PBN}$ neuron projection to the VPMpc to generate an associative memory using taste as a CS indicated no conditioned taste aversion formation when paired with brief photostimulation, while projections to the CeA and ovBNST did (Chen et al., 2018), suggesting that either the relayed signal is the wrong modality for combining with CS taste information, or that a specific temporal activation pattern different from that tested is required to form an association (e.g.

longer-term activation that better mimics visceral illness). Hence, it is surprising that associative learning to a tone generated conditioned freezing behavior, while association with a taste did not alter preference, even though the VPMpc is an integral part of the ascending taste network (Liu and Fontanini, 2015). More work assessing the response patterns of individual VPMpc neurons to diverse sensory modalities and their contribution to conditioned taste aversion is required to resolve these paradoxes.

Previous work in rats indicates that PBN projections to the CeA are capable of eliciting both escape behaviors and fear learning in addition to driving place avoidance (Sato et al., 2015), while in mice it has been demonstrated that activation of CGRP-receptor neurons in the CeA is sufficient to act as a US to drive associative fear learning, and that silencing these neurons prior to conditioning attenuates conditioned-fear responses (Han et al., 2015). We activated both the rostral and caudal CeA terminal fields of $CGRP^{PBN}$ neurons and were surprised that neither manipulation was individually capable of generating a fear memory, suggesting a number of possibilities that may give rise to these findings: 1) It is possible that $CGRP^{PBN}$ neurons are only one component of the PBN projection to CeA and other PBN cell types are important for aversive learning, 2) CGRP-receptor neurons in the CeA may make up a larger population than those activated by $CGRP^{PBN}$-neuron terminal stimulation and receive input from secondary sources that are important for aversive learning; 3) direct activation of neurons in the CeA may be more efficient than terminal stimulation and may thus be able to drive associative learning; and 4) since the mice used in our study are heterozygous for CGRP, wholly intact neuropeptide signaling may be required for association formation derived from PBN to CeA stimulation (Okutsu et al., 2017). In support of the first two possibilities, we observed that inhibiting $CGRP^{PBN}$ neuron terminals in the CeA during foot-shock delivery had no effect on associative fear learning, suggesting that the relayed activity from $CGRP^{PBN}$ neurons to the CeA during the foot shock is not necessary for the CS-US association. This is in apparent contrast to previous work demonstrating that silencing CGRP-receptor neurons in the CeA prior to conditioning attenuates conditioned responses to the CS (Han et al., 2015). However, that manipulation

was permanent and failed to distinguish between association formation and recall, which our US-only inhibition did, suggesting that reactivation of CGRP-receptor neurons in the CeA after conditioning may underlie the observed reductions in conditioned responding. Based on these observations and our data implicating $CGRP^{PBN}$ neuron projections to the CeA in generating robust unconditioned-responses, we propose an alternate model wherein $CGRP^{PBN}$ neuron connections to the CeA, PSTN, SI, and ovBNST drive unconditioned responses to the US, post-conditioning activation of BLA neurons by the CS reactivates the CeA to generate conditioned responses (Kim et al., 2017), and $CGRP^{PBN}$ neuron connections to the SI and VPMpc primarily mediate the role of $CGRP^{PBN}$ neurons in associative-fear learning, a compelling arrangement given that in rats, these two downstream partners are the most directly invested in cortical circuits (Cechetto and Saper, 1987; Wenk, 1997). Our data establish partially separable ascending routes from $CGRP^{PBN}$ neurons for generating unconditioned responses and forming associative memories to aversive stimuli.

Supplemental figures

Figure 1—figure supplement 1

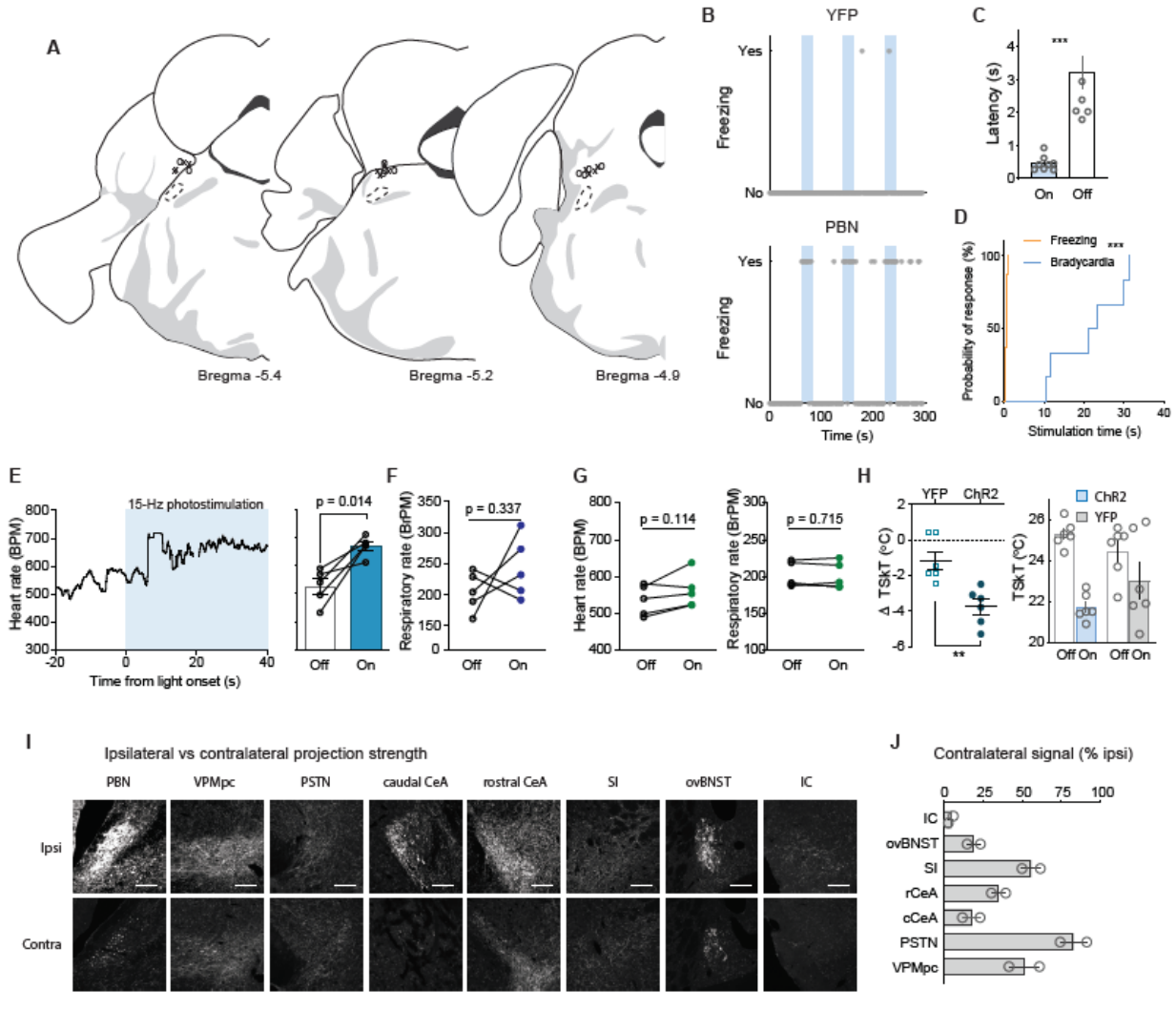

Figure 1—figure supplement 1. Fiber placement, autonomic measurements, and contralateral projection strength

(**A**) Position of fiberoptic cannula tips for CGRP^{PBN} neuron stimulation. (**B**) Example of freezing behavior in response to repeated 30-Hz photostimulation of CGRP^{PBN} neurons. (**C**) Latency to freeze during stimulation and post-stimulation epochs (some data points outside axis limits; n=8, paired t-test, *t(7)* = 5.681, p = 0.0007). **(D)** Survival curve comparing latencies of freezing and bradycardia responses to 30-Hz photostimulation of CGRP^{PBN} neurons (n=8 freezing, n=6 heartrate, Mantel-Cox Logrank test Chi square = 13.13, p = 0.0003). (**E**) Effect of 15-Hz photostimulation of CGRP^{PBN} neurons on heart rate (n=5, paired t-test, *t(4)* = 4.173, p = 0.014). (**F**) Effect of 15-Hz photostimulation of CGRP^{PBN} neurons respiratory rate (n=5, paired t-test, *t(4)* = 1.09, p = 0.34). (**G**) Effect of 15-Hz photostimulation in YFP-expressing control animals on heart rate (left), and respiratory rate (right) (n=5, paired t-tests, heart rate *t(4)* = 2.02, p = 0.12; respiration *t(4)* = 0.39, p = 0.71). (**H**) Vasoconstriction elicited by 30-Hz photostimulation of CGRP^{PBN} neurons, change in tail-skin temperature (left), and absolute tail-skin temperature (right) (n=6,6; ChR2, YFP, Welch's unpaired t-test, *t(9.64)* = 3.92, **p = 0.0031). (**I**) Ipsi- and contralateral fluorescent images of CGRP^{PBN}-neuron projection targets from mouse unilaterally expressing DIO-YFP in CGRP^{PBN} neurons. Scale bar: 100 µm. (**J**) Contralateral projection strength relative to ipsilateral fluorescent signal in each projection target structure (n=2). Data are represented as mean±SEM.

Figure 2—figure supplement 1

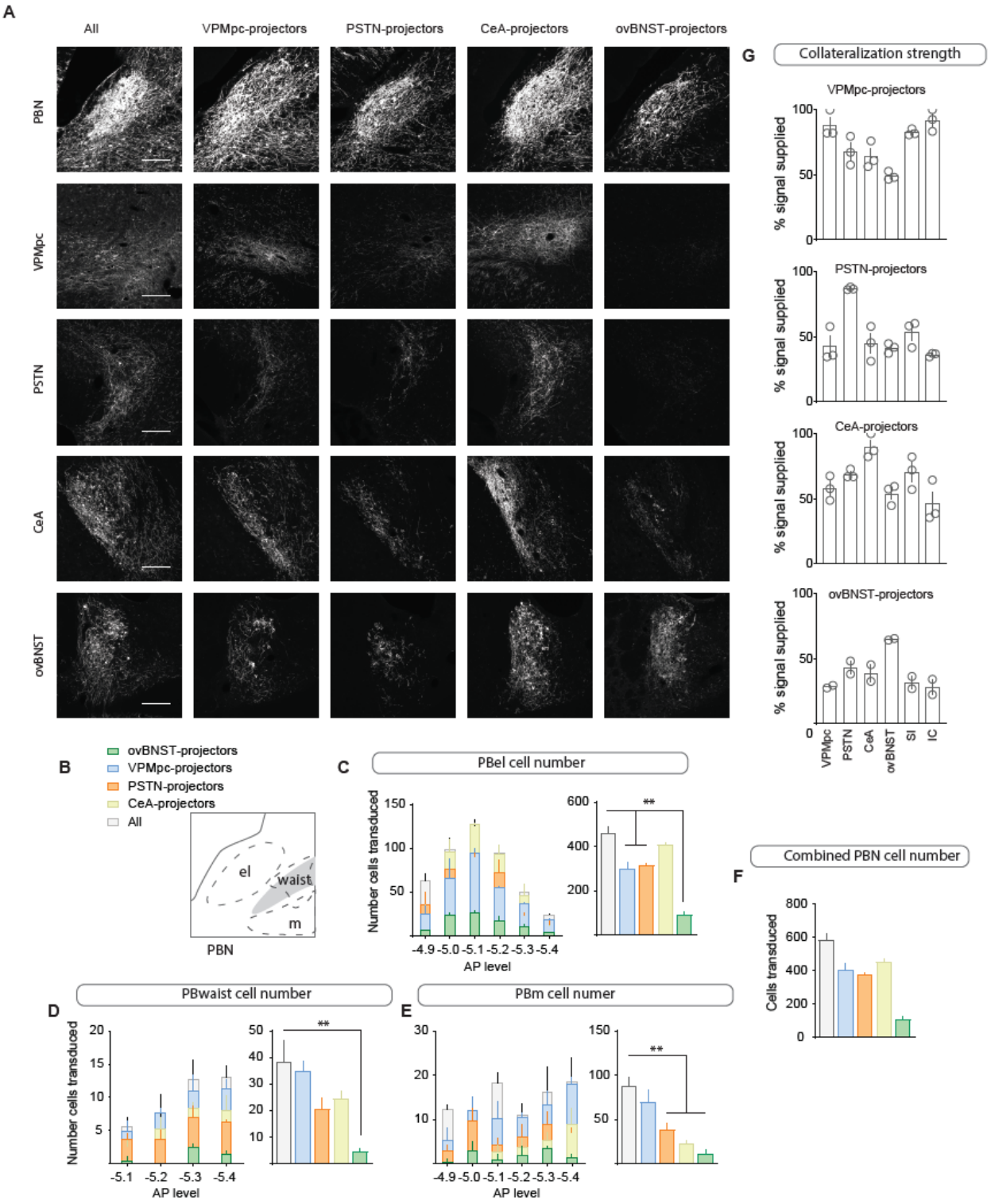

Figure 2—figure supplement 1. Collateralization to forebrain targets by CGRP^{PBN} neurons

(**A**) Fluorescent images of CGRP^{PBN} neurons and their projection targets from mice expressing YFP in either all CGRP^{PBN} neurons or those projecting to the VPMpc, PSTN, CeA, or ovBNST. Scale bar: 100 µm. (**B-F**) Cell counts across the AP-axis in various PBN subnuclei of CGRP^{PBN} neurons transduced with the help of retrogradely transported Flp injected into the VPMpc, PSTN, CeA, or ovBNST (n=3 per condition). Significance for ordinary one-way ANOVAs with subsequent Dunnett correction for multiple comparisons ((C) $F_{4,9}$ = 31.17, p < 0.0001; (D) $F_{4,9}$ = 10.81, p = 0.0017; (E) $F_{4,9}$ = 6.05, p = 0.012; pairwise comparisons **p < 0.01). (**G**) Collateralization coefficients for each projection target calculated for each projection-specific subset of CGRP^{PBN} neurons. Data are represented as mean±SEM.

Figure 3—figure supplement 1

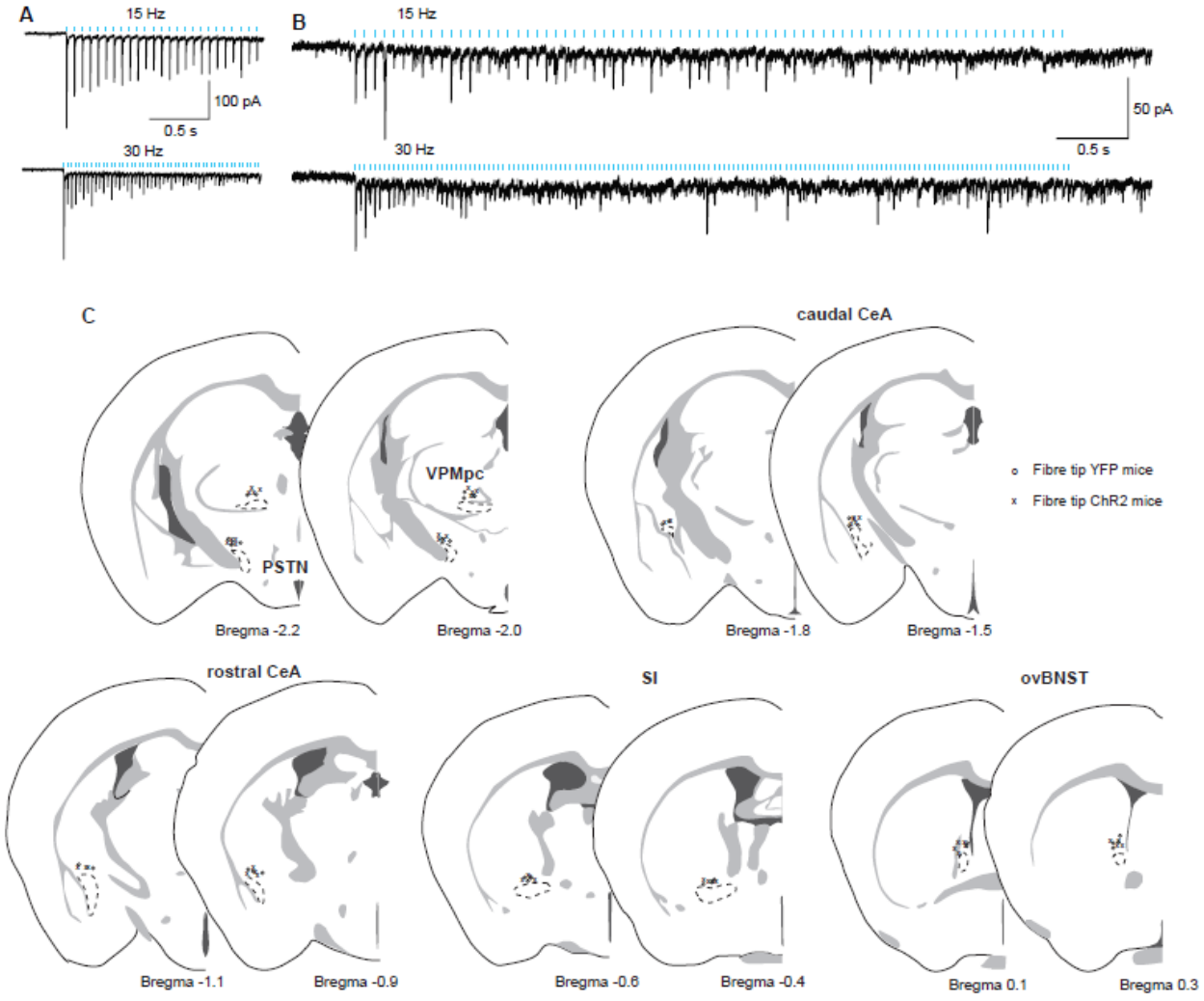

Figure 3—figure supplement 1. Verification of terminal stimulation of CGRP^{PBN} neuron projections

(**A-B**) Postsynaptic neurons are reliably activated by 15- (top) and 30-Hz (bottom) photostimulation of CGRP^{PBN} neuron terminals (5 cells from 2 mice, 2 cells represented). (**C**) Position of fiber-optic cannula tips for projection-specific terminal photostimulation in control (o) and experimental (x) groups.

Figure 3—figure supplement 2

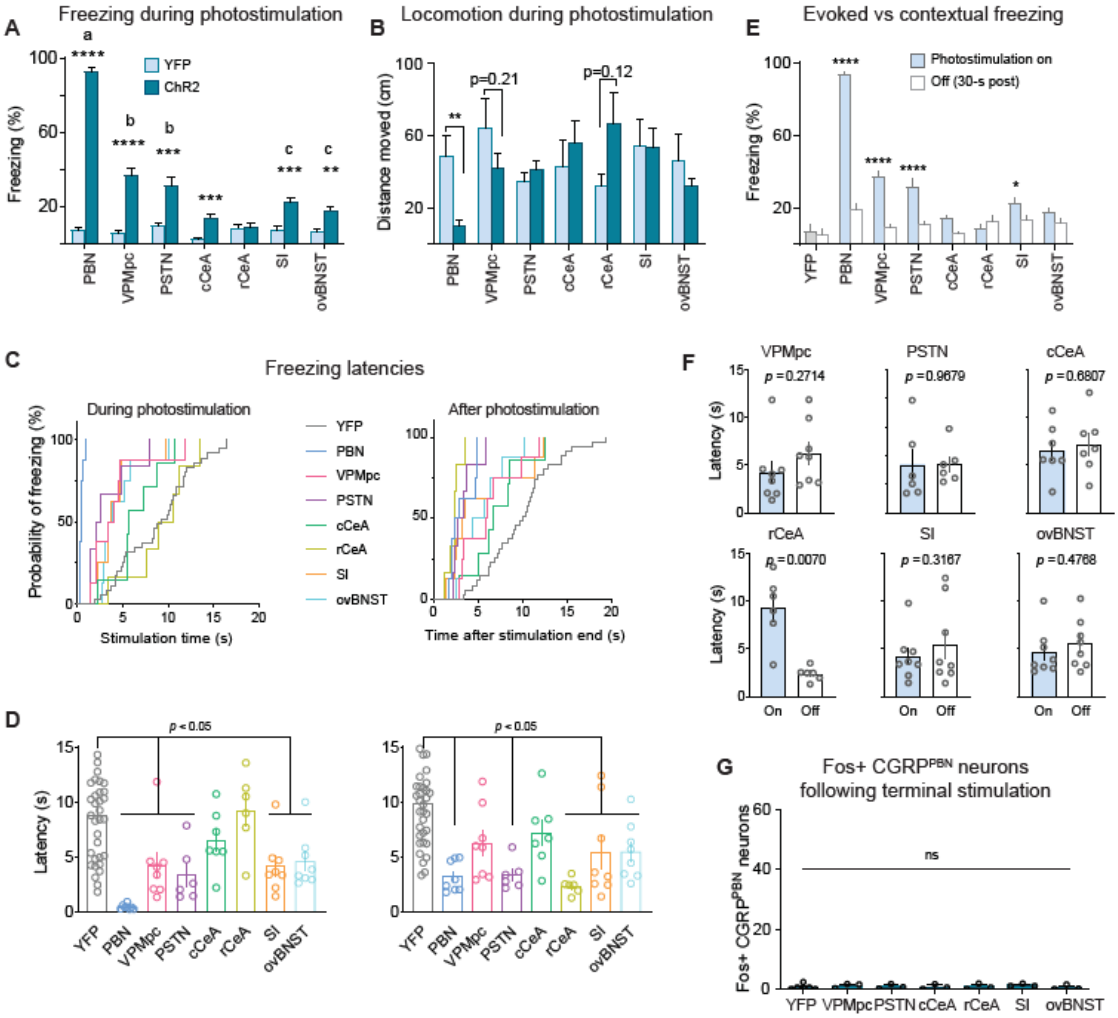

Figure 3—figure supplement 2. Freezing behavior elicited by photostimulation of CGRP^{PBN} neuron terminals

(**A**) Freezing behavior from each animal collapsed across stimulation epochs. Photostimulation of CGRP^{PBN} neurons resulted in robust freezing behavior not replicated by activation of any individual projection (significant group effect in two-way ANOVA, $F_{6,253}$ = 75.73, p < 0.0001; subsequent Sidak pairwise comparisons, **p < 0.01; ***p < 0.001). (**B**) Average distance moved for each animal during stimulation epochs; only stimulation of CGRP^{PBN} neurons significantly reduced locomotion (Welch's unpaired t-tests, PBN n=7,6 (ChR2, YFP), *t(5.91)* = 3.37, p = 0.0153; rCeA n = 6,5, *t(6.30)* = 1.88, p = 0.1066). **(C)** Survival curves comparing average latencies of freezing responses during (left) and after (right) photostimulation of CGRP^{PBN} neuron terminals or cell bodies (YFP control n=35, PBN n=8, VPMpc n=8, PSTN n=6, cCeA n=7, rCeA n=6, SI n=8, ovBNST n=8; Mantel-Cox Log-rank test, Chi-squared = 168.1, p < 0.0001). **(D)** Average freezing response latencies during (left) and after (right) photostimulation (n same as in **C**). Significance for ordinary one-way ANOVAs with subsequent Tukey's correction for multiple comparisons. Left: $F_{7,78}$ = 9.00, p < 0.0001; right: $F_{7,78}$ = 8.73, p < 0.0001. **(E)** Comparison of freezing behavior from each stimulation/post-stimulation epoch collapsed for each animal (3 values per animal) (significant treatment effect in two-way ANOVA, $F_{7,345}$ = 116.4, p < 0.0001; subsequent Sidak pairwise comparisons, *p < 0.05; ****p < 0.0001) **(F)** Comparison of freezing-bout response latencies during and after photostimulation of CGRP^{PBN} neuron-terminals (paired t-tests, VPMpc n=8, *t(7)* = 1.19, p > 0.05; PSTN n=6, *t(5)* = 0.04, p > 0.05; cCeA n=7, *t(6)* = 0.43, p > 0.05; rCeA n=6, *t(5)* = 4.41, p = 0.007; SI n=8, *t(7)* = 1.08, p > 0.05; ovBNST n=8, *t(7)* = 0.75, p > 0.05). (**G**) Photostimulation of CGRP^{PBN}-neuron terminals did not induce Fos in CGRP^{PBN} neurons (ordinary one-way ANOVA, $F_{6,17}$ = 0.37, p = 0.89).

Figure 3—figure supplement 3

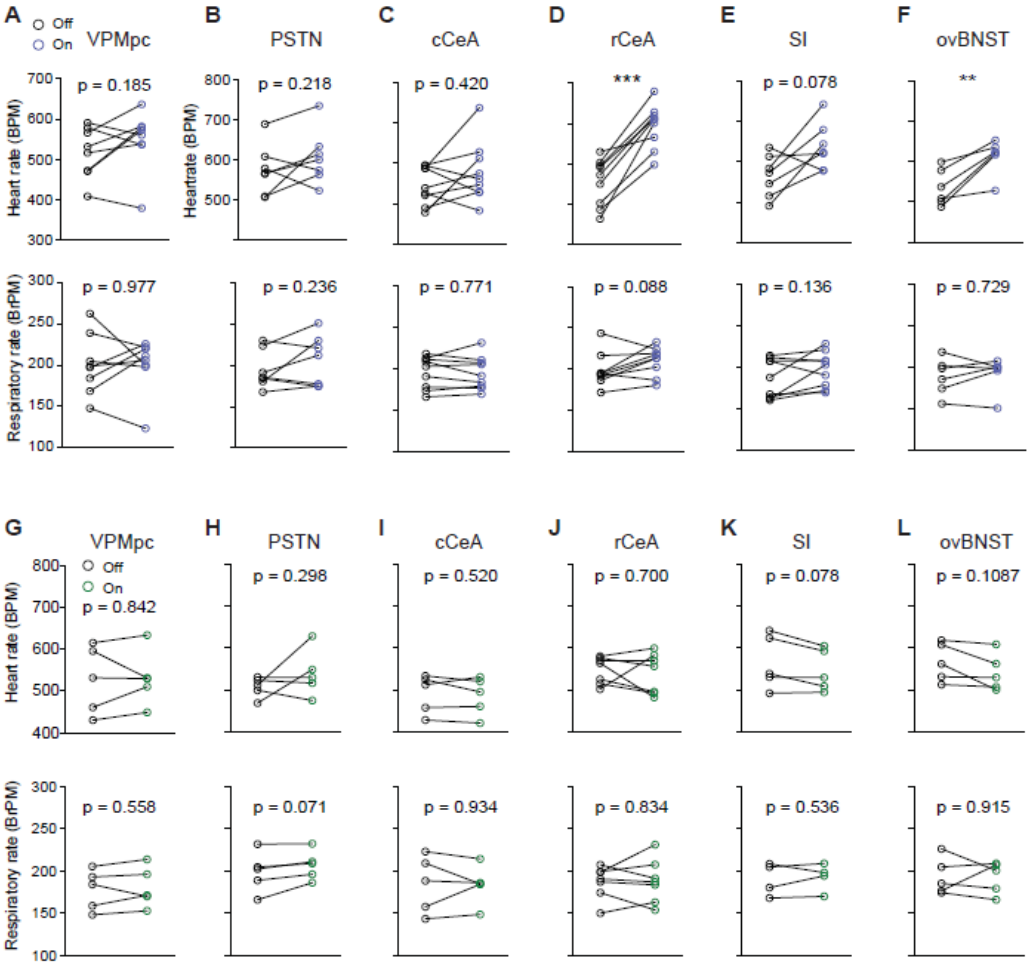

Figure 3—figure supplement 3. Physiological responses to photostimulation of CGRP^{PBN} neuron terminals (**A**) Autonomic responses to 15-Hz photostimulation of CGRP^{PBN} neuron terminals in the VPMpc (n=8, paired t-test, heart rate *t(7)* = 1.47, p = 0.19; respiration *t(7)* = 0.03, p > 0.05). (**B**) Autonomic responses to 15-Hz photostimulation of CGRP^{PBN} neuron terminals in the PSTN (n=7, paired t-test, heart rate *t(6)* = 1.37, p > 0.05; respiration *t(6)* = 1.32, p > 0.05). (**C**) Autonomic responses to 15-Hz photostimulation of CGRP^{PBN} neuron terminals in the cCeA (n=6, paired t-test, heart rate *t(5)* = 0.90, p > 0.05; respiration *t(5)* = 0.31, p > 0.05). (**D**) Autonomic responses to 15-Hz photostimulation of CGRP^{PBN} neuron terminals in the rCeA (n=9, paired t-test, heart rate *t(8)* = 7.65, p < 0.0001; respiration *t(8)* = 1.94, p > 0.05). (**E**) Autonomic responses to 15-Hz photostimulation of CGRP^{PBN} neuron terminals in the SI (n=7, paired t-test, heart rate *t(6)* = 2.48, p = 0.048; respiration *t(6)* = 1.66, p > 0.05). (**F**) Autonomic responses to 15-Hz photostimulation of CGRP^{PBN} neuron terminals in the ovBNST (n=6, paired t-test, heart rate *t(5)* = 4.35, p = 0.0074; respiration *t(5)* = 0.36, p > 0.05). (**G-L**) Autonomic responses to 15-Hz light delivery in control animals. Data represented as mean±SEM.

Figure 4—figure supplement 1

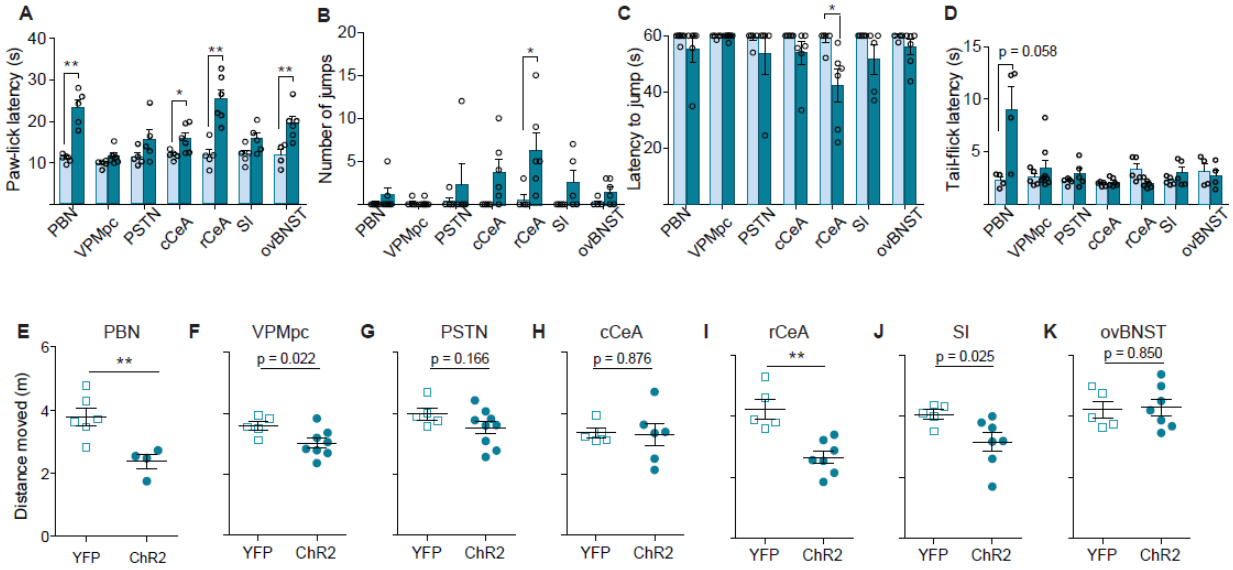

Figure 4—figure supplement 1. Activation of CGRP^{PBN} terminals in the rCeA potentiates nocifensive responses
(**A**) Response latency on 52°C hot plate increased by stimulating CGRP^{PBN} neurons or projections to the cCeA, rCeA, or ovBNST prior to exposure, consistent with stress-induced analgesia (significance for Welch's unpaired t-test; PBN n=6,5 (ChR2, YFP); *t(4.31)* = 6.22, **p = 0.0027; cCeA n=6,5; *t(6.21)* = 2.76, *p = 0.0315; rCeA n=6,5; *t(8.00)* = 5.00, **p = 0.0011; ovBNST n=6,4; *t=(7.91)* = 3.57, **p = 0.0074). (**B**) Number of jumps in 1-min exposure to 52°C hot plate increased by stimulating CGRP^{PBN} neuron terminals in the rCeA (Welch's unpaired t-test, *t(5.85)* = 2.69, *p = 0.0369; n=6,5). (**C**) Latency to jump was also reduced by rCeA-terminal activation (Welch's unpaired t-test, *t(5.73)* = 2.80, *p = 0.0329; n=6,5). (**D**) Tail-flick latency upon tail submersion in 52.5 °C water bath was not significantly affected by either somata or terminal photostimulation of CGRP^{PBN} neurons (Welch's unpaired t-test, p > 0.05). (**E-K**) Distance moved during RTPP assay pairing one side of a novel chamber with photostimulation of CGRP^{PBN}-neuron terminals or somata (significance for Welch's unpaired t-test). Data are represented as mean±SEM.

Figure 6—figure supplement 1

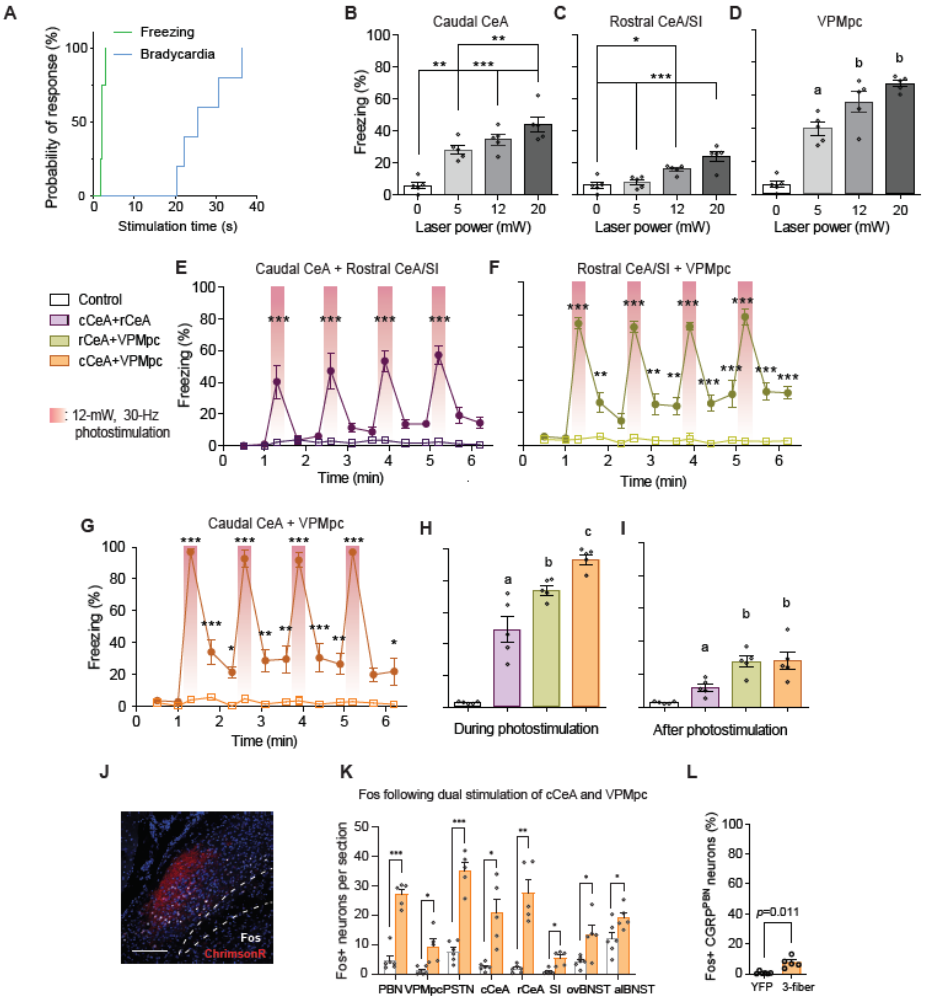

Figure 6—figure supplement 1. Coincident activation of CGRP^{PBN} neuron projections using ChrimsonR causes profound freezing responses
(**A**) Survival curve comparing latencies of freezing and bradycardia responses to simultaneous 30-Hz photostimulation of CGRP^{PBN} neuron terminals in the VPMpc and cCeA (n=4 freezing, n=5 heart rate, Mantel-Cox Log-rank test, Chi-square = 9.03, p = 0.0027). **(B-H)** Freezing responses to simultaneous optogenetic activation of multiple CGRP^{PBN}-neuron terminal fields using ChrimsonR. (**B-D**) Freezing behavior during 30-Hz photostimulation of increasing power of CGRP terminal fields in (B) the cCeA (n=5), (C) rCeA (n=5), or (D) the VPMpc (n=5). Significance for one-way ANOVA with subsequent Tukey correction for multiple comparisons. (**E**) Freezing behavior in response to simultaneous activation of CGRP terminals in the rostral and caudal CeA (n=5,4 (ChR2, control), significant effect of group in two-way repeated-measure ANOVA, $F_{1,7}$ = 41.27, p = 0.0004; subsequent Sidak pairwise comparisons, ****p < 0.0001). (**F**) Freezing behavior in response to simultaneous activation of CGRP^{PBN} terminals in the rostral CeA and VPMpc (n=5,4; significant effect of group in two-way RM ANOVA, $F_{1,7}$ = 173.5, p < 0.0001; subsequent Sidak pairwise comparisons, **p < 0.01; ***p < 0.001). (**G**) Freezing behavior in response to simultaneous activation of CGRP^{PBN} terminals in the caudal CeA and VPMpc (n=5,4, significant effect of group in two-way RM ANOVA, $F_{1,7}$ = 118.3, p < 0.0001; subsequent Sidak pairwise comparisons, *p < 0.05). (**H**) Comparison of averaged freezing behavior for each stimulation combination during the stimulation epoch (n=5,4, one-way ANOVA, $F_{3,16}$ = 72.18, p < 0.0001; subsequent Tukey correction for multiple comparisons, dissimilar letters above columns of data indicate statistical differences between groups). (**I**) Comparison of averaged freezing behavior for each stimulation combination during the post-stimulation epoch (n=5,4, one-way ANOVA, $F_{3,16}$ = 14.04, p < 0.0001; subsequent Tukey correction for multiple comparisons). (**J**) Representative image showing ChrimsonR:tdTomato expression in CGRP^{PBN} neurons (red) and Fos expression (white) following activation of terminals in the cCeA and VPMpc. Scale bar: 100 µm.(**K**) Quantification of number of Fos-positive neurons in the PBN and forebrain targets following simultaneous activation of CGRP^{PBN} neuron terminals in the cCeA and VPMpc (n=5), or light delivery in a YFP-expressing control (n=6). Significance for Welch's unpaired t-tests. (**L**) Quantification of the number of CGRP^{PBN} neurons expressing Fos following simultaneous activation of terminals in the cCeA and VPMpc (n=5), or light delivery in a YFP-expressing control (n=6) (Welch's unpaired t-test, $t(4.40)$ = 4.26, p = 0.0106).

Figure 7—figure supplement 1

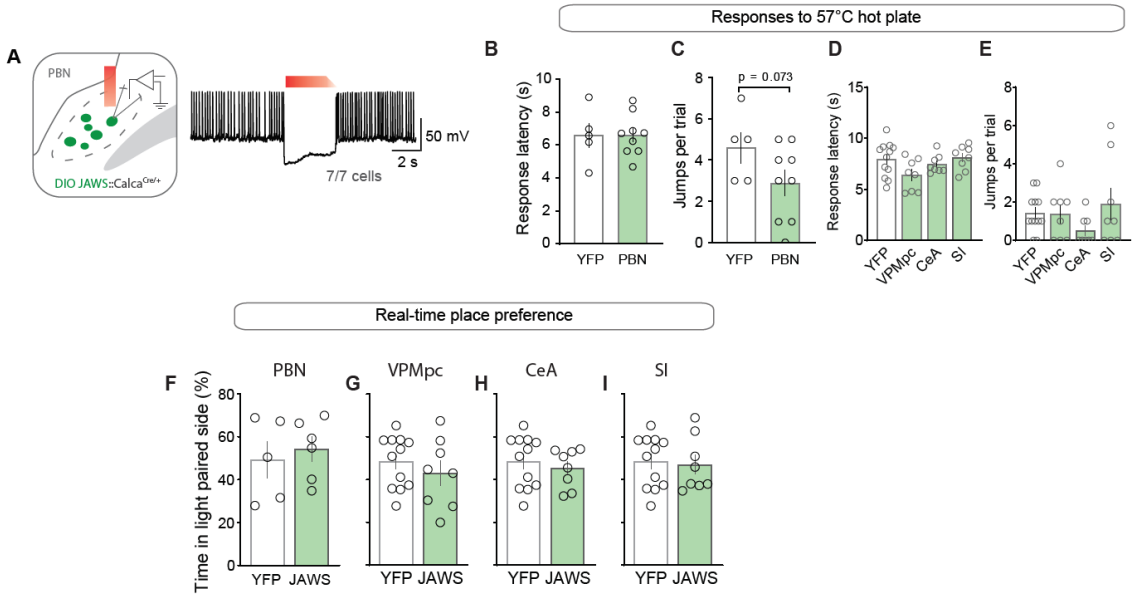

Figure 7—figure supplement 1. Photoinhibition of CGRP^{PBN} neurons or projections does not affect nocifensive responses or alter place preference (**A**) Representative recording of action potentials from a CGRP^{PBN} neuron. Red-light photostimulation (3 s on and 1 s ramp-down) effectively suppressed firing rate of CGRP^{PBN} neurons with minimal rebound excitation (7 cells from 2 mice). (**B**) Nociceptive response latency to 57°C hot plate with photoinhibition of CGRP^{PBN} neurons (2-s on, 1-s ramp, 1-s off for 30-s trial) (Welch's unpaired t-test, $t(7.28)$ = 0.07, p > 0.05; n=8,5). (**C**) Number of jumps on 57°C hot plate during 30-s trial with photoinhibition of CGRP^{PBN} neurons (Welch's unpaired t-test, $t(9.02)$ = 2.03, p = 0.0734; n=8,5). (**D**) Nociceptive response latency to 57°C hot plate with photoinhibition of CGRP^{PBN} terminals in the VPMpc, CeA, or SI (n=8 per group) relative to controls (n=12) (one-way ANOVA, $F_{3,32}$ = 2.46, p = 0.0808). (**E**) Number of jumps on 57°C hot plate during 30-s trial with photoinhibition of CGRP^{PBN} terminals in the VPMpc, CeA, or SI (n=8 per group) relative to controls (n=12) (one-way ANOVA, $F_{3,32}$ = 1.26, p = 0.3057). (**F-I**) Photoinhibition of CGRP^{PBN} neurons or individual projections in one side of chamber did not influence place preference (Welch's unpaired t test; PBN $t(7.22)$ = 0.48, p > 0.05, n=8,5; VPMpc $t(12.17)$ = 0.81, p > 0.05, n=8,12; CeA $t(17.72)$ = 0.62, p > 0.05, n=8,12; SI $t(14.64)$ = 0.24, p > 0.05, n=8,12. Data represented as mean±SEM.

II. Dissecting central amygdala control of salience and valence coding for aversive stimuli

Both classical and recent work points to the pontine parabrachial nucleus (PBN) as providing the crucial nociceptive input to the lateral and capsular CeA (CeLC) necessary for aversive memory formation (Bernard and Besson, 1988a; Bernard et al., 1992; Choi et al., 2020; Gauriau and Bernard, 2002; Han et al., 2015; Yu et al., 2017). Shaping this incoming information bias is the underlying structure of the ascending signal: input to the PBN from somatic and visceral pathways is biased by subregion (Gauriau and Bernard, 2002), with various PBN subnuclei in turn sending segregated input to specific partners in downstream CeA subnuclei (Bester et al., 1997; Tokita et al., 2010). Of special interest is the external lateral PBN (PBel), a source of calcitonin gene-related peptide (CGRP) input to CGRP-receptor (Calcrl) neurons in the CeLC demonstrated to be necessary for associative fear learning (Han et al., 2015). Surprisingly, while PBel CGRP+ neurons are broadly tuned to aversive stimuli of both somatic and visceral origin (e.g. illness, pain, itch) (Campos et al., 2018), the PBel is not the primary target of the nociceptive spino-parabrachial pathway (Chiang et al., 2020; Choi et al., 2020) but is instead the target of rich excitatory input from the ascending vagal viscerosensory pathway via the nucleus of the solitary tract (NTS) (Roman et al., 2016), with indirect spinal input likely added on through intra-PBN excitatory microstructure (Chiang et al., 2020). This arrangement suggests an intriguing possibility: that PBel->CeLC CGRP signaling may be providing valence and salience as an integrated measure of internal state, rather than somatic-specific nociceptive tone. Supporting this idea is the fact that signaling of the excitatory neuropeptide CGRP itself within the CeA, while entirely lacking the temporal dynamics of the stimulus, contributes both to affective-behavioral responses and associative learning to pain (van den Burg and Stoop, 2019; Han et al., 2005; Okutsu et al., 2017; Shinohara et al., 2017).

To begin to dissect the role of CeLC Calcrl+ neurons in differentially contributing to valence and salience signaling to aversive stimuli, we started with the possibility of functional segregation by spatial

location, as recent evidence suggests that the CeA can be parcellated along its rostrocaudal axis (Han et al., 2015; Kim et al., 2017; Sanford et al., 2017). Specifically, caudal CeA Calcrl+ neurons co-express PKCδ and are located in both the lateral and capsular subregions, while rostrally CeA Calcrl+ neurons are restricted to the CeC and do not co-express PKCδ (Han et al., 2015; Kim et al., 2017). Taking advantage of this arrangement, we traced the efferent connections of CeA Calcrl+ neurons across their rostrocaudal extent and determined that rostral CeA Calcrl+ neurons are integrated into extra-amygdalar hypothalamic and basal forebrain circuits, while caudal CeA Calcrl+ neurons primarily target extended amygdalar structures. This led to the joint hypotheses that rostral neurons would be more canonically nociceptive and biased towards salience signaling (Bernard et al., 1992; Dringenberg and Vanderwolf, 1997; Swerdlow et al., 1984; Unal et al., 2015), with caudal regions biased towards interoceptive signals and valence signaling (Ahrens et al., 2018; Botta et al., 2015; Cai et al., 2014).

Diverging connectivity and function of CeA Calcrl^{+} neurons based on spatial location

Since aversive stimulus salience and valence putatively relayed to the CeLC by PBel^{CGRP} neurons are separable stimulus features, we sought to determine whether the intrinsic organization of downstream CeA Calcrl^{+} neurons could support separable functions through divergent connectivity. Bolstering this possibility is recent evidence suggesting that the CeA may be functionally segregated along its rostrocaudal axis, as both cell marker expression (Han et al., 2015; Kim et al., 2017; Sanford et al., 2017), subnucleus organization (Kim et al., 2017), and upstream expression of BLA pronociceptive neurons (Kim et al., 2016) vary rostro-caudally. To answer this, we used small, targeted injections to express anterograde tracers (DIO-Syn-GFP and mCherry) unilaterally in rostral and caudal CeA Calcrl^{+} neurons, and then sectioned the entire brain to assess putative complementary efferent connectivity (Fig. 1a, Extended Data Fig 1a). In support of previous work identifying only sparse connections from the CeLC to either midbrain or hindbrain structures (Kim et al., 2017; Petrovich and Swanson, 1997), we saw synaptic labeling

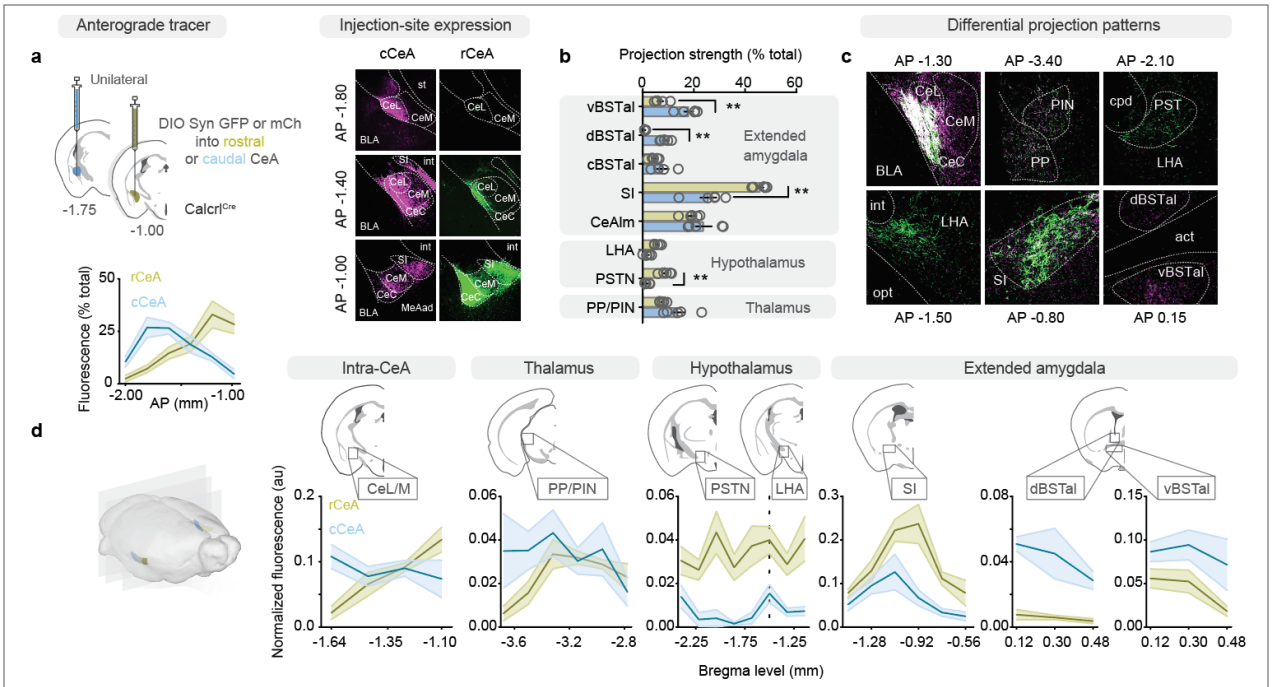

Fig. 1 | Calcrl^{CeA} neurons exhibit different projection patterns depending on their spatial location. a, Unilateral injections of different anterograde tracers (AAV1-DIO-Syn:GFP or mCherry) into the rostral and caudal CeA of Calcrl$^{Cre/+}$ mice resulted in complementary expression across the rostrocaudal axis. **b,** Expression of anterograde tracer in the rostral vs caudal CeA lead to varying levels of fluorescence in most downstream targets (two-way ANOVA with Sidak's post hoc with correction for multiple comparisons). **c,** Expression of fluorescent tracer in rostral (green) or caudal (magenta) Calcrl^{CeA} neurons in various efferent projections sites. **d,** Fluorescence in downstream targets relative to cumulative projection intensity. Data are represented as mean±SEM. Scale bar: 100 µm. **p < 0.01. See also Extended Data Fig. 1.

restricted to forebrain structures, including the anterolateral bed nucleus of the stria terminalis (BNSTal), dorsomedial and ventrolateral basal forebrain (substantia innominata, SI (Jolkkonen et al., 2002)), lateral hypothalamic area (LH and parasubthalamic nucleus (PSTN)), and posterior paralaminar thalamic structures (peripeduncular (PP) and posterior intralaminar (PIN) nuclei (Linke et al., 2000)) (Fig. 1b-c). Notably, there were marked differences in tracer expression depending on tracer cell location, with rostral injections only leading to strong synaptic labeling in the SI, LH, and PSTN, while caudal injections led to greater labeling within the CeM and BNSTal (Fig. 1b-d). Both injections led to comparable expression in the PP and PIN (Fig. 1d). Comparing tracer cell location across both CeA subnuclei and the rostrocaudal axis, we found that caudal injections, as intended, led to greater expression in caudal regions of the CeA, but also biased expression towards the CeL, while rostral injections were biased towards the CeC

(Extended Data Fig 1a-b). Correlating the strength of synaptic labeling in each of the downstream targets with 1) number of cells transfected in the CeL, 2) the CeC, 3) the entire CeA proper, or 4) the rostrocaudal bias of the injection to assess the relative contribution of each factor to efferent connectivity patterns revealed that synaptic labeling in the SI, LH and PSTN was best-predicted by injections with strong rostral expression bias, while labeling in the dorsal and ventral BSTal was best predicted by the number of cells transfected in the CeL, with a weaker association to caudal expression bias (Extended Data Fig 1b-d).

Of note, we observed that rostral CeA Calcrl^{+} neurons tended to project to the downstream targets of PBel CGRP^{+} neurons recently found to best initiate passive fear responses (Bowen et al., 2020). As the CeA is a GABAergic structure and PBel CGRP^{+} neurons promote freezing behavior by activating their downstream targets, this led to the prediction that rostral CeA Calcrl^{+} neurons may act to promote active defensive strategies, while the canonical disinhibitory connections between caudal CeA Calcrl^{+} neurons and extended amygdala structures are better suited for promoting passive strategies such as freezing behavior. To determine whether this is indeed the case, we selectively expressed channelrhodopsin-2 in rostral or caudal CeA Calcrl^{+} neurons and placed fiberoptic cannulae over the rostral or caudal CeA to bias activation to one or the other location (Fig. 2a). Mice were then placed in a novel context and intermittently photostimulated while locomotion and light-evoked behavioral responses, including grooming, backing, rearing, and freezing were measured (Fig. 2b-c). We observed that the responses generated by the two populations were in opposition: stimulation of rostral CeA Calcrl^{+} neurons elicited an immediate backing phenotype (Fig. 2b-d), followed by bursts of rapid forward locomotion and ending with dramatic post-stimulation freezing behavior (Fig. 2b-h), together reminiscent of responses to salient aversive external stimuli such as foot shock (Fanselow, 1982). In contrast, caudal CeA Calcrl^{+} neurons led to intermittent bouts of locomotion and freezing behavior during photostimulation, with mild freezing behavior lasting into the post-stimulation time window (Fig. 2b-h). We also assessed the effect of stimulation on autonomic measures, as the CeA through its connectivity is positioned to orchestrate both

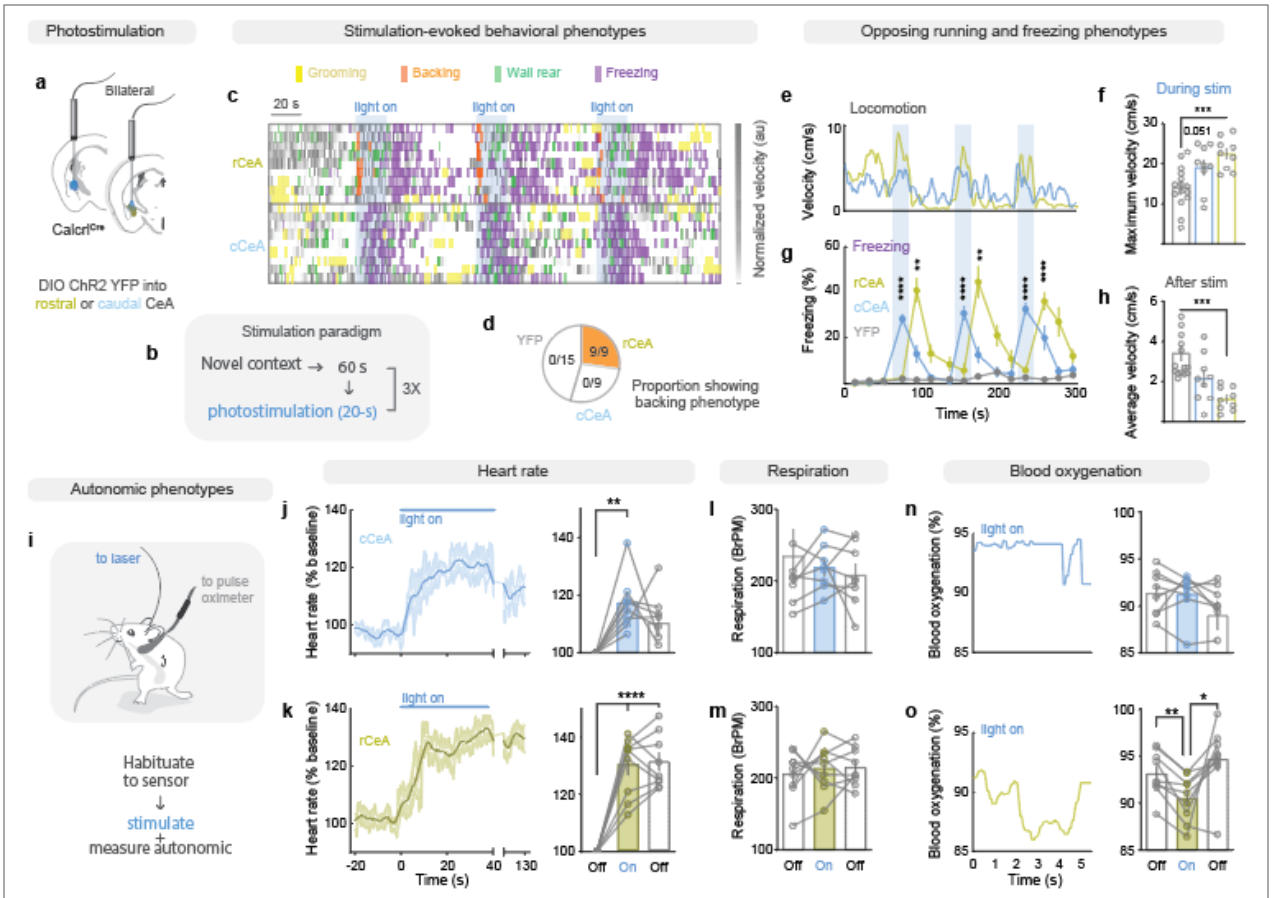

Fig.2 | Photostimulation of rostral CeA Calcrl⁺ neurons generates a panic-like phenotype while photostimulation of caudal Calcrl⁺ neurons promotes mild freezing behavior. a, Bilateral injections of DIO-ChR2 YFP and fiber placement into the rostral or caudal CeA of Calcrl$^{Cre/+}$ mice allowing photostimulation of Calcrl^{CeA} neurons in either location. **b,** Experimental paradigm for intermittent photostimulation in a novel context. **c**, Raster plots of behavior during intermittent stimulation of either rostral or caudal CeA Calcrl⁺ neurons. **d**, Pie chart summarizing frequency of backing-up phenotype observed during photostimulation of rostral CeA Calcrl⁺ neurons. **e**, 10X smoothed, moving-window-averaged velocity across experimental time windows. **f**, Photostimulation of rostral CeA Calcrl⁺ neurons elicited robust increases in locomotion (one-way ANOVA with subsequent Dunnett's multiple comparisons test). **g,** Photostimulation of caudal CeA Calcrl+ neurons elicited freezing behavior, while stimulation of rostral Calcrl^{CeA} neurons promoted freezing behavior during the post-stimulation epoch (two-way RM-ANOVA with subsequent Tukey's multiple comparisons test). **h,** Photostimulation of rostral CeA Calcrl⁺ neurons suppressed locomotion during the post-stimulation epoch (one-way ANOVA with subsequent Dunnett's multiple comparisons test). **i,** Experimental paradigm for photostimulating while recording changes in autonomic activity. **j-k**, Photostimulation of caudal and rostral CeA Calcrl⁺ neurons caused tachycardia (one-way ANOVA with subsequent Dunnett's multiple comparisons test). **l-m,** Photostimulation either group did not affect respiration. **n-o,** Photostimulation of rostral CeA Calcrl⁺ neurons caused transient hypoxia (one-way ANOVA with subsequent Dunnett's multiple comparisons test). Data represented as mean±SEM. See also Extended data Fig. 2.

behavioral and autonomic responses to threat (LeDoux et al., 1988; Tovote et al., 2016) and has been implicated in autonomic-affective disorders such as panic (Leibold et al., 2016; Ziemann et al., 2009). We measured heart rate, respiration, and blood oxygenation with a pulse oximeter while photostimulating

either population (Fig. 2i). We observed that stimulation of caudal CeA Calcrl$^+$ neurons led only to mild tachycardia (to 117.3±2.7% baseline (mean±sem)), while stimulation of rostral CeA Calcrl$^+$ neurons led to robust tachycardia (to 130.0±2.7% baseline (mean±sem)) and caused transient hypoxia (Fig. 2j-o), perhaps due to the dramatic increase in heart rate without a corresponding increase in respiration (Fig. 2m). Together these data reveal that the extrinsic organization and function of putative nociceptive neurons of the CeA varies depending on spatial location, suggesting a mechanism by which behavior and affect can be controlled by a single state or stimulus in a complementary manner.

Orchestration of nocifensive responses by rostral CeA Calcrl$^+$ neurons

While differences in intrinsic functional capabilities became apparent from our stimulation studies, we reasoned that visualization of calcium dynamics (correlates of neural activity) from individual neurons in vivo (Ghosh et al., 2011) would allow us to investigate whether there are differences in response profiles of CeA Calcrl$^+$ neurons depending on spatial location suggestive of an incoming information bias. We expressed a calcium-sensitive fluorophore (GCaMP6m) specifically in CeA Calcrl$^+$ neurons, allowing us to record calcium dynamics from individual Calcrl$^+$ neurons in either the rostral or caudal CeA depending on the placement of the graded-index lens (Fig. 3a, Extended Data Fig 3a), then extracted and processed background-subtracted, motion-corrected signals from raw video using the miniscope 1-photon imaging signal-extraction pipeline (MIN1PIPE) (Lu et al., 2018). To determine whether CeA Calcrl$^+$ neurons are activated by noxious thermal stimuli, we subjected mice to a hot plate test and found that most neurons responded (Fig. 3b-c), and overall, both activated populations had elevated activity for the duration of the test (117/167 in the rostral CeA, 102/164 in the caudal CeA, Fig. 3b-d, Extended Data Fig 3b). In contrast to PBel CGRP$^+$ neurons that are robustly activated by painful stimuli under anesthesia, we observed that anesthesia potently suppressed responses to noxious stimuli delivered across the body in CeA Calcrl$^+$

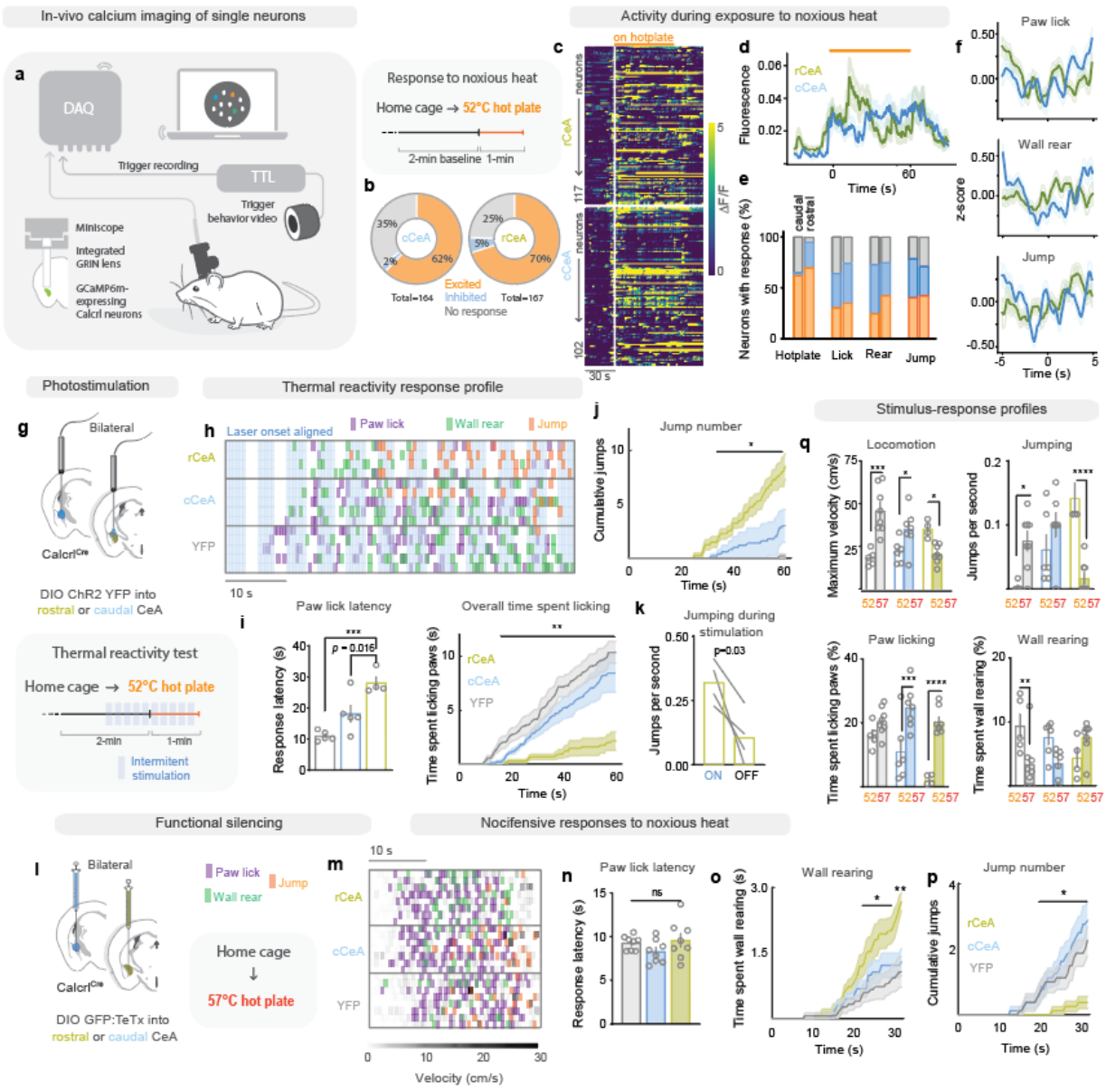

Fig.3 |Both rostral and caudal CeA Calcrl+ neurons are activated by noxious heat but only the rostral population is necessary for nocifensive behaviors. **a,** Schema outlining method for measuring single-cell calcium activity in freely behaving animals and experimental paradigm for measuring time-locked responses to noxious heat. **b,** Heatmaps of ΔF/F in responsive Calcrl-expressing neurons in the rostral and caudal CeA during exposure to 52 °C hot plate (n=117/167 neurons from 5 mice for the rostral CeA and n=102/164 neurons from 4 mice for the caudal). **c,** Pie chart summarizing proportion of rostral or caudal CeA Calcrl+ neurons responding to noxious heat. **d,** Average fluorescence of heat-activated rostral and caudal CeA Calcrl+ neurons across stimulus exposure. **e,** Proportion of rostral or caudal CeA Calcrl+ neurons with significant activity modulation during different stimulus or behavioral events. **f,** Population-activity averages during behaviors exhibited in response to noxious heat. **g,** Experimental paradigm for photostimulation of either rostral or caudal Calcrl^{CeA} neurons during exposure to noxious heat. **h,** Raster plot of behaviors aligned to intermittent light delivery during exposure to 52 °C hot plate. **i,** Photostimulation of rostral CeA Calcrl+ neurons delayed initial nociceptive response (one-way ANOVA with subsequent Dunnett's multiple comparisons test) and resulted in decreased time spent licking paws throughout the test (two-way RM-ANOVA with subsequent Tukey's multiple comparisons test). **j,** Photostimulation of rostral CeA Calcrl+ neurons caused robust potentiation of jumping responses (two-way RM-ANOVA with subsequent Tukey's multiple comparisons test). **k,** Jumping elicited by stimulation of rostral CeA Calcrl+ neurons occurred with greater frequency during stimulation epochs (paired t-test). **l,** Experimental paradigm for functional silencing of rostral or caudal CeA Calcrl+ neurons to measure contribution of Calcrl+ neurons to nocifensive behaviors. **m,** Raster plot of behaviors exhibited on hot plate in experimental and control animals. **n,** No change in response latency by mice with functionally silenced CeA Calcrl+ neurons, **o,** Silencing rostral CeA Calcrl+ neurons increased frequency of wall rearing and **p,** reduced jumping behavior in response to 57 °C hotplate (two-way RM-ANOVA with subsequent Tukey's multiple comparisons test). **q,** Stimulus response profiles in different experimental groups (one-way ANOVA with subsequent Dunnett's multiple comparisons test). Data represented as mean±SEM. *p < 0.05; **p < 0.01; ***p < 0.001; ****p < 0.0001. See also Extended data Fig. 3 and 4.

neurons (Extended Data Fig 3c-d). We categorized activity dynamics for the two populations during nocifensive behaviors observed during the test (Fig. 3e), and observed no clear patterns, although both populations tended to be inhibited by paw licking (which functions to reduce paw temperature), while rostral neurons had slightly elevated activity during wall rearing (Fig. 3e-f).

As the activity of downstream networks is additionally shaped by the ongoing sensory context, we altered the activity of CeA Calcrl^{+} neurons during an ongoing aversive event to test how the signals relayed by CeA Calcrl^{+} neurons are integrated with state (Fig. 3g). Intermittent stimulation of rostral CeA Calcrl^{+} neurons during a hot-plate test slowed the initial response to heat and suppressed paw licking throughout the trial, while robustly potentiating jumping (Fig. 3h-j). Aligning each subject's trial to intermittent light delivery, we observed that most of the jumping occurred while stimulation was ongoing (Fig. 3k). In contrast, pre-stimulation, or stimulation of caudal CeA Calcrl^{+} neurons had no effect on these measures (Fig. 3h-j, Extended Data Fig. 3a-d). Since these effects could be due to simple addition of locomotor phenotypes without necessarily reflecting a causal role in nociceptive processing, we selectively silenced rostral or caudal CeA Calcrl^{+} neurons through targeted expression of the light chain of tetanus toxin (TeTx) to assess their contribution to nocifensive behaviors (Fig. 3l, Extended Data Fig. 3e-g). With this manipulation targeted to the rostral CeA, we saw increased time spent rearing on the wall and a dramatic attenuation in jumping elicited by 57 °C hot-plate exposure (Fig. 3m-p). Silencing caudal CeA Calcrl^{+} neurons had no effect on these measures, and neither manipulation affected response latency (Fig. 3m-p). Correlating the number and location of cells transduced with TeTx to jumping attenuation, we found it was predicted best by the number of cells transduced in the CeC (Extended Data Fig. 3i-j). Comparing stimulus-response profiles from control mice to those with altered CeA Calcrl^{+} neuron activity, we found that the behavioral outcome of hot-plate tests of increasing temperatures was inverted relative

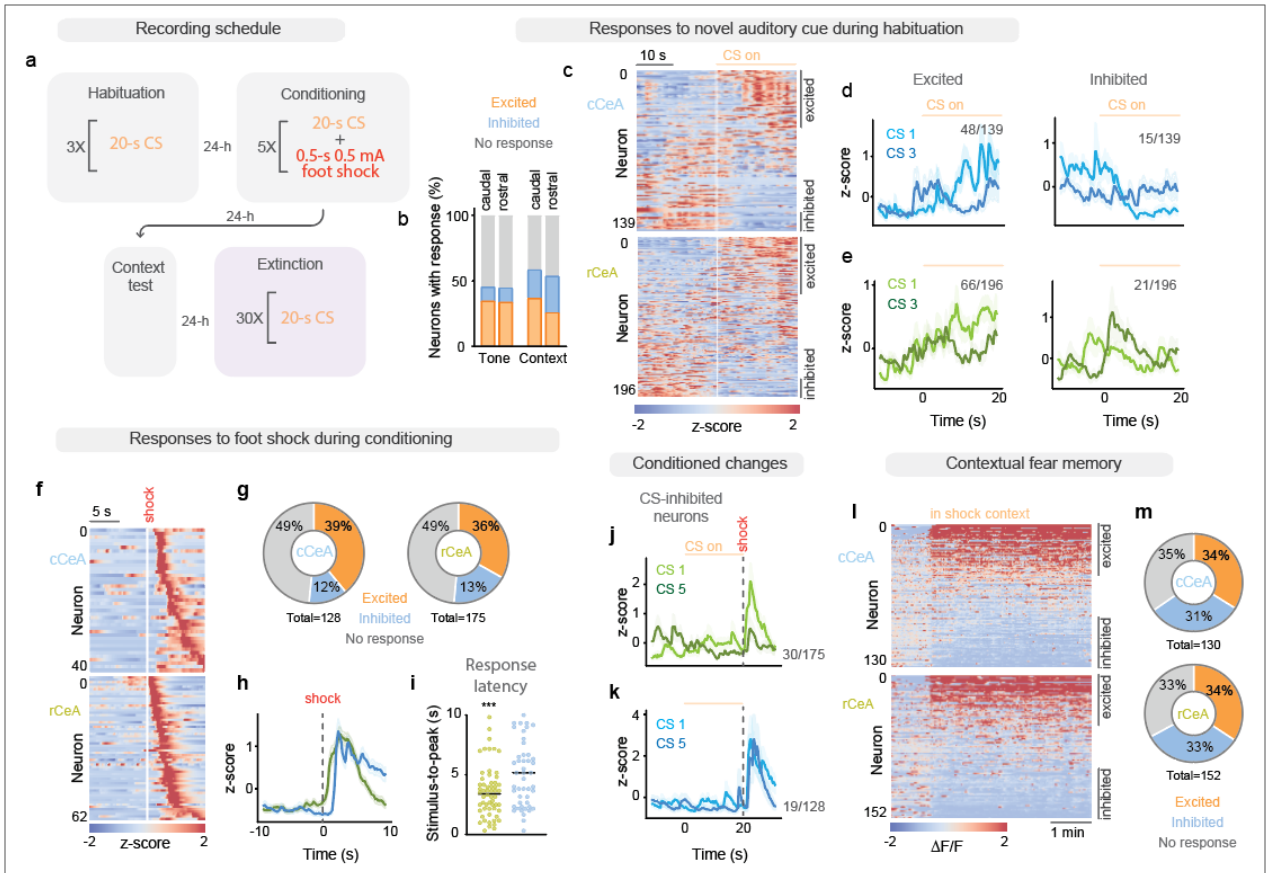

Fig. 4 | Rostral and caudal CeA Calcrl⁺ neurons exhibit different activity dynamics in response to foot shock and conditioned fear. **a,** Schema illustrating recording schedule during different phases of an auditory and contextual fear learning paradigm. **b-c,** Both rostral and caudal CeA Calcrl⁺ neurons are activated upon exposure to a novel context and auditory cue (proportions from n=139 neurons from 3 mice for the caudal CeA and n=196 neurons from 5 mice for the rostral). **d-e,** Activity of caudal CeA Calcrl⁺ neurons that responded to the first CS delivery is attenuated by the third delivery. **f,** Heatmaps of shock-responsive neuron z-scores during the peri-shock period of the first shock sorted in ascending order by stimulus-to-peak latency (n=40/128 neurons from 3 mice for the caudal CeA and n=62/175 neurons from 5 mice for the rostral). **g,** Proportion of neurons from each area responding to the first shock delivered during conditioning. **h,** Activity traces of shock-activated neurons from the rostral or caudal CeA. **i,** Rostral CeA Calcrl⁺ neurons foot-shock response peaks faster than caudal CeA Calcrl⁺ neurons (bar at mean, Student's unpaired t test). **j-k,** Data from neurons inhibited during the final CS (n=19/128 neurons from 3 mice for the caudal CeA and n=30/175 from 5 mice for the rostral). **j,** Calcrl neurons in the rostral CeA that become inhibited by the CS throughout conditioning exhibit an attenuated response to shock in the final conditioning trial, while **k,** caudal neurons do not. **l-m,** Both rostral and caudal CeA Calcrl⁺ neurons respond similarly upon re-exposure to the conditioning context (proportions for n=130 cells from 3 mice for the caudal CeA and n=152 cells from 5 mice for the rostral). Line graphs represented as mean±SEM. ***p < 0.001. See also Extended data Fig. 3.

to control mice for locomotion, jumping, and wall rearing if the activity of rostral CeA Calcrl⁺ neurons was reversed (Fig. 3q), suggesting an integral role in scaling nocifensive responses to stimulus intensity.

Contribution of both populations of Calcrl⁺ neurons to associative fear learning

We postulated that although rostral and caudal CeA Calcrl⁺ neurons responded similarly during exposure to noxious heat, their response dynamics during auditory fear conditioning, which involves rapid

construction of prediction signals from a brief but salient aversive stimulus and neutral CS that acquires valence, might reveal differences (Fig. 4a).

Both rostral and caudal CeA Calcrl^{+} neurons responded to the novel auditory cue (CS) and context during the habituation session prior to conditioning (Fig. 4b-c). This response dissipated in caudal CeA Calcrl^{+} neurons following multiple CS exposures as the mice became acclimated (Fig. 4d). During the conditioning session, we recorded calcium activity during each of the 5 CS-US pairing trials. To identify foot shock-responsive neurons we extracted data around the first foot shock, then categorized neurons as shock responsive if they responded for >2.5 s in the 10-s window (>3 SD from baseline) following shock delivery. Under this criteria, similar proportions of rostral and caudal CeA Calcrl^{+} neurons were US responsive (66/128 in caudal CeA, 50 excited; 83/175 in rostral CeA, 62 excited) (Fig. 4f-g). However, while the peak responses were similar for both populations, the stimulus-to-peak latency was shorter in shock-responsive rostral CeA Calcrl^{+} neurons (Fig. 4h-i), while caudal CeA Calcrl^{+} neurons showed prolonged elevated activity following delivery of the first shock (Fig. 4h). Assessing the effect of conditioning on the dynamics of CeA Calcrl^{+} neurons, we observed that the proportion of rostral CeA Calcrl^{+} neurons inhibited (defined as >3 SD below baseline for >5 s of the 20-s CS) by the CS increased by ~50% by the fifth CS (from 23 to 30), while caudal CeA Calcrl^{+} neurons remained consistent. Conversely, the number of neurons excited by the CS decreased steadily across conditioning for both populations (from 39 to 22 in the caudal; from 60 to 42 in the rostral). Examining the change in activity of neurons inhibited by the final CS across conditioning for both populations, we observed that Calcrl+ neurons inhibited during the final CS in the rostral CeA were not inhibited during the first CS but exhibited dramatic shock excitation that became suppressed by conditioning (Fig. 4j). Conversely, Calcrl+ neurons from the caudal CeA that responded similarly during the final CS showed no attenuation of shock responses across learning (Fig. 4k). These findings suggest that rostral CeA Calcrl^{+} neurons are recipients of a predictive inhibitory signal that acts to suppress the salience of an expected aversive event (Ozawa et al., 2017). Both rostral and caudal CeA

Calcrl$^+$ neurons responded when mice were returned to the conditioning context 24 h later, with equal proportion excited and inhibited (Fig. 4l-m).

To test whether the different response dynamics observed during conditioning translated into different functional roles in affective learning, we selectively silenced rostral or caudal CeA Calcrl$^+$ neurons prior to conditioning (Fig. 5a). While silencing rostral CeA Calcrl$^+$ neurons led to a reduction in shock reactivity (Fig. 5b), silencing either population profoundly attenuated conditioned freezing response to the CS during conditioning, although this effect was attenuated in the recall test 24 h later (Fig. 5c-d). Interestingly, silencing caudal CeA Calcrl$^+$ neurons prior to conditioning abolished contextual fear memory, while silencing rostral CeA Calcrl$^+$ neurons had a similar, less dramatic effect (Fig. 5g), suggesting that caudal Calcrl$^+$ neurons, which exhibit a slower, more prolonged response to foot shock may be better able to support contextual fear memory formation. Consistent with the entire population contributing to associative fear learning, fear memory strength was best-predicted by the overall number of cells transduced with TeTx in the CeA rather than expression within a particular region (Extended Data Fig. 4a-b), and activation of neither population alone was able to substitute for a foot shock in a fear conditioning paradigm (Extended Data Fig. 4c-d). We were also interested to examine the role of each population in mediating changes in affect driven by noxious stimulation, so we looked at anxiety behavior on an elevated plus maze before and after exposing TeTx-silenced mice to a foot shock. This revealed that while by itself activation of neither population was anxiogenic (Extended Data Fig. 4e), silencing caudal CeA Calcrl$^+$ neurons led to a basal reduction in anxiety state while silencing rostral CeA Calcrl$^+$ neurons attenuated foot shock-induced anxiogenesis (Extended Data Fig. 4f-h).

Since the majority of CeA Calcrl$^+$ neurons activated during fear conditioning showed robust US responses and the activity of foot shock responsive neurons within the CeL contributes to later plasticity in the LA that underlies association formation (Yu et al., 2017), we limited inhibition of CeA Calcrl$^+$ neurons to the period immediately around the foot shock (beginning 0.5-s before and ending 5-s after) using the

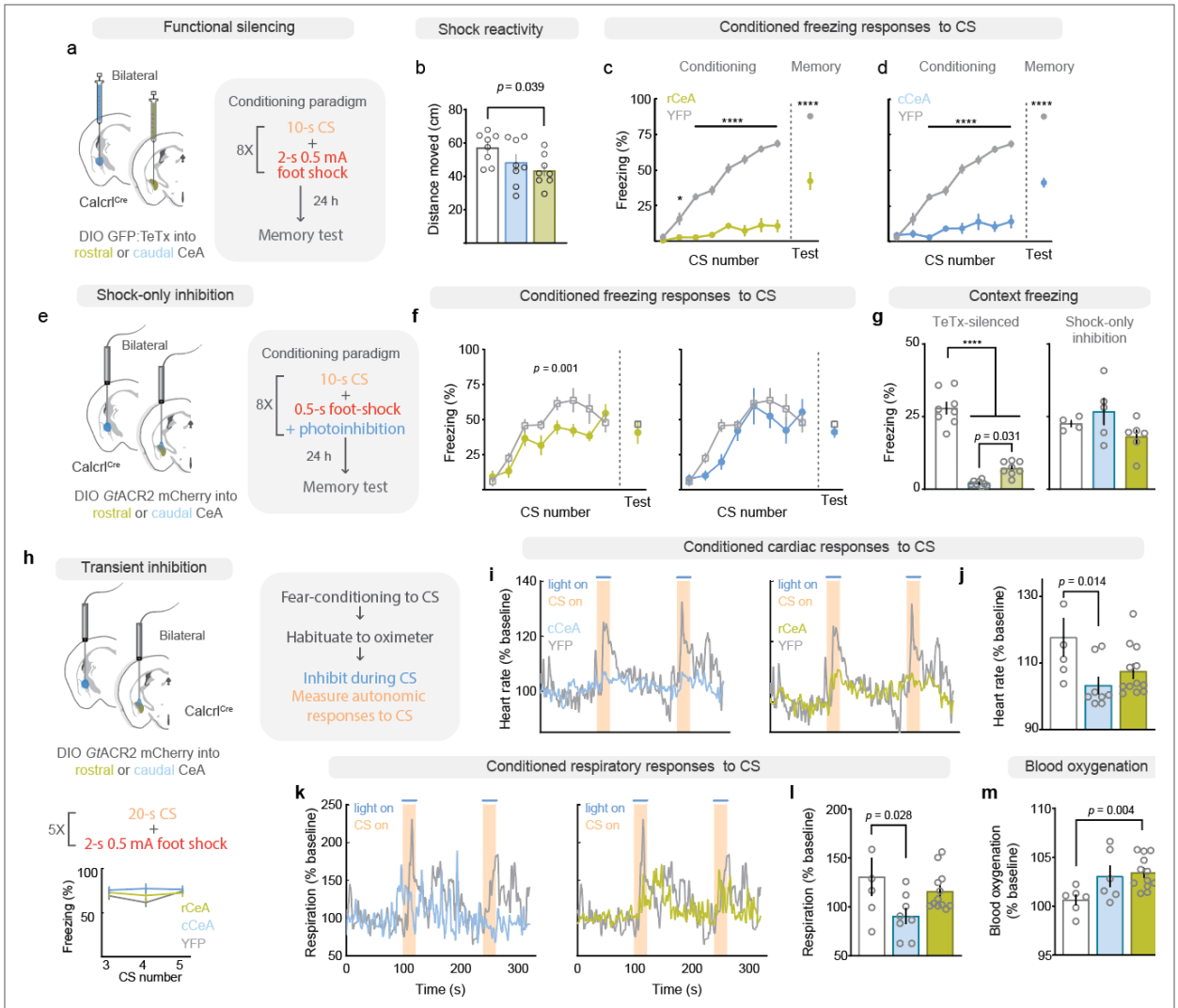

Fig. 5 | Silencing either rostral or caudal CeA Calcrl+ neurons attenuates conditioned fear behaviors, but only the caudal population contributes to conditioned autonomic responses. a, Experimental paradigm for silencing caudal or rostral CeA Calcrl$^+$ neurons and generating conditioned-fear responses. **b,** Silencing rostral CeA Calcrl$^+$ neurons attenuated locomotor responses to foot shock during conditioning (one-way ANOVA with subsequent Dunnett's multiple comparisons test). **c-d,** Freezing behavior to auditory CS co-terminating with a foot shock was attenuated by silencing either rostral or caudal CeA Calcrl$^+$ neurons (two-way RM-ANOVA with subsequent Sidak's multiple comparisons test). **e,** Schematic outlining paradigm for transient inhibition of CeA Calcrl$^+$ neurons using a blue-light activated chloride channel during foot-shock delivery in auditory fear conditioning. **f,** Freezing behavior to auditory CS during conditioning attenuated for rostral CeA Calcrl$^+$ neuron-inhibited group, but fear-memory recall 24 h following conditioning was intact (two-way RM-ANOVA with subsequent Sidak's multiple comparisons test). **g,** Freezing in the conditioning context by mice with silenced or shock-only inhibited CeA Calcrl$^+$ neurons (one-way ANOVA). **h,** Schematic of paradigm for transiently inhibiting CeA Calcrl$^+$ neurons in fear-conditioned mice while measuring conditioned autonomic responses to CS delivery. Line graph is freezing behavior of experimental and control mice during final CS of conditioning. **i,** 10X smoothed, mean heart rate in animals with or without Calcrl-neuron inhibition in the rostral or caudal CeA. **j,** Inhibiting caudal CeA Calcrl$^+$ neurons attenuates conditioned tachycardia in response to CS (one-way ANOVA with subsequent Dunnett's multiple comparisons test). **k,** 10X smoothed mean respiratory rate in animals with or without Calcrl-neuron inhibition in rostral or caudal CeA during CS delivery. **l,** Inhibiting caudal CeA Calcrl$^+$ neurons attenuated the increase in respiratory rate elicited by CS delivery (one-way ANOVA with subsequent Dunnett's multiple comparisons test). **m,** Inhibiting rostral CeA Calcrl$^+$ neurons during CS delivery lead to a paradoxical increase in blood oxygenation (one-way ANOVA with subsequent Dunnett's multiple comparisons test). Data represented as mean±SEM. *p < 0.05; ****p < 0.0001. See also Extended data Fig. 5.

blue light activated anion channelrhodopsin *Gt*ACR2 (Govorunova et al., 2015) (Fig. 5e). While transiently inhibiting rostral CeA Calcrl$^+$ neurons during the foot shock led to a slight attenuation of freezing behavior during conditioning, this effect was not maintained in the recall test 24-h later (Fig. 5f), and there was no attenuation in freezing behavior in the conditioning context (Fig. 5g). To examine whether CeA Calcrl$^+$ neurons contribute to conditioned autonomic responses in which a formerly neutral cue attains both emotional valence and elicits robust physiological responses to address impending threat, we conditioned mice to asymptotic freezing levels to a CS with a foot-shock US (Fig. 5h), then recorded autonomic activity while delivering a CS and simultaneously inhibiting CeA Calcrl$^+$ neurons. This experiment revealed that both tachycardia and hyperventilation evoked by CS delivery were attenuated by inhibiting caudal CeA Calcrl$^+$ neurons (Fig. 5i-l), while inhibiting rostral CeA Calcrl$^+$ neurons led to a paradoxical increase in blood oxygenation (Fig. 5m).

Differential weighting of motivation and valence by rostral and caudal Calcrl neurons

While real-time perception of a stimulus involves the integrated quality of its salience and valence to motivate appropriate action, remembered value is a clearer measure of pure valence (e.g., visceral signals such as hunger and satiety lack salience and require long exposure with external cues to deliver valence). To disentangle how CeA Calcrl$^+$ neurons might influence the salience and valence to external cues, we used a real-time, place-avoidance paradigm, where a subject can avoid or prolong neural stimulation depending on their location within a two-sided chamber (Fig. 6a). Mice rapidly learned to avoid the side of the chamber paired with CeA Calcrl$^+$ neuron photostimulation, spending only ~15% of their time on the stimulation side throughout a 15-min trial (Fig. 6b). When tested 24 h later, we noticed that mice trained with stimulation of caudal CeA Calcrl$^+$ neurons retained their aversion, while those trained with stimulation of rostral CeA Calcrl$^+$ neurons had reduced aversion (Fig. 6c-d), suggesting that while potently aversive in real-time, the remembered valence is only efficiently consolidated with caudal Calcrl$^+$ neuron

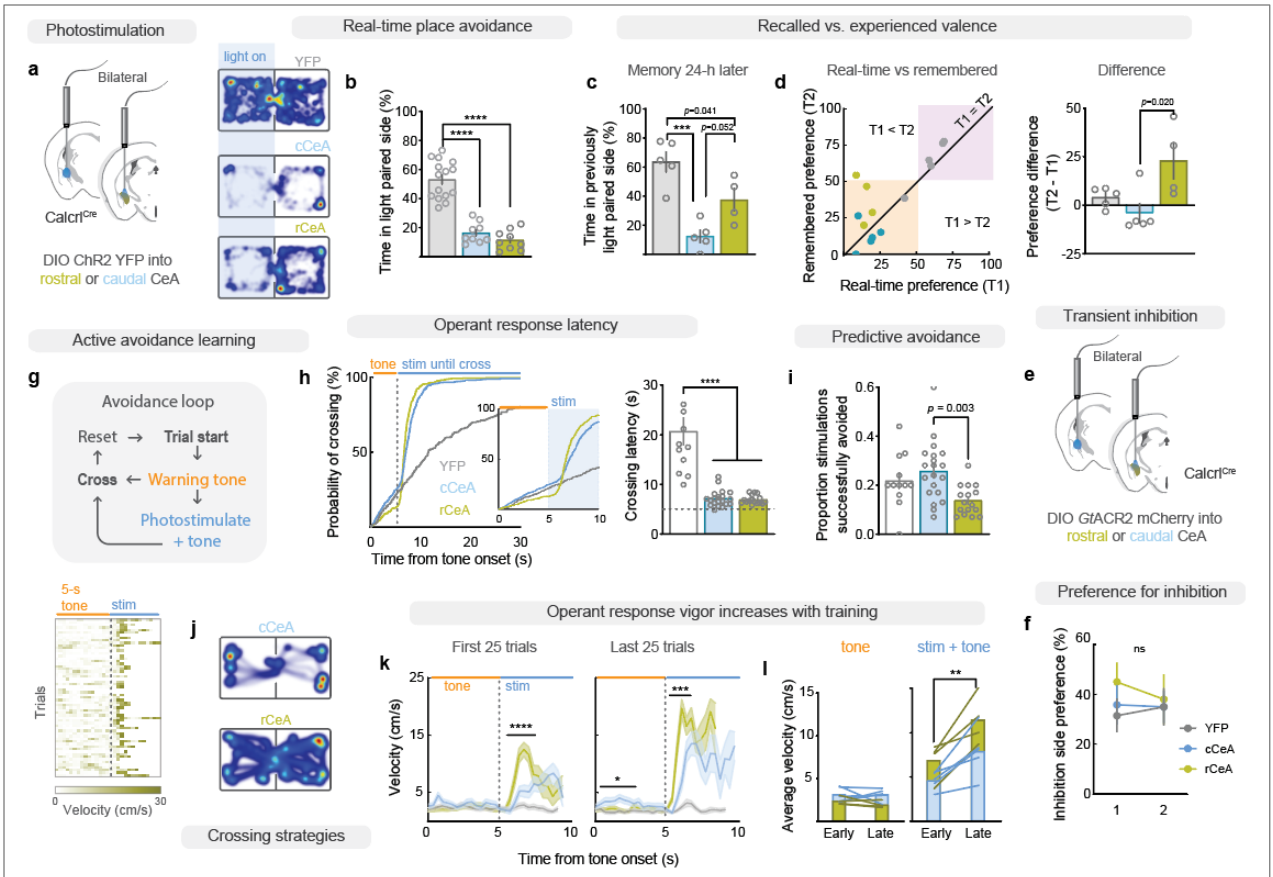

Fig. 6 | Rostral and caudal CeA Calcrl+ neurons differentially weight motivation and valence to drive avoidance learning.
a, Experimental paradigm for photostimulating either rostral or caudal CeA Calcrl^{+} neurons in one side of a novel chamber to measure changes in real-time place preference. **b,** Activation of either population causes robust avoidance of the light-paired side (significance for one-way ANOVA with subsequent Dunnett's multiple comparisons test). **c-d,** When re-exposed to the chamber 24-h later without stimulation, caudal-stimulated mice continue to have a strong aversion to the previously light-paired side while rostral-stimulated mice have a weakened recollection (orange quadrant indicates side-avoidance, purple side-preference) (significance for one-way ANOVA with subsequent Dunnett's multiple comparisons test). **e-f,** Experimental paradigm for testing effect of Calcrl-neuron inhibition on real-time, place preference and lack of effect compared to YFP controls. **g,** Illustration of active avoidance paradigm, where photostimulation is preceded by an auditory cue and crossing to the other side of the chamber resets the trial, with a 30-s inter-trial interval. Raster plot (bottom) of velocity across trials for rostral CeA Calcrl^{+} stimulated mouse during warning tone and stimulation prior to crossing. **h,** Photostimulation of either population promoted a rapid operant response with low crossing latency (dashed line indicates stimulation onset) (significance for one-way ANOVA with subsequent Dunnett's multiple comparisons test). **i,** Caudal-stimulated mice were more likely to cross during the predictive cue than rostral-stimulated mice (significance for one-way ANOVA with subsequent Dunnett's multiple comparisons test). **j,** Representative heatmaps of animal locations during the 10-s window preceding warning-tone delivery. **k,** Locomotion in early and late training trials during the tone and stimulation delivery. **l,** Average velocity increased during stimulation for both stimulation groups (significance for two-way RM-ANOVA with subsequent Tukey's multiple comparisons test). Data represented as mean±SEM. **p < 0.01; ***p < 0.001; ****p < 0.0001.

stimulation. Interestingly, transient inhibition of Calcrl neurons had no effect on place preference, suggesting the basal activity of the neurons does not support inhibition-based learning (Fig. 6e-f).

We wondered how this might translate to an active active-avoidance paradigm, where instead of passively avoiding stimulation through choosing one side of a chamber the subject must make an operant

response (crossing sides) to terminate noxious stimulation or avoid it entirely by using a predictive cue to cross to safety during a warning period (Fig. 6g). We found that both groups of mice responded by crossing sides with greater rapidity than YFP controls (Fig. 6h). However, across three days of training, neither group learned to take advantage of the cue to avoid stimulation entirely compared to the control mice (Fig. 6i). We also noticed that, despite rostral CeA Calcrl^{+} neuron stimulation leading to more vigorous crossing responses both early and late in training relative to caudal stimulation (Fig. 6k-l), both groups' crossing latencies were comparable (Fig. 6h). This was due in part to the two groups of mice utilizing different strategies: the rostral group waited for the next trial throughout the chamber, whereas the caudal group waited in stereotyped locations, increasing crossing efficiency (Fig. 6j). Together these data suggest that rostral CeA Calcrl^{+} neurons generate a highly motivating aversive signal, while caudal CeA Calcrl^{+} neurons are better able to assign long-term valence to external cues to promote learning, and that both efficiently drive avoidance.

While noxious external stimuli are notable for their high salience and ability to motivate vigorous behavior to drive avoidance, aversive internal stimuli are profoundly demotivating and project valence onto external cues over time to condition aversion (Garcia et al., 1968). We postulated that an aversive viscerosensory stimulus would differentially activate rostral and caudal CeA Calcrl^{+} neurons because of their differing capacities to affect motivation and valence, and investigated their responses to a visceral US (intraperitoneal injection of lipopolysaccharide (LPS), which mimics bacterial infection and causes visceral malaise) and conditioned aversion to a palatable novel diet consumed before illness (Garcia et al., 1955) (Fig. 7a). As expected, more neurons in the caudal CeA were excited by LPS (mean $\Delta F/F > 0.5$ relative to baseline during 1 or more of post-injection time periods), and with shorter latency, than in the rostral CeA (74/138 neurons in caudal; 52/176 in rostral) (Fig. 7b-d). We tested how this difference in responsivity to illness translated to behavior and found that while stimulation of either population was sufficient to suppress ingestive behavior (Extended Data Fig. 5a-c), only silencing caudal CeA Calcrl^{+} neurons

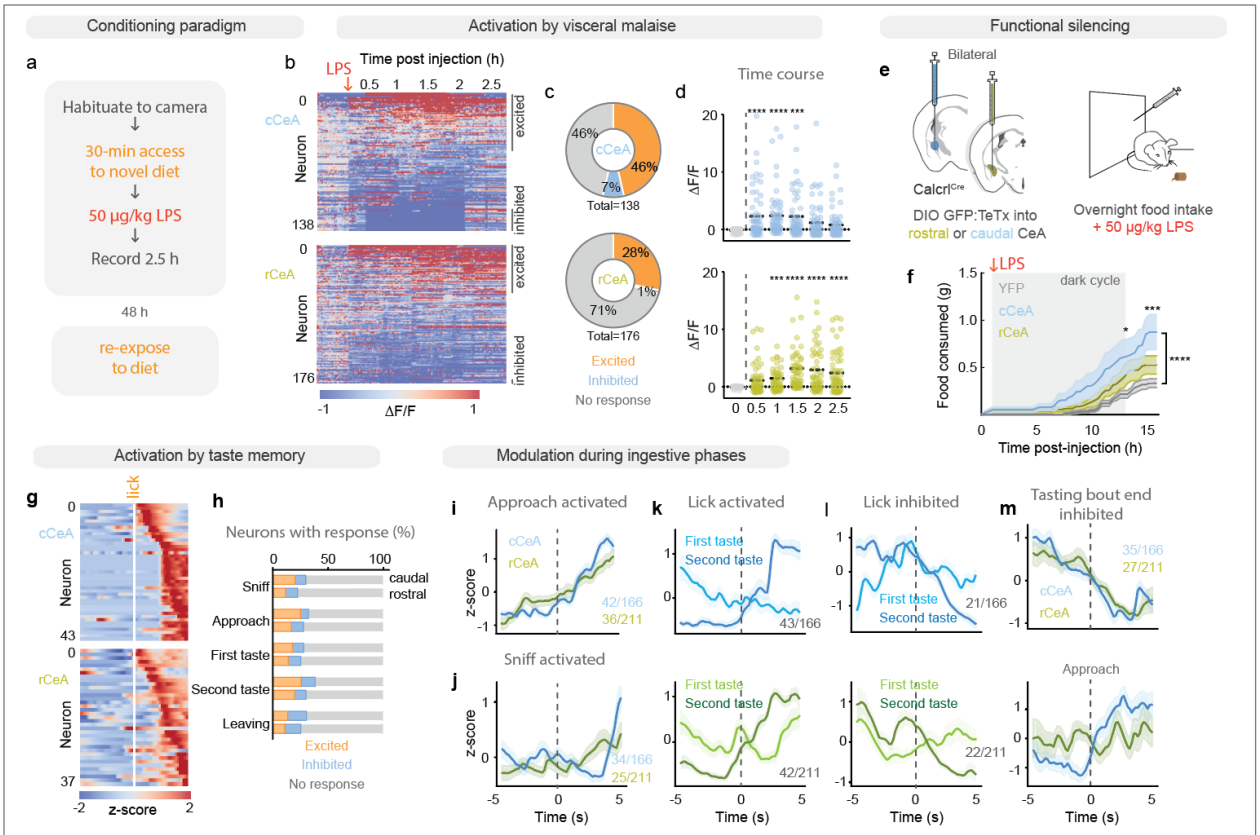

Fig. 7 | Caudal CeA Calcrl+ neurons are preferentially activated by aversive visceral signals and contribute to illness-induced anorexia, but both populations respond during recall of aversive visceral memory. a, Timeline of experimental paradigm for recording calcium activity of rostral or caudal CeA Calcrl$^+$ neurons elicited by administration of a visceral illness mimetic (LPS) and conditioned taste aversion. **b,** Heatmap of ΔF/F for individual neurons during each of the 2-min recording blocks across the 2.5-h recording window. **c,** Proportion of CeA Calcrl$^+$ neurons with responses to LPS administration (from n=138 neurons from 4 mice for the caudal CeA and n=176 neurons from 5 mice for the rostral). **d,** ΔF/F of individual Calcrl neurons in the caudal or rostral CeA exhibiting a significant increase in activity during any of the recording blocks, across all the recording blocks (lines at mean, n=64/138 neurons from 4 mice for the caudal CeA and n=50/176 neurons from 5 mice for the rostral) (Wilcoxan Signed Rank test). **e,** Schematic of paradigm for silencing rostral or caudal CeA Calcrl$^+$ neurons and measuring visceral illness-induced anorexia. **f,** Silencing caudal CeA Calcrl$^+$ neurons attenuated anorexia caused by visceral illness (two-way RM ANOVA with Tukey's multiple comparisons test). **g,** Heatmaps of lick-responsive neuron z-scores during the peri-bout period sorted in ascending order by peak-response latency from mice with conditioned aversion to tastant (n=43/166 neurons from 4 mice for the caudal CeA and n=37/211 neurons from 5 mice for the rostral). **h,** Proportion of neurons with significant changes in activity during various behavioral events. **i,** Neurons activated by approach towards lick spout (n=42/166 neurons caudal and n=36/211 neurons rostral). **j,** Neurons activated by sniffing following tastant availability (n=34/166 neurons caudal and n=25/211 neurons rostral). **k-l,** Activity of neurons activated or inhibited by second bout of licking plotted for first and second tasting bouts (n=43/166 caudal and n=42/211 rostral activated and n=21/166 caudal and n=22/211 rostral inhibited). **m,** Activity of neurons inhibited following the second taste (top) and the preceding approach (bottom) (n=35/166 neurons caudal and n=27/211 neurons rostral). Data represented as mean±SEM. *p < 0.05; ***p < 0.001; ****p < 0.0001.

attenuated anorexia caused by visceral malaise (Fig. 7e-f). Despite being necessary for anorectic responses to visceral malaise, mice lacking caudal CeA Calcrl$^+$ neuron function did not alter normal daily overall food intake or meal patterns (Extended Data Fig. 5d-h), suggesting they are not necessary to signal satiety.

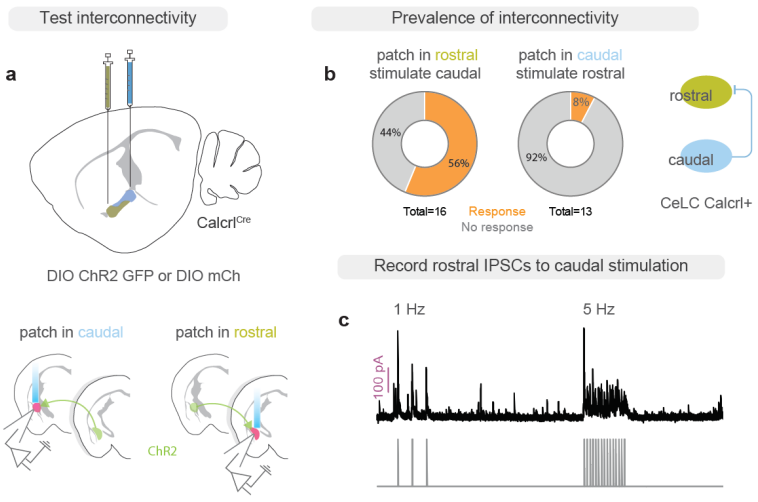

Fig. 8 | Interconnectivity between rostral and caudal Calcrl^{CeA} neurons.
a, Experimental paradigm for photostimulating terminals of either rostral or caudal CeA Calcrl+ neurons while recording post-synaptic responses from Calcrl+ neurons in opposite pole of CeA using slice electrophysiology. **b,** Proportion of Calcrl+ neurons from rostral or caudal CeA responding to terminal stimulation of Calcrl+ neurons from opposite pole. **c,** Representative post-synaptic response from a rostral Calcrl+ neuron receiving inhibitory monosynaptic input from caudal Calcrl+ fibers. Top, IPSCs from recorded neuron; bottom, light trains of photostimulation.

To assess how these intrinsic differences in viscerosensory responsivity might translate to post visceral-conditioning associations with external cues, we examined the activity of both populations during re-exposure to the novel diet that had been paired with visceral illness. We found that, in contrast to the purely visceral signal of malaise, both populations responded in similar proportions to recalled taste aversion (43/166 neurons in caudal CeA, 42/211 neurons in rostral CeA). We examined the neural activity across different phases after placing the spout in the cage: first sniff, first approach, first and second taste, and leaving (Fig. 7g-h). Overall, CeA Calcrl^{+} neurons were more likely to be excited by approach and licking and inhibited by leaving, whereas caudal Calcrl+ neurons additionally demonstrated elevated responses during a second bout of licking relative to the initial taste (Fig. 7g-l). This led us to consider neurons that became inhibited following cessation of the second taste that preceded leaving, as these neurons might oppose continued ingestion of the potentially toxic food. Interestingly, caudal CeA Calcrl^{+} neurons with this response profile were potently activated during approach, whereas rostral CeA Calcrl^{+} neurons were not (Fig. 7m). Thus, caudal CeA Calcrl^{+} neurons can convey the valence of an approaching event.

We were motivated by the apparent opposing roles of rostral and caudal CeA Calcrl^{+} neurons in motivating responses or affecting long-term valence to assess whether they were joined by intrinsic inhibitory connections which could further support execution of distinct roles through cross- or disinhibitory mechanisms that distinguish CeA function (Fadok et al., 2017; Letzkus et al., 2015). We paired

small, targeted expression of ChR2 in Calcrl^{+} neurons in the rostral or caudal poles of the CeA with expression of a fluorescent reporter (mCherry) in the opposite pole (Fig. 8a), then sliced and recorded from Calcrl^{+} neurons in the reporter-expressing area and tested for interconnectivity by delivering trains of light, which should activate terminals of any forward- or back-projecting Calcrl^{+} neurons expressing ChR2 and cause IPSCs in connected neurons. We found that there was directionally biased connectivity: about half (9/16) of rostral CeA Calcrl^{+} neurons received inhibitory synaptic input from caudal Calcrl^{+} neurons (Fig. 8b-c) while very few caudal neurons received input from rostral Calcrl^{+} neurons (1/13; Fig. 8b). This cannot be accounted for by a simple bias in subnucleus connectivity (i.e., the rostral population being restricted to the CeC and the caudal including more CeL), as previous work has shown balanced mutual cross-inhibition between CeC and CeL populations (Kim et al., 2017).

Discussion

We show that neurons of the nociceptive CeA are functionally segregated by spatial location, with rostral CeA Calcrl^{+} neurons driving highly motivated defensive responses to noxious external stimuli while caudal CeA Calcrl^{+} neurons are more likely to respond to aversive viscerosensory stimuli and control learned valence. The activity of both populations is integrated to contribute to associative fear learning, which involves complex layering of broader affect with salient auditory and nociceptive stimuli. Despite more than half of rostral Calcrl^{+} neurons receiving inhibition from caudal neurons, we find that the majority of both populations are activated by most noxious stimuli. This suggests that their joint activity is primarily shaped by incoming sensory drive except in situations with internally biased noxious stimulation such as visceral pain, which biases activity towards the negative valence-encoding caudal population at the expense of motivation.

These studies complement a large body of work examining cell type- and projection-specific functions of CeA circuits in appetitive and defensive behaviors. The CeA has a rich community of cell

populations noted for their cross-inhibitory connections controlling active and passive conditioned fear (Fadok et al., 2017; Gozzi et al., 2010), conveying uncertainty and causing anxiety (Botta et al., 2015; Jo et al., 2018; Tye et al., 2011), promoting and suppressing nociception and conditioned freezing (Ciocchi et al., 2010; Haubensak et al., 2010; Herry et al., 2008; Wilson et al., 2019), controlling ingestion and satiety (Cai et al., 2014; Kim et al., 2017), and creating hierarchies of defensive strategies (Isosaka et al., 2015). A hallmark of these competing populations is their differential activation by sensory input which allows a sensory state to bias the competition between the two populations to flexibly shape behavior (Fadok et al., 2017; Kim et al., 2017). CeA Calcrl^{+} neurons are at least partially defined by the rich excitatory input they receive from PBel CGRP^{+} neurons, which appears to be uniform across the rostrocaudal extent of the CeA (Bowen et al., 2020). Despite this shared input, caudal Calcrl^{+} neurons inhibit rostral Calcrl^{+} neurons, supporting the idea that "cell-types" within the CeA must be defined by more than expression profile, and perhaps require definition by both response profiles and connectivity in addition to canonical cell-type labels.

Based on the responses generated by both populations, caudal CeA Calcrl^{+} neurons are at first tempting to categorize as fear$_{ON}$ neurons because they promote freezing behavior, yet they are activated by shock, tend to be inhibited by the CS after conditioning, and share very little overlap with CeL SOM^{+} neurons (Han et al., 2015). They comprise a subset of CeLC PKCδ^{+} neurons that promote freezing behavior (Kim et al., 2017) that are also inhibited by conditioned fear (Haubensak et al., 2010). It is also tempting to categorize them as CeL PKCδ^{+} neurons since they are involved in suppressing ingestive behaviors, yet while inhibiting CeL PKCδ^{+} neurons attenuated anorexia in response to a number of anorectic agents including LiCl (another US used for conditioned taste aversions), it did not do so for LPS (Cai et al., 2014), suggesting that caudal Calcrl^{+} neurons comprise a subset of CeLC neurons not entirely accounted for by CeA PKCδ^{+} neurons. Rostral CeA Calcrl^{+} neurons are more readily categorized since they are robustly US-activated and inhibited by the CS, suggesting they fit within the canonical fear$_{OFF}$ descriptor. Moreover,

their US-responses diminish with conditioning, suggesting they may be functionally downstream of LA neurons that establish a prediction signal that inhibits US salience across training (Ozawa et al., 2017). We were surprised that, despite upstream PBel CGRP$^+$ neurons displaying robust nociceptive responses under anesthesia (Campos et al., 2018), the majority of CeA Calcrl$^+$ neurons did not respond to painful stimulation delivered across the body when anesthetized. The classical studies recording from nociceptive CeA neurons under anesthesia would not have included CeA Calcrl$^+$ neurons (Bernard et al., 1992). This suggests that CeA Calcrl$^+$ neurons may be inhibited by recently identified, anti-nociceptive anesthesia-activated CeA neurons (Hua et al., 2020).

We were drawn to studying the divergent function of CeA Calcrl$^+$ neurons because they are members of a notoriously heterogeneous structure that bivalently controls a rich array of behaviors, yet are the recipients of a remarkably homogeneous input from the PBel, from neurons that are activated by almost everything of negative valence (Campos et al., 2018). Based on studies examining the role of CGRP peptide in CeA nociceptive processing (Okutsu et al., 2017; Shinohara et al., 2017) and the observation that PBel CGRP$^+$ neuron activity scales with stimulus intensity (Campos et al., 2018), we hypothesized that CeA Calcrl$^+$ neurons would drive avoidance of aversive stimuli in part by differentially biasing signaling of stimulus valence and salience.

Valence is defined as the direction of an emotion, whether positive or negative, and is directly related to the behavioral goal of approach or avoidance, while salience is related to the chance a stimulus requires an organism to make an action. These are orthogonal features of stimulus quality, as perception related to salience is influenced by arousal, but not the valence of secondary stimulus (Sutherland and Mather, 2018). As such, salience can predict response vigor – under optimal control, cues with better predictive capacity justify more vigorous action (Shadmehr et al., 2019). Throughout our studies, we noticed that while CeA Calcrl$^+$ neurons uniformly promoted avoidance behavior, indicating they relayed a negative valence signal, the rostral CeA Calcrl$^+$ neurons were uniquely able to generate robust, highly

motivated behavioral responses both during basal conditions and when activated during an ongoing noxious event. Moreover, the responses generated were rapid, but tended to not promote long-term alterations in behavior through learning. Conversely, caudal CeA Calcrl^{+} neurons generated passive defensive behavioral responses and had dramatic effects on long-term avoidance behavior towards neutral stimuli, suggesting preferential integration with internal state and negative valence processing. Together these data suggest that rostral CeA Calcrl^{+} neurons are responsible for the first phases of nociceptive processing, generating a robustly actionable, salient signal that initially drives avoidance, perhaps in part through rich connections to basal forebrain circuits supporting cortical arousal (Dringenberg and Vanderwolf, 1997; Jolkkonen et al., 2002), while caudal CeA Calcrl^{+} neurons become activated later and relay a long-term valence signal that is integrated with external stimuli to promote long-term aversion. These findings have implications for understanding phases of nociceptive processing, and also encourage further examination of integration between canonical valence-salience systems (e.g. midbrain, ventral striatum, basal forebrain) with the more classically categorized affective systems within which the CeA is embedded (Beyeler et al., 2016; Jo et al., 2018; Namburi et al., 2015; Zweifel et al., 2011).

Supplemental Figures
Extended Data Fig. 1

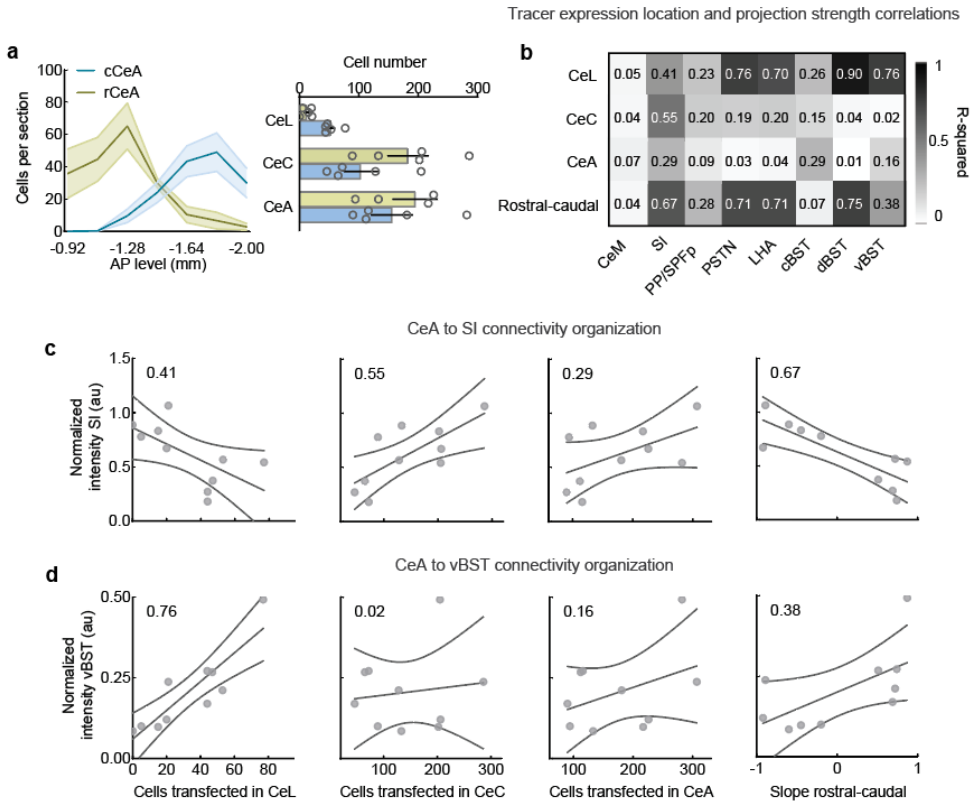

Extended data Fig. 1 | Tracer expression patterns correlated with downstream terminal labeling.
a, Number of cells expressing tracer per section across the rostrocaudal axis for rostral versus caudal viral targeting (left) and summary of cell number per CeA subregion for different injection types (right). **b,** Correlation coefficients between CeA tracer-expression profiles (number of cells per subregion or rostral vs caudal expression bias) and synaptic labeling observed in downstream targets. Darker colors indicate higher R-squared values; numbers are R-squared values for each correlation. **c-d,** Linear regression of CeA tracer-expression profiles vs **c,** SI or **d,** ventral alBST synaptic labeling; R-squared values for each correlation given in upper-left corner of graph. For statistical information see Supplementary Table 1. Related to Fig. 1.

Extended Data Fig. 2

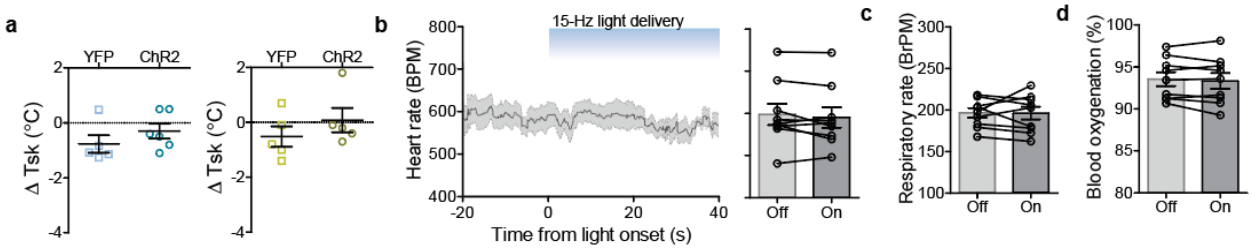

Extended data Fig. 2 | Control autonomic measurements. a, Effect of stimulating rostral or caudal CeA Calcrl^{+} neurons on vasoconstriction (unpaired Student's t test). **b,** Heart rate measurements from control animals during 15-Hz photostimulation (paired Student's t test). **c,** Summary of control animals' respiratory rate before and during light delivery (paired Student's t test). **d,** Blood oxygenation in control mice before and during light delivery (paired Student's t test). For statistical information see Supplementary Table 1. Related to Fig. 2.

Extended Data Fig. 3

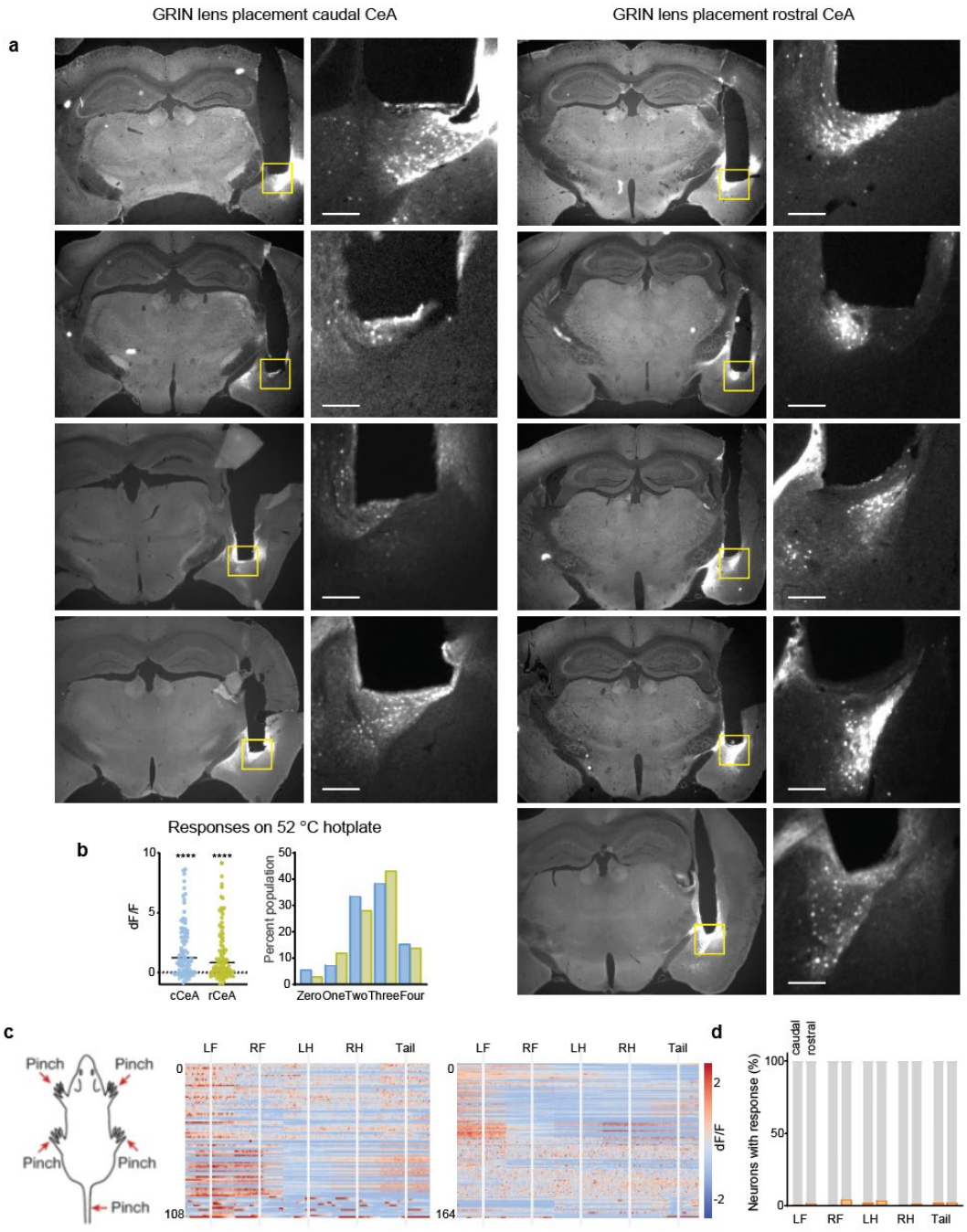

Extended data Fig. 3 | Lens placement and anesthetized pinch responses. a, Images of lens placement for caudal (4) and rostral (5) targeting cohorts Scale bar: 200 µm. **b,** Mean deltaF/F signal for responsive neurons during the 1-min hotplate trial (Wilcoxan signed rank test) (left) and proportion of neurons responding to one or more of hotplate, paw lick, wall rear, or jump. **c,** Heatmap of deltaF/F in response to pinches to the four paws and tail under anesthesia. **d,** Summary of number of neurons activated, inhibited, or not responding to each of the pinches (categorized as responsive if >2.5 sd above baseline for >1.5 -s of the 2-s pinch). Related to Fig. 3.

Extended Data Fig. 4

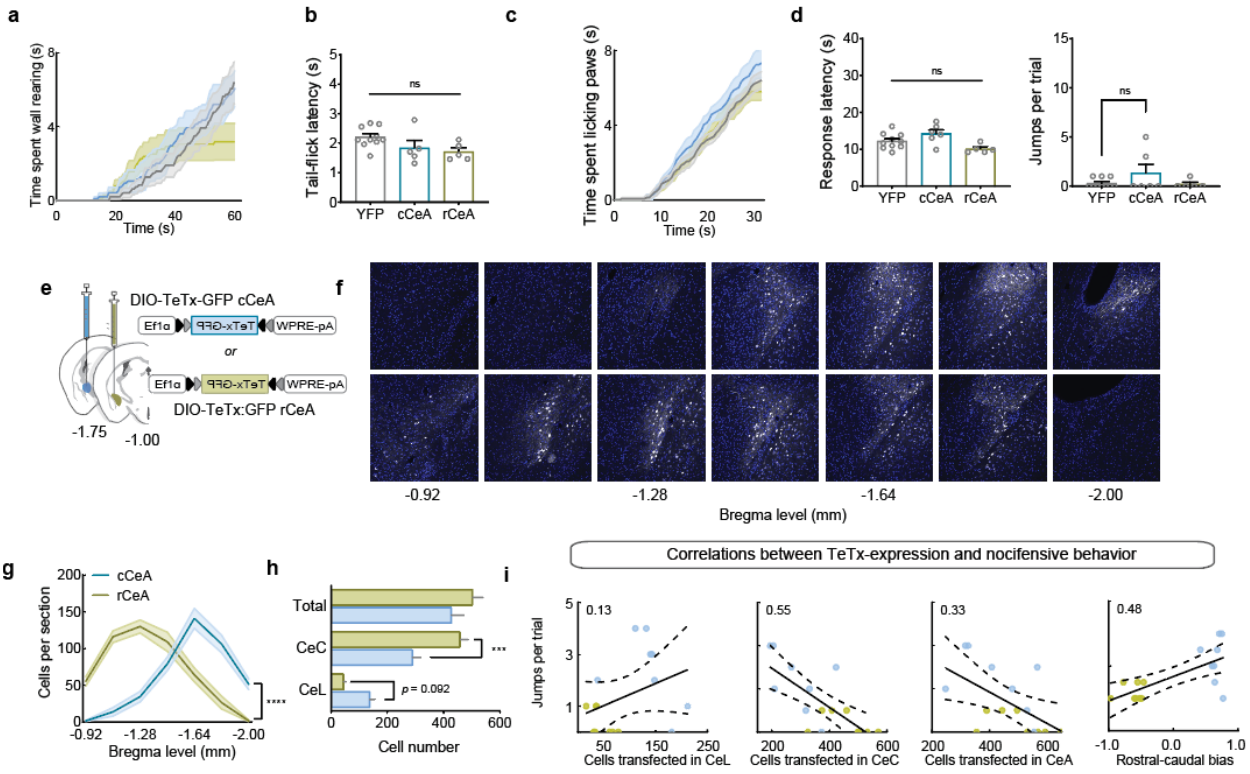

Extended data Fig. 4 | Pre-stimulation does not affect nociceptive responses and capsular expression of TeTx correlates with nocifensive response attenuation. **a,** Effect of CeA Calcrl^{+} neuron photostimulation on wall rearing during the hotplate test (52 °C) (two-way RM ANOVA). **b,** Effect of CeA Calcrl^{+} neuron photostimulation on tail-flick latency (measure of spinal algesia, 52 °C water bath) (one-way ANOVA). **c,** Effect of silencing CeA Calcrl^{+} neurons on time spent paw licking during hotplate test (57 °C) **d,** Pre-stimulating CeA Calcrl^{+} neurons for 5-min at 15-Hz does not affect nocifensive behavior in response to a 52 °C hotplate test. **e-g,** Selective expression of TeTx in the rostral or caudal CeA. **h,** Quantification of cells transduced in CeA subnuclei from each injection type. **i,** Correlations between CeA TeTx-expression profiles (number of cells per subregion or rostral vs caudal expression bias) and jumping behavior on 57 °C hotplate. R-squared for each linear relationship is listed in upper left corner of each graph. Data represented as mean±SEM. **p < 0.01; ***p < 0.001. For statistical information see Supplementary Table 1. Related to Fig. 3.

Extended Data Fig. 5

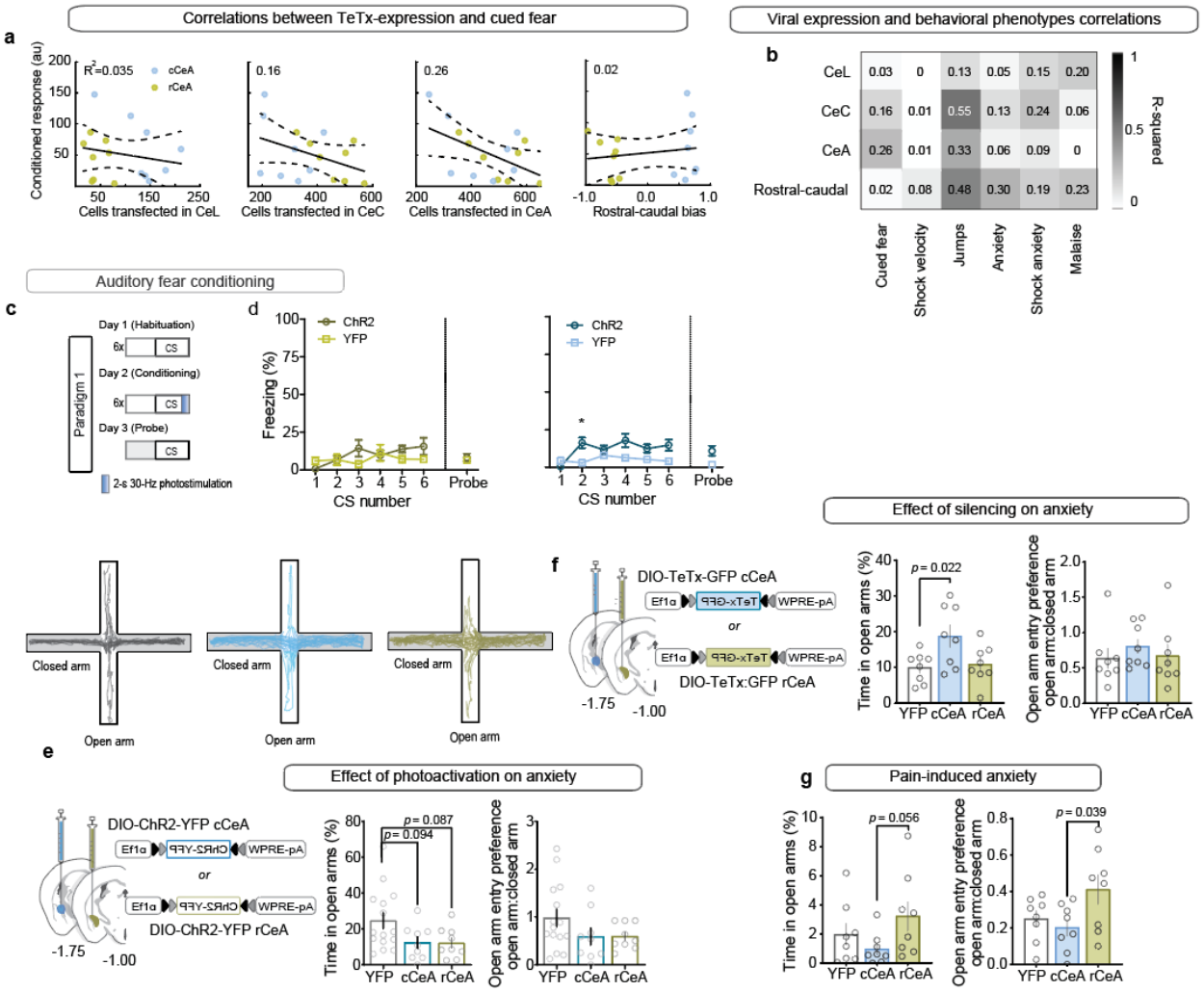

Extended data Fig. 5 | Viral expression correlation with associative fear learning and shock-induced anxiety. a, Correlations between CeA TeTx-expression profiles (number of cells per subregion or rostral vs caudal expression bias) and strength of conditioned fear responses (area under the curve for cued freezing during conditioning). **b,** Correlation coefficients between CeA TeTx-expression profiles (number of cells per subregion or rostral vs caudal expression bias) and behavioral responses. **c,** Freezing behavior during 20-s auditory CS co-terminating with 2-s of 30-Hz photostimulation of rostral or caudal CeA Calcrl$^+$ neurons (two-way RM ANOVA with Sidak's multiple comparisons test). **e,** Time spent in open arms and open arm entry preference in mice with photostimulation of CeA Calcrl$^+$ neurons (one-way ANOVA with Tukey's multiple comparisons test). **f,** Basal anxiety behavior in mice with silenced rostral or caudal CeA Calcrl$^+$ neurons (one-way ANOVA with Tukey's multiple comparisons test). **g,** Anxiety behavior in control and mice with silenced CeA Calcrl$^+$ neurons after challenging with 0.5 mA foot shock (one-way ANOVA with Tukey's multiple comparisons test). Data represented as mean±SEM. *p < 0.05. For statistical information see Supplementary Table 1. Related to Fig. 5.

Extended Data Fig. 6

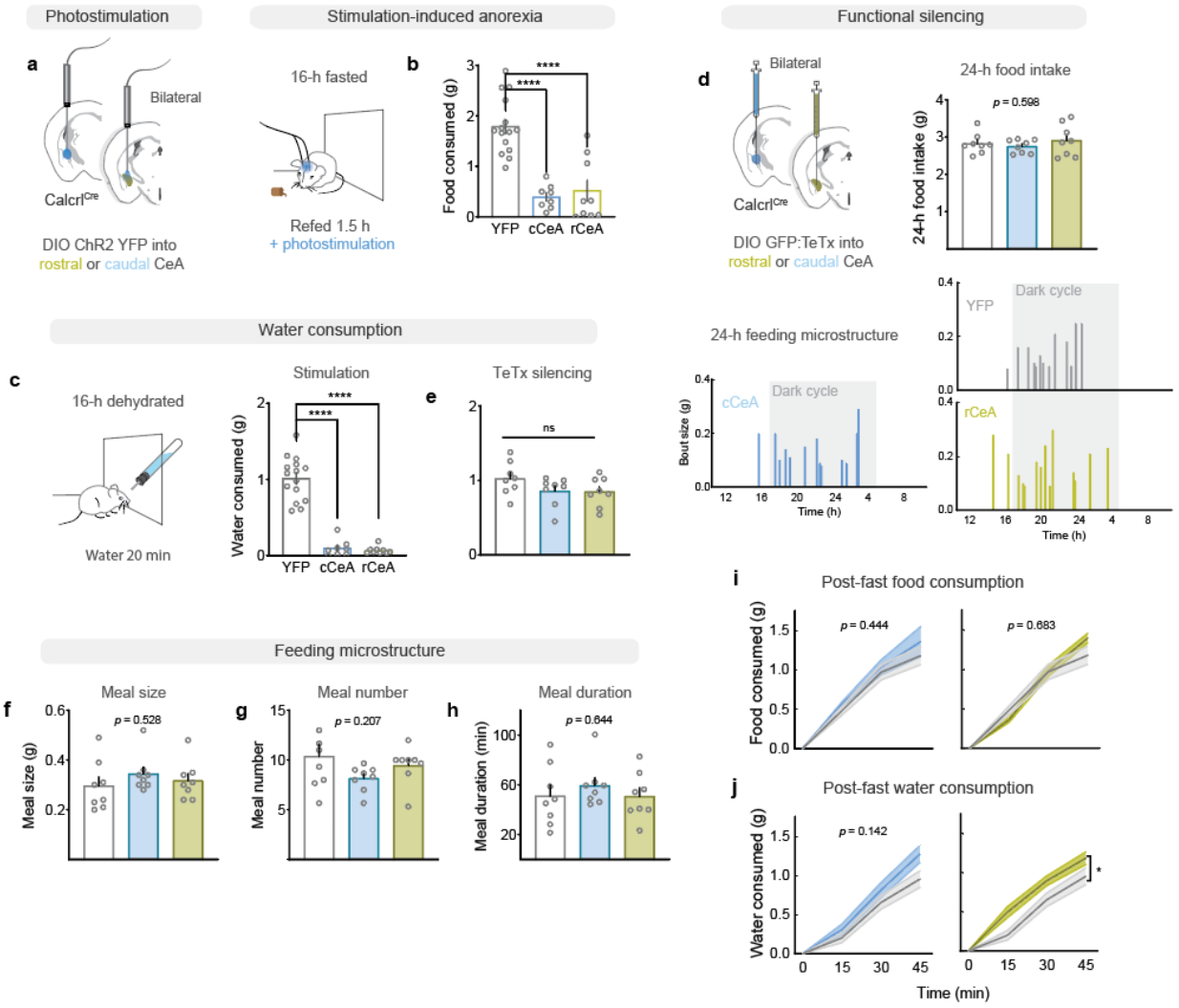

Extended data Fig. 6 | Activation of either rostral or caudal Calcrl^{CeA} neurons potently suppresses ingestive behaviors, but neither are required for normal satiety. a-b, 1.5-h food intake in fasted mice with photostimulation of either rostral or caudal CeA Calcrl^{+} neurons (one-way ANOVA with Dunnett's multiple comparisons test). **c,** Water consumption in dehydrated mice with photostimulation of either rostral or caudal CeA Calcrl^{+} neurons (one-way ANOVA with Dunnett's multiple comparisons test). **d,** 24-h food intake and feeding bout patterns in mice with silenced CeA Calcrl^{+} neurons (one-way ANOVA). **e,** Water consumption in dehydrated mice with silenced CeA Calcrl^{+} neurons (one-way ANOVA). **f-h,** Meal size, number, and duration in mice with silenced CeA Calcrl^{+} neurons (one-way ANOVA). **i,** Food-intake in fasted mice with transient inhibition of CeA Calcrl^{+} neurons using the light-activated anion channelrhodopsin *Gt*ACR2 (two-way RM-ANOVA). **j,** Water-intake in fasted/refed mice with transient inhibition of CeA Calcrl^{+} neurons using the light-activated anion channelrhodopsin *Gt*ACR2 (two-way RM-ANOVA). Data represented as mean±SEM. *p < 0.05. For statistical information see Supplementary Table 1. Related to Fig. 7.

Conclusions

The goal of this thesis is to delineate systems underpinning affective processing of aversive stimuli at the level of the PBN and CeA, focusing on the complementary roles played by $CGRP^{PBN}$ neurons, their various projections, and $Calcrl^{+}$ neurons in the CeA. Previous work in the lab demonstrated that $CGRP^{PBN}$ neurons are activated by diverse threats and contribute generally to defensive responses and that CeA $Calcrl^{+}$ neurons are required for associative fear learning. The experiments described here extend these studies by demonstrating that:

1. $CGRP^{PBN}$ neurons have a profound effect on physiology in addition to behavior and affect.
2. $CGRP^{PBN}$ neurons collateralize to forebrain targets in partially separable subpopulations.
3. The physiological and behavioral responses generated by $CGRP^{PBN}$ neuron stimulation depend on stimulation frequency.
4. Function is segregated across the $CGRP^{PBN}$ neuron-forebrain circuit, with extended amygdalar and basal forebrain/thalamic partners eliciting distinct affective and behavioral responses.
5. Two previously unstudied targets (the SI and VPMpc) contribute to associative fear learning.
6. Some phenotypes are only generated by combined activation of projections.
7. Rostral and caudal CeA $Calcrl^{+}$ neurons have diverging connectivity.
8. Rostral CeA $Calcrl^{+}$ neurons cause active defensive responses while caudal neurons promote freezing behavior.
9. CeA $Calcrl^{+}$ neurons have profound effects on physiology in addition to behavior and affect.
10. CeA $Calcrl^{+}$ neurons are robustly activated by noxious somatic stimuli but are inhibited by anesthesia.
11. Activation of rostral CeA $Calcrl^{+}$ neurons scales nocifensive responses to threat intensity.

12. Rostral and caudal CeA Calcrl^{+} neurons have different response dynamics to foot shock both initially and following learning.
13. CeA Calcrl^{+} neurons are activated by contextual fear memories.
14. Silencing either rostral or caudal CeA Calcrl^{+} neurons prior to conditioning profoundly attenuates fear learning.
15. Shock-only inhibition of CeA Calcrl^{+} neurons does not recapitulate effects of total neuronal silencing on fear memory formation.
16. Caudal CeA Calcrl^{+} neurons are necessary for contextual fear learning.
17. Caudal CeA Calcrl^{+} neurons contribute to conditioned autonomic responses.
18. Activation of rostral CeA Calcrl^{+} neurons generates a highly motivating but transient avoidance signal.
19. Activation of caudal CeA Calcrl^{+} neurons forms strongly aversive memories to external stimuli.
20. Caudal CeA Calcrl^{+} neurons have robust activation by aversive visceral stimuli.
21. Silencing caudal CeA Calcrl^{+} neurons attenuates anorexia in response to visceral malaise.
22. Both rostral and caudal CeA Calcrl^{+} neurons are reactivated by recall of an aversive taste memory.

Future Directions

These experiments show that although $CGRP^{PBN}$ neurons are homogeneously activated by diverse multi-sensory threats (Campos et al., 2018), that the general negative valence signal they relay is broken down across forebrain nuclei to differentially control distinct aspects of defensive behavior, including active and passive fear responses, sympathetic and parasympathetic outflow, affect, and associative learning. What remains unknown is how the differentiation process is accomplished – is activity in downstream sites biased by distinct incoming sensory informational contexts, such that situational differences promote distinct responses through combinations of downstream sites that form ensembles, or is it instead due to differences in their extrinsic connectivity and preferential integration into downstream circuitry controlling physiology and behavior? Especially deserving of attention is the PBN→thalamus and PBN→SI connections which are implicated in contributing to associative fear learning, but not formation of conditioned taste aversion. It would be revealing to establish the genetic identity of these downstream partners and record their activity during both CS-US pairing and memory recall to assess how activity dynamics are developed at each node. Another important step is establishing a connection from the PBN to the BLA, the site where CS-US association occurs. While it is known that activation within the nociceptive CeA is required for plasticity in the LA, the route from the CeA to LA is as yet unidentified (Yu et al., 2017). Classic intersectional polysynaptic tracing studies are a good model for this direction (Livneh et al., 2017).

Another point of interest is the contribution made by $CGRP^{PBN}$ neurons to reinforcing associative fear memories during recall. Which upstream or downstream sites contribute to this process, and are they the same ones as are involved in initial memory formation? This concept has the potential to influence how we perceive memory reconsolidation, as depending on the answer, remembering a noxious event

could potentially be the creation of a virtual US that shapes and reinforces the original memory, while providing a path to association with novel contextual cues.

My experiments dissecting the role of CeA Calcrl^{+} neurons in associative fear learning demonstrated that while silencing either population attenuated association strength, transiently inhibiting either population just during US delivery did not affect the strength of the consolidated memory. This is at odds with other experiments that saw significant attenuation when inhibiting CeL PKCδ+ neurons during a similar peri-shock window (Yu et al., 2017). It would be revealing to inhibit Calcrl neurons using a red-light activated opsin placed to allow inhibition of the majority of these neurons, since we saw that the best predictor of the effect of silencing was the overall number of neurons infected with TeTx, rather than expression within any particular region within the CeA. Another factor that could have affected this result is the length of time the neurons were inhibited – our recordings indicated activity following the shock remained elevated for 10s of seconds, while inhibition was restricted to a much shorter window. Given that many of the caudal Calcrl^{+} neurons had tonically elevated activity after the shock for the remainder of the conditioning period, it may also be the case that this standing activity contributes to plasticity in downstream circuits by driving them closer to baseline, or through inhibiting competing circuits. It would be revealing to inhibit during the entire ITI, and potentially even following conditioning when the animal has elevated stress and anxiety to see if that affects association strength.

We began by describing the CGRP^{PBN} → forebrain circuit as primarily being responsible for relaying signals related to internal state. So far, we have primarily focused on how this valence signal is used to flavor perception of external stimuli by integrating salience and valence signaling onto the preexisting sensory context. What about truly visceral stimuli such as satiety and malaise, both controlled by vagal c-type afferents that can be loosely categorized as nociceptive? Recent work suggests that although multiple downstream targets of CGRP^{PBN} neurons can suppress appetite and condition taste aversions (Chen et al., 2018), the individual actors are not necessary for normal satiation or memory formation. This

is perhaps due to redundancy within the circuit, as the downstream targets contact many of the same partners and can hence stand in for each other when either one is silenced. Hence, it would be revealing to silence pairs of downstream targets implicated in malaise and satiety (e.g. the CeA and ovBST or CeA and PSTN). Understanding the integration of internal state with external stimuli can provide insight into how the brain assigns value, and how this information is used to shape the long-term processes of memory and homeostasis.

Methods

Animals

Calca$^{Cre/+}$ and *Cacrl*$^{Cre/+}$ mice (C57Bl/6 background) were generated and maintained as described (Carter et al., 2013; Han et al., 2015). Male and female mice were used for all studies. Following stereotaxic surgery, mice were singly housed for at least 3 wk prior to and during experimentation with *ad libitum* access (unless noted otherwise) to standard chow diet (LabDiet 5053) in temperature- and humidity-controlled facilities with 12-h light/dark cycles. All animal care and experimental procedures were approved by the Institutional Animal Care and Use Committee at the University of Washington.

Virus production

AAV9-Flex-ChrimsonR:tdTomato was purchased from UNC GTC Vector Core (AV6556B; $4.5x10^{12}$ viral particles/mL). AAV1-DIO-GFP:TeTx, AAV1-DIO-GtACR2-mCherry, AAV1-DIO-ChR2:YFP, AAV1-DIO-JAWS:GFP, rAAV2-retro-Flp, AAV1-Cre_{on}-Flp_{off}-ChR2-YFP, AAV1-Cre_{on}-Flp_{on}-ChR2-YFP and AAV1-DIO-YFP viral vectors were produced by transfecting HEK cells with each of these plasmids plus pDG1 (AAV1 coat stereotype) helper plasmid; viruses were purified by sucrose and CsCl gradient centrifugation steps, and re-suspended in 0.1 M phosphate-buffered saline (PBS) at about 10^{13} viral particles/mL.

Stereotaxic surgery

Section I: Bilateral stereotaxic injections of virus (0.28 µl per side) into the PBN of *Calca*$^{Cre/+}$ mice were achieved as described (Carter et al., 2013). In mice used for ChR2-optogenetic experiments, two custom-made fiber-optic cannulas were implanted bilaterally above the PBN (AP 4.70 mm, ML ± 1.50 mm, DV 2.90 mm), VPMpc (AP 1.90 mm, ML ± 1.25 mm, DV 3.65 mm), PSTN (AP -1.80 mm, ML ± 1.50 mm, DV 4.60 mm), cCeA (AP 1.50 mm, ML ± 3.10 mm, DV 4.30 mm), rCeA (AP 0.70 mm, ML ± 2.85 mm, DV 4.50 mm), SI (AP 0.30 mm, ML ± 1.80 mm, DV 4.40 mm), or BNST (AP +0.20 mm, ML ± 1.20 mm, DV 4.00 mm). For three-fiber, dual-stimulation experiments, three custom-made fiber-optic cannulae were implanted in the

left hemisphere, one above the rCeA/SI (AP 0.60 mm, ML – 2.50 mm, DV 4.40 mm), one above the cCeA (head inclined at a 10° angle; AP 2.15 mm, ML – 3.30 mm, DV 4.10 mm), and one above the VPMpc (AP 1.95 mm, ML – 1.00 mm, DV 3.80 mm). For JAWS-photoinhibition experiments, fiber placement was same for PBN, VPMpc and SI; fibers for CeA were placed at AP 1.10 mm, ML ± 3.00 mm, DV 3.85 mm. For all experimental mice, fiber-optic cannulae were affixed to the skull with C&B Metabond (Parkell) and dental acrylic. Mice were allowed to recover for 3 wk before the start of behavioral tests. For collateralization-tracing experiments rAAV2-retro Flp virus was injected (0.48 µl unilaterally) into the VPMpc (AP 1.92 mm, ML ± 1.00 mm, DV 3.85 mm), PSTN (AP -1.90 mm, ML ± 1.50 mm, DV 4.70 mm), CeA (AP 1.10 mm, ML ± 3.10 mm, DV 4.10 mm), or ovBNST (AP +0.20 mm, ML ± 1.00 mm, DV 4.00 mm) and INTRSECT virus (0.35 µl unilaterally) was injected into the PBN. Tracing mice were sacrificed 4-wk after virus injection.

Section II: Bilateral stereotaxic injections of virus (0.1-0.21 µl per side) into the CeA of *Calcrl*$^{Cre/+}$ mice were achieved as described (Han et al., 2015), except targeted to the rostral or caudal thirds of the CeA (rCeA AP -0.70 mm, ML ± 2.95 mm, DV 4.35 mm; rCeA AP 1.40mm, ML ± 3.12 mm, DV 4.15 mm). In mice used for optogenetic experiments, two custom-made fiber-optic cannulas were implanted bilaterally above the rostral or caudal CeA, 0.25 mm above the site of injection and were affixed to the skull with C&B Metabond (Parkell) and dental acrylic. Mice were allowed to recover for 3 wk before the start of behavioral tests. Tracing mice were sacrificed 4-wk after virus injection.

Photostimulation and inhibition

ChR2 - After recovery from surgery, mice were acclimated to dummy cables attached to the implanted fiber-optic cannulas. For behavioral and autonomic studies, bilateral branching fiber-optic cables (200-µm diameter, Doric Lenses) were attached to the head of each mouse before experimentation. Light-pulse trains (10 ms) were delivered at 15 Hz, or 30 Hz as described below. Stimulation paradigms were programmed using a Master8 (AMPI) pulse stimulator that controlled a blue-light laser (473 nm;

LaserGlow). The power of light exiting each side of the branching fiberoptic cable was adjusted to 15 ± 0.5 mW. *ChrimsonR* – Same as above, except stimulation was kept to 30 Hz, and the pulse stimulator controlled a red-light laser (660 nm; LaserGlow). The power of light exiting the single fiberoptic (for single-projection terminal stimulation) was adjusted to 5, 12, or 20 mW as described below. For dual-projection terminal stimulation, the light exiting each side of the branching fiberoptic cable was adjusted to 12± 0.5 mW. *JAWS* – acclimation same as above, except light was delivered (634-nm, Shanghai Lasers) as 2-s on 1-s ramp 1-s off for continuous inhibition during behavior (e.g. hot-plate test, RTPP), or 3.5-s on 1-s ramp beginning 0.5-s before each 2-s foot shock during foot-shock conditioning. The power of light exiting each side of the branching fiberoptic cable was adjusted to 8 ± 0.5 mW. Gt*ACR2* – acclimation and delivery parameters same as above for JAWS, except light was 473nm.

Criteria for exclusion from analysis

Mice were excluded from individual test data if 1) they became immobilized due to tangled fiber-optic patch cords during the behavioral tests, 2) they escaped the arena during photostimulation, or 3) there was limited error-free data collected in pulse-oximeter physiological measurements (this only occurred with respiratory measures). Mice were excluded from all analysis if post-hoc histological examination revealed that viral expression was weak or unilateral, or that fiber-optic cannulae were not appropriately targeted over the projection-site of interest. Locations of fiber tips for all animals for Section I that passed the expression and placement criteria are summarized in Section I Figure S3. There was also progressive dropout due to headcap loss requiring animal sacrifice during the study; all data were included up to that point pending histological analysis.

Slice electrophysiology

Mice were anesthetized with Euthasol (0.2 ml, i.p.) and intracardially perfused with 4-6 °C cutting solution containing (in mM): 92 N-methyl-D-glucamine, 2.5 KCl, 1.25 NaH_2PO_4, 30 $NaHCO_3$, 20 HEPES, 25 D-glucose, 2 thiourea, 5 Na-ascorbate, 3 Na-pyruvate, 0.5 $CaCl_2$, 10 $MgSO_4$. Coronal slices (300 µm) were cut with a vibratome (Leica VT1200) and kept in the same cutting solution at 33 °C for 12 min. Slices were transferred to a 25°C recovery solution containing (in mM): 124 NaCl, 2.5 KCl, 1.25 NaH_2PO_4, 24 $NaHCO_3$, 5 HEPES, 13 D-glucose, 2 $CaCl_2$, 2 $MgSO_4$. Recordings were made in artificial cerebral spinal fluid (aCSF) containing (in mM) 126 NaCl, 2.5 KCl, 1.2 NaH_2PO_4, 26 $NaHCO_3$, 11 D-glucose, 2.4 $CaCl_2$, 1.2 $MgCl_2$ continuously perfused at 33 °C. All solutions were continuously bubbled with 95%:5% O_2:CO_2 (pH 7.3-7.4, 300-310 mOsm). Patch-clamp recordings were obtained with a MultiClamp 700B amplifier (Molecular Devices) and filtered at 2 kHz.

JAWS Photoinhibition – $CGRP^{PBN}$ neurons expressing AAV1-DIO-JAWS-GFP were identified via epifluorescence and action potentials were recorded in current clamp with patch electrodes (3-5 MΩ) containing (in mM): 135 K-gluconate, 10 HEPES, 4 KCl, 4 Mg-ATP, 0.3 NA-GTP (pH 7.35, 280 mOsm). To assess the effects of CGRP terminal inhibition, excitatory-post synaptic currents (EPSCs) were recorded in voltage clamp at -70 mV from neurons in the CeA surrounded by JAWS:GFP-positive fibers. Patch electrodes (3-5 MΩ) contained (in mM): 117 Cs- $MeSO_3$, 20 HEPES, 0.4 EGTA, 2.8 NaCl, 5 TEA, 4.92 Mg-ATP, 0.47 Na-GTP (pH 7.35, 280 mOsm). Red light (634 nm, Shanghai Laser) was delivered with a fiber optic placed in the bath above the slice (3 s for action potential recordings and 30 s for EPSCs with 1 s ramp down). EPSCs were analyzed with an automated detection protocol in Mini Analysis Program v.6.0.7 (Synaptosoft) software and manually checked for accuracy.

Postsynaptic EPSCs – To verify CGRP connectivity to post-synaptic neurons, light-evoked EPSCs were recorded from cells surrounded by ChR2:YFP-positive fibers in each downstream site. Neurons were held

in voltage clamp at -70 mV and EPSCs were evoked by 10-ms pulses of blue light delivered through the objective via a 470 nm LED (ThorLabs). Events were analyzed in Clampfit v.11.0.3 (Molecular Devices).

Behavioral measures

Order of experiments – Section I: Mice were acclimated to handling and attachment of fiber-optic patch cords for 1 wk, followed by auditory fear conditioning, elevated-plus-maze test, RTPP, unconditioned freezing responses to stimulation in open field, hot-plate test, tail-flick latency test, tail-skin temperature test, autonomic measurements. All replicates were biological (test repetition in biologically distinct samples), not technical (test repetition in same biological sample). Not all cohorts of mice were exposed to all experimental tests – there were biological replicates of mice for PBN photostimulation, and cCeA, SI, and ovBNST terminal photostimulation. The second groups were added for auditory fear conditioning (n=3,1 (ChR2, YFP) SI only), unconditioned freezing (n=3,1 ovBNST and SI), and EPM behavioral data (ovBNST and SI), and for the PBN only, plethysmography measurements of respiratory rate (n=6). Some early groups of PBN stimulation were only tested for unconditioned freezing responses (n=3). Other variances in group numbers are due to exclusion from individual tests due to adverse events during the test or drop-out due to damaged fiber-optic cannulae (see exclusion criteria, above). Section II: Cohort 1 (ChR2): Mice were acclimated to handling and attachment of fiber-optic patch cords for 1 wk, followed by auditory fear conditioning, elevated-plus-maze test, RTPP, unconditioned freezing responses to stimulation in open field, hot-plate test, tail-flick latency test, tail-skin temperature test, autonomic measurements. Cohort 2 (ChR2): Mice were acclimated to handling and attachment of fiber-optic patch cords for 1 wk, elevated-plus-maze test, RTPP, active-avoidance, unconditioned freezing responses to stimulation in open field, hot-plate test, autonomic measurements. Cohort 3 (TeTx): Mice were acclimated to handling and housed in BIODAQ for habituation for 1 wk, daily food intake measured for 1 wk, LPS-induced anorexia, rehoused in standard cages for 1 wk, elevated-plus-maze test, auditory fear

conditioning. Cohort 4 (*Gt*ACR2): Mice were acclimated to handling and attachment of fiber-optic patch cords for 1 wk, followed by RTPP, auditory fear conditioning, conditioned autonomic measurements.

Auditory fear conditioning – The fear-conditioning chamber was a square arena (25 x 25 cm) with metal walls, two speakers attached on opposite walls, and a metal grid floor that consisted of a circuit board that delivers electrical shock (Coulbourn Instruments). A USB camera was connected to the personal computer and video tracking software (EthoVision XT 10, Noldus Technology) controlled the circuit and recorded the data. Day 1: Mice were attached to fiberoptic patch cords and allowed to habituate for 5 min in their home cage prior to introduction to conditioning context. After free exploration of the context for 1 min, 6 CS tones (tone: 10 kHz 20 s, 60 dB) were played at random intervals, with an average inter-trial interval (ITI) of 2 min. Day 2: Mice were attached and allowed to explore for 1 min; then 6 CS presentations (20 s, 60 dB, 10 kHz) were played at random intervals, with an average ITI of 2 min and each co-terminated with a 2-s light train (30 Hz, 15 mW). Following the sixth CS-US pairing, mice remained in the context for 1 min before being returned to their home cage. Day 3: Mice were attached to fiberoptic patch cords and habituated as before, but then they were placed in a novel context (25 x 25 cm, semitransparent plexiglass). After 2 min of free exploration, one tone CS was played. All the trials were recorded by a USB camera attached to the personal computer and the time spent freezing (during the tone), defined as immobility up until any movement of the head or body, was manually scored with a stopwatch (experimenter was blind to treatments). *With photoinhibition* – same as above, except 2-s light train was replaced with a 2-s 0.5-mA footshock with red or blue light delivery for photoinhibition (8 mW, 3.5-s on, 1-s ramp off, turned on 0.5-s before the shock and ending 2.5 s later).

Elevated-plus maze (EPM) – The custom-made EPM consisted of 2 sets of crossed arms (2 arms enclosed by 30-cm tall transparent plexiglass, 2 arms open), each 50 cm long and 8 cm wide, set 65 cm above floor. Mice were attached to fiber optic patch cords and allowed to habituate for 10 min in their home cage prior to introduction to the EPM. Mice were placed in an open arm, 10 cm out, facing the center, with the

fiber optic patchcord (4 m long) secured to the ceiling above the center of the maze. Mice were allowed to explore the arena for 10 min with optogenetic stimulation (15 Hz, 2 s on/2 s off). The sessions were recorded by a USB camera attached to a personal computer and were analyzed using video-tracking software (EthoVision XT 10).

Real-time place preference (RTPP) – Section I: The testing apparatus was a custom-made, three-chambered box (two 18 x 20 cm chambers joined by a 10 x 20 cm start chamber) constructed of opaque black plexiglass with a cement floor. One chamber had walls with vertical pink stripes (2 cm wide), the other had horizontal pink stripes (2 cm wide), and the start chamber had no stripes. Mice were attached to fiber-optic patch cords and allowed to habituate for 10 min in their home cage prior to introduction to the test box. Mice were then introduced to the start chamber and allowed to explore freely during the 15-min trial. One chamber of the box was assigned as the light-paired side. Each time the mouse crossed into the stimulation chamber it received 15-Hz photostimulation or 2-s on 1-s ramp 1-s off trains of photoinhibition until it left the light-paired side. Behavioral data were recorded via a USB camera interfaced with EthoVision software (Noldus Information Technologies). Section II: the same, except the apparatus was a two-chambered box.

Active avoidance paradigm – The testing apparatus was a custom-made, two-chambered box (two 25 x 25 cm chambers joined by an empty strip). Mice were attached to fiber-optic patch cords and allowed to habituate for 10 min in their home cage prior to introduction to the test box. Mice were then introduced to one side of the chamber and allowed to explore freely during the 15-min trial. After 1-min the avoidance loop began: a 10-kHz warning tone was generated, 5-s after tone onset the mouse received 15-Hz photostimulation. Both the tone and photostimulation were switched off when the mouse crossed to the opposite chamber, which also reset the loop with a 30-s inter-trial interval. Sessions were capped at 35-min and mice received 3 days of training. Behavioral data were recorded via a USB camera interfaced with EthoVision software (Noldus Information Technologies).

Stimulation in open field – Mice were attached to fiber-optic patch cords and allowed to habituate for 5 min in their home cage prior to placement in the arena (40 x 40 cm, white plexiglass walls). One minute after introduction to the arena it received 30-s photostimulation (30 Hz, 15 mW) 3 times with 60-s inter-stimulation intervals. The sessions were recorded with a USB camera attached to a personal computer and the time spent freezing, defined as immobility up until any movement of the head or body, was manually scored with a stopwatch (experimenter was blind to treatments). Locomotor data was collected using video-tracking software (EthoVision XT 10).

Hot-plate test – Photostimulation: Section I: Mice were attached to fiber-optic patch cords and allowed to habituate for 10 min in their home cage prior to stimulation. Following habituation, mice received photostimulation (30 Hz, 8 s on/5 s off, 15 mW) for 7 min prior to exposure to the hot plate. After terminating photostimulation to prevent freezing interfering with responses to heat (for $CGRP^{PBN}$ neuron manipulation studies; stimulation was 3 s on/2 s off for Calcrl+ CeA manipulation studies and was maintained during the test), mice were placed on the pre-heated aluminum plate (15 x 15 cm, set to 52 ºC) of the Hot/Cold Plate Analgesia Meter (Coulbourn Instruments). The transparent Plexiglas chamber (15 x 15 x 20 cm) prevented the mouse from escaping. The latency of the responses to the heat (paw lick, or jump) was measured manually by the experimenter with a stopwatch during the 60-s trials. Trials were recorded with a USB camera attached to a personal computer, and later jump number (jump counted when all 4 limbs left floor) and the latency to the first jump were manually scored with a stopwatch. Section II: Same as above, except photostimulation (30-Hz, 3-s on 2-s off) was ongoing during testing. *Photoinhibition* – same as above, except the hot plate was set to 57 ºC, and photoinhibition (2-s on 1-s ramp 1-s off throughout trial) began immediately prior to placing the subject on the plate. Trial terminated at 30 s.

Tail-flick-latency test – Mice were attached to fiber-optic patch cords and allowed to habituate for 10 min in their home cage prior to stimulation. Following habituation, mice received photostimulation (30 Hz, 8

s on/5 s off, 15 mW) for 7 min. After ending photostimulation (to prevent freezing interfering with tail-flick reflex), the mouse was restrained within a thick cloth, with only its tail protruding, and its tail was partially submerged (1/2 of its length) into water maintained at 52.5 ºC (± 0.2 ºC). The tail-flick latency in response to heat was manually scored with a stopwatch. Trials were cut-off at 15-s if no response occurred.

ChrimsonR or ChR2, single-fiber, freezing responses – Mice were attached to a single, fiber-optic patch cord and allowed to habituate in their home cage for 5 min. After habituation, they were placed into an empty, clean, standard cage, and allowed to explore for 2 min, then they received 10-s photostimulation (30 Hz, 5, 12, or 20 mW). The sessions were recorded with a USB camera attached to a personal computer and the time spent freezing, defined as immobility up until any movement of the head or body, was manually scored with a stopwatch (experimenter was blind to treatments).

Food and water intake measurements – Food was removed from mice 2-h before the dark cycle. 16-h later mice were attached to patch cords and habituated for 5 min. Then a single pellet and water were made available and 15 Hz 3 s on/2 s off photostimulation was delivered during the 1-h refeeding. For re-hydration studies water was removed and the trial was 10-m long.

Conditioned taste Aversion (CTA) Assay – For calcium imaging experiments, ad libitum-fed mice were presented with a test tube of vanilla-flavored Ensure approximately 2 h after the onset of the light cycle. Twenty min after the first lick, mice were injected with LPS and the Ensure bottle was removed after 4 h. Activity of CeA Calcrl^{+} neurons was measured every 30 min for 2 min following the injection and 48-h following conditioning, when Ensure was made available for 10-m following a 2-min baseline period and neuronal activity was measured.

BIODAQ meal pattern measurements – Mice were habituated to BIODAQ cages for 7 days prior to bout and meal size data being collected. For the LPS-induced anorexia experiment, mice were given a 50 ug/kg injection of LPS 1-h before the dark cycle.

Autonomic measurements

Tail-skin temperature measurements – Mice were attached to fiber-optic patch cords and allowed to habituate for 10 min in their home cage prior to stimulation. Following habituation, a baseline thermal image of the tail was taken using an infrared camera (FLIR E4; FLIR Instruments). After 2 min of photostimulation (30 Hz, 8 s on/5 s off), a second thermal image was taken. Images were uploaded and analyzed using the software provided (FLIR Tools). Temperature data were taken from 1/3 of length below the base of the tail.

Pulse-oximeter measurements – Mice were habituated to dummy collar sensors (Starr Life Sciences) for 12 h overnight prior to secondary habituation to collar sensors and attached cables (Starr Life Sciences). After a full day of habituation, hair was removed from the sensor areas (circumference of neck) to allow trans-dermal infrared penetration, and mice were switched to dummy collar sensors overnight. The next morning, collar sensors and attached cables were placed on the mice, which habituated for at least 30 min prior to patch-cord attachment. Mice were then attached to fiber-optic patch cords and returned to their home cage and allowed to habituate for 1-2 h, until heart rate and respiration became stable. The collar sensors were attached to a pulse oximeter (MouseOx Plus, Starr Life Sciences) via 3-m cables, and the pulse oximeter was attached to a personal computer via USB. Eventually 5 min of baseline was recorded using the software (Conscious Software Module, Starr Life Sciences), after which the mouse received 3 min of photostimulation (15 or 30 Hz) followed by 1 min of post-stimulation measurements. Recordings were exported and analyzed in Excel.

Conditioned autonomic responses – Mice were conditioned to freeze to a 10-kHz tone using a 2-s 0.5 mA foot shock delivered 5x as described above. They were prepared for pulse-oximeter measurements as described above and were attached to fiber-optic patch cords, but were placed in with access to a tone generator to deliver the CS. After habituation and baseline recordings the 20-s CS was delivered 2X with a 1-m ITI with simultaneous light-inhibition using the blue-light activated anion channel *Gt*ACR2.

Plethysmography measurements – A new cohort of mice (n=6) was generated to stimulate $CGRP^{PBN}$ neuron somata to measure respiration rate by plethysmography because pulse-oximeter measurements were unable to resolve respiratory rate during somata stimulation. Animals were briefly anesthetized, attached to a bilateral fiber optic patch cord with a rotary joint, and placed in a barometric chamber supplied with room air (21% O2, 200 ml/min). The chamber was sealed for each recording session, which consisted of 5 recording blocks, 30 s each, centered around 10 s of stimulation (30 Hz) during which the pressure difference was measured between the experimental and reference chamber with a differential pressure transducer. Signals were amplified, digitized, and low-pass filtered (0.1 Hz). Data were collected and analyzed using pCLAMP 9.0 software (Molecular Devices).

Calcium imaging

Mice were prepared for calcium imaging as described (Resendez et al., 2016). Briefly, 3 wk after viral injection, mice were anesthetized with isoflurane and implanted with a microendoscope lens (6.1 mm length, 0.5 mm diameter; Inscopix #100-000588) with assistance of a ProView implant kit (Inscopix, #100-000754) that allowed visualization of fluorescent activity during implantation. The lens was targeted to be ~200–300 μm above the neurons using the following coordinates: cCeA (AP 1.50 mm, ML ± 3.10 mm, DV 4.30 mm), rCeA (AP 0.70 mm, ML ± 2.85 mm, DV 4.50 mm). One week after lens implantation, mice were anesthetized and a baseplate (Inscopix, #100-000279) was implanted above the lens. The baseplate

provides an interface for attaching the miniature microscope during calcium imaging experiments, but at other times a baseplate cover (Inscopix, #100-000241) was attached to prevent damage to the microendoscope lens. Calcium fluorescence was recorded at 6 frames/s. The recording parameters were based on pilot studies that demonstrated the least amount of photobleaching while allowing sufficient detection of fluorescent activity. Ethovision XT10 (Noldus Technology) was used to trigger and synchronize calcium recordings with behavioral video recordings.

Calcium imaging data analysis

Raw video files were cropped and 2x spatial downsampled using Inscopix analysis software, then all recordings from an individual session were concatenated in ImageJ. Concatenated files were motion-corrected, processed, and signal extracted using the MIN1PIPE integrated imaging processing pipeline (Lu et al., 2018), using auto-seeds and 9-10 (average neuron diameter in px) dpi setting. Seeds-cleansed traces were imported and analyzed in Python, using indexes of behavior-frame locations exported from analyzed Ethovision XT10 files to align.

Histology

Stimulation prior to euthanasia – Mice were attached to fiber-optic patch cords and allowed to habituate for 10 min in their home cage, after which they received 25 min of photostimulation (30 Hz, 3 s on/2 s off). Then they were detached from the patch cords and left in their home cage for 70 min until euthanasia.

Histology and microscopy – Mice were anesthetized with Beuthansia (0.2 ml, i.p.; Merck) and perfused transcardially with PBS followed by 4% PFA in PBS. Brains were post-fixed overnight in 4% PFA at 4 ºC, cryoprotected in 30% sucrose, frozen in OCT compound (ThermoFisher), and stored at -80 ºC. Coronal

sections (30 µm) were cut on a cryostat (Leica Microsystems) and collected in cold PBS. For immunohistochemistry experiments, sections were washed three times in PBS with 0.2% Triton X-100 (PBST) for 5 min and incubated in blocking solution (3% normal donkey serum in PBST) for 1 h at room temperature. Sections were incubated overnight at 4 ^{o}C in PBST with primary antibodies including: rabbit anti-c-Fos (1:2000, Abcam, ab190289), goat anti-c-Fos (1:500, Santa Cruz Biotechnology, sc-52), chicken-anti-GFP (1:10000, Abcam, ab13970). After 3 washes in PBS, sections were incubated for 1 h in PBS with secondary antibodies: Alexa Fluor 488 donkey anti-chicken, Alexa Fluor Cy5 donkey anti-chicken, Alexa Fluor 594 donkey anti-mouse, Cy5 donkey anti-goat, and/or Cy5 donkey anti-rabbit (1:500, Jackson ImmunoResearch). Tissue was washed 3 times in PBS, mounted onto glass slides, and coverslipped with Fluoromount-G (Southern Biotech). Fluorescent images were acquired using a confocal microscope. All digital images were processed in the same way between experimental conditions to avoid artificial manipulation between different datasets.

Collateral tracing quantification – Coronal sections (30 µm) were collected in 180-µm series and stained for YFP (chicken-anti-GFP; Alexa Fluor Cy5 donkey anti-chicken). Fluorescent images (20X magnification) of each projection target were acquired using a confocal microscope, with the same settings used across all samples and subjects. Across subjects, on average 6 PBN images, 3 VPMpc images, 5 PSTN images, 6 CeA images, 5 SI images, 4 ovBNST images, and 8 IC images were collected from each brain. Area-specific, pixel-intensity measures for each image/projection target were analyzed in Image-J. Background was subtracted for each image using the average fluorescence from a region of the image outside the projection target analyzed. Pixel-intensity values were summed across individual sections to give the total for each projection target. This value was normalized to either 1) the total pixel intensity values for all areas within subject for % total projection strength, a measure of the contribution of the individual projection to the total projection distribution for the subject or 2) the area-specific pixel intensity in

control mice expressing tracer in all CGRP neurons for % maximal pixel intensity, a measure of the projection strength relative to the control condition.

Collateralization coefficient – To calculate the relative importance of a target structure for contributing the signal in other projection regions we calculated the difference between the normalized Flp_{on} and Flp_{off} fluorescent signal conditions within each downstream region. This value, which ranges between -1 and +1, equals 0 when fluorescence in the downstream structure is equal when driven only by target-projectors and when only target-projectors are excluded. We set this 0 value to equal 50% by making 50% the y-intercept, then scaled by 50% so that when values are at their maximal (at either +1 or -1), the value reaches either 0 or 100%.

$$CC_a = \frac{([\mathrm{F_a}]_{\mathrm{FlpON_b}} - [\mathrm{F_a}]_{\mathrm{FlpOFF_b}})}{[\mathrm{F_a}]_{\mathrm{YFP}}} \times 50\% + 50\%$$

Here the target structure of interest is *b*, and the collateralization coefficient is being calculated for its relationship with area *a*. Each target structure (i.e. the VPmpc, PSTN, CeA, ovBNST) will have a number of collateralization coefficients for its relationship with other downstream structures (n=6 structures -1 target = 5). We then averaged across subjects to get the mean collateralization coefficient for each target-area combination and compared the distribution of these values across target areas to assess their relative collateralization tendencies.

Quantification and statistical analysis

All data were analyzed using Prism 8.0 (GraphPad Software) as described in Supplemental Information. In brief, no tests were used to determine normality of data distributions or to pre-determine sample size; sample size was chosen based on past experience with expected effect sizes. Within-subject data was analyzed using two-sided, paired t-tests; across subject analysis was done with a combination of Welch's

t tests (unpaired, correction for no assumption of equal standard deviations), ordinary one-way ANOVA (with Tukey's or Dunnettt's correction for multiple comparisons), and ordinary or repeated measure two-way ANOVAs (with Sidak's correction for multiple comparisons). For two-way ANOVAs, P-value for Treatment (i.e. ChR2 vs YFP) <0.05 is indicated to the right of each graph, and post-hoc row analyses' P-values <0.05 are listed above individual data points.

References

Ahrens, S., Wu, M. V, Furlan, A., Hwang, G.-R., Paik, R., Li, H., Penzo, M.A., Tollkuhn, J., and Li, B. (2018). A Central Extended Amygdala Circuit That Modulates Anxiety. J. Neurosci. *38*, 5567–5583.

Barsy, B., Kocsis, K., Magyar, A., Babiczky, Á., Szabó, M., Veres, J.M., Hillier, D., Ulbert, I., Yizhar, O., and Mátyás, F. (2020). Associative and plastic thalamic signaling to the lateral amygdala controls fear behavior. Nat. Neurosci. *23*, 625–637.

Basbaum, A.I., Bautista, D.M., Scherrer, G., and Julius, D. (2009). Cellular and molecular mechanisms of pain. Cell *139*, 267–284.

Bernard, J.F., and Besson, J.M. (1988a). Convergence of nociceptive information on the parabrachio-amygdala neurons in the rat. C R Acad Sci III *307*, 841–847.

Bernard, J.F., and Besson, J.M. (1988b). Convergence of nociceptive information on the parabrachio-amygdala neurons in the rat. C. R. Acad. Sci. III. *307*, 841–847.

Bernard, J.F., and Besson, J.M. (1990). The spino(trigemino)pontoamygdaloid pathway: electrophysiological evidence for an involvement in pain processes. J. Neurophysiol. *63*, 473–490.

Bernard, J.F., Huang, G.F., and Besson, J.M. (1992). Nucleus centralis of the amygdala and the globus pallidus ventralis: electrophysiological evidence for an involvement in pain processes. J. Neurophysiol. *68*, 551–569.

Bernard, J.F., Huang, G.F., and Besson, J.M. (1994). The parabrachial area: electrophysiological evidence for an involvement in visceral nociceptive processes. J. Neurophysiol. *71*, 1646–1660.

Bernard, J.F., Dallel, R., Raboisson, P., Villanueva, L., and Le Bars, D. (1995). Organization of the efferent projections from the spinal cervical enlargement to the parabrachial area and periaqueductal gray: a {PHA}-L study in the rat. J. Comp. Neurol. *353*, 480–505.

Bester, H., Besson, J.M., and Bernard, J.F. (1997). Organization of efferent projections from the parabrachial area to the hypothalamus: a Phaseolus vulgaris-leucoagglutinin study in the rat. J. Comp. Neurol. *383*, 245–281.

Beyeler, A., Namburi, P., Glober, G.F., Simonnet, C., Calhoon, G.G., Conyers, G.F., Luck, R., Wildes, C.P., and Tye, K.M. (2016). Divergent Routing of Positive and Negative Information from the Amygdala during Memory Retrieval. Neuron *90*.

Blair, H.T., Schafe, G.E., Bauer, E.P., Rodrigues, S.M., and LeDoux, J.E. (2001). Synaptic plasticity in the lateral amygdala: a cellular hypothesis of fear conditioning. Learn. Mem. *8*, 229–242.

Blanchard, R.J., and Blanchard, D.C. (1969). Crouching as an index of fear. J. Comp. Physiol. Psychol. *67*, 370–375.

Botta, P., Demmou, L., Kasugai, Y., Markovic, M., Xu, C., Fadok, J.P., Lu, T., Poe, M.M., Xu, L., Cook, J.M., et al. (2015). Regulating anxiety with extrasynaptic inhibition. Nat. Neurosci. *18*, 1493–1500.

Bourgeais, L., Monconduit, L., Villanueva, L., and Bernard, J.F. (2001a). Parabrachial internal lateral neurons convey nociceptive messages from the deep laminas of the dorsal horn to the intralaminar thalamus. J. Neurosci. *21*, 2159–2165.

Bourgeais, L., Gauriau, C., and Bernard, J.F. (2001b). Projections from the nociceptive area of the central nucleus of the amygdala to the forebrain: a {PHA}-L study in the rat. Eur. J. Neurosci. *14*, 229–255.

Bourgeais, L., Gauriau, C., Monconduit, L., Villanueva, L., and Bernard, J.-F. (2003). Dendritic domains of nociceptive-responsive parabrachial neurons match terminal fields of lamina I neurons in the rat. J. Comp. Neurol. *464*, 238–256.

Bowen, A.J., Chen, J.Y., Huang, Y.W., Baertsch, N.A., Park, S., and Palmiter, R.D. (2020). Dissociable

control of unconditioned responses and associative fear learning by parabrachial CGRP neurons. Elife *9*.
van den Burg, E.H., and Stoop, R. (2019). Neuropeptide signalling in the central nucleus of the amygdala. Cell Tissue Res. *375*, 93–101.
Cai, H., Haubensak, W., Anthony, T.E., and Anderson, D.J. (2014). Central amygdala PKC-δ(+) neurons mediate the influence of multiple anorexigenic signals. Nat. Neurosci. *17*, 1240–1248.
Campos, C.A., Bowen, A.J., Schwartz, M.W., and Palmiter, R.D. (2016). Parabrachial CGRP neurons control meal termination. Cell Metab. *23*, 811–820.
Campos, C.A., Bowen, A.J., Han, S., Wisse, B.E., Palmiter, R.D., and Schwartz, M.W. (2017). Cancer-induced anorexia and malaise are mediated by CGRP neurons in the parabrachial nucleus. Nat. Neurosci. *20*, 934–942.
Campos, C.A., Bowen, A.J., Roman, C.W., and Palmiter, R.D. (2018). Encoding of danger by parabrachial CGRP neurons. Nature *555*, 617–622.
Carter, M.E., Soden, M.E., Zweifel, L.S., and Palmiter, R.D. (2013). Genetic identification of a neural circuit that suppresses appetite. Nature *503*, 111–114.
Cechetto, D.F., and Saper, C.B. (1987). Evidence for a viscerotopic sensory representation in the cortex and thalamus in the rat. J. Comp. Neurol. *262*, 27–45.
Chen, J.Y., Campos, C.A., Jarvie, B.C., and Palmiter, R.D. (2018). Parabrachial CGRP neurons establish and sustain aversive taste memories. Neuron *100*, 891--899.e5.
Chiang, M.C., Nguyen, E.K., Canto-Bustos, M., Papale, A.E., Oswald, A.-M.M., and Ross, S.E. (2020). Divergent Neural Pathways Emanating from the Lateral Parabrachial Nucleus Mediate Distinct Components of the Pain Response. Neuron.
Choi, S., Hachisuka, J., Brett, M.A., Magee, A.R., Omori, Y., Iqbal, N.-A., Zhang, D., DeLisle, M.M., Wolfson, R.L., Bai, L., et al. (2020). Parallel ascending spinal pathways for affective touch and pain. Nature *587*.
Chuong, A.S., Miri, M.L., Busskamp, V., Matthews, G.A.C., Acker, L.C., Sørensen, A.T., Young, A., Klapoetke, N.C., Henninger, M.A., Kodandaramaiah, S.B., et al. (2014). Noninvasive optical inhibition with a red-shifted microbial rhodopsin. Nat. Neurosci. *17*, 1123–1129.
Ciocchi, S., Herry, C., Grenier, F., Wolff, S.B.E., Letzkus, J.J., Vlachos, I., Ehrlich, I., Sprengel, R., Deisseroth, K., Stadler, M.B., et al. (2010). Encoding of conditioned fear in central amygdala inhibitory circuits. Nature *468*, 277–282.
D'amour, F.E., and Smith, D.L. (1941). A method for determining loss of pain sensation. J. Pharmacol. Exp. Ther. *72*, 74–79.
Davis, M., and Whalen, P.J. (2001). The amygdala: Vigilance and emotion. Mol. Psychiatry *6*, 13–34.
Dong, H.-W., and Swanson, L.W. (2004). Organization of axonal projections from the anterolateral area of the bed nuclei of the stria terminalis. J. Comp. Neurol. *468*, 277–298.
Dringenberg, H.C., and Vanderwolf, C.H. (1997). Neocortical activation: Modulation by multiple pathways acting on central cholinergic and serotonergic systems. Exp. Brain Res. *116*, 160–174.
Duvarci, S., Popa, D., and Paré, D. (2011). Central amygdala activity during fear conditioning. J. Neurosci. *31*, 289–294.
Espejo, E.F., and Mir, D. (1993). Structure of the rat's behaviour in the hot plate test. Behav. Brain Res. *56*, 171–176.
Fadok, J.P., Krabbe, S., Markovic, M., Courtin, J., Xu, C., Massi, L., Botta, P., Bylund, K., Müller, C., Kovacevic, A., et al. (2017). A competitive inhibitory circuit for selection of active and passive fear responses. Nature *542*, 96–100.
Fadok, J.P., Markovic, M., Tovote, P., and Lüthi, A. (2018). New perspectives on central amygdala function. Curr. Opin. Neurobiol. *49*.
Fanselow, M.S. (1982). The postshock activity burst. Anim. Learn. Behav. *10*, 448–454.

Fanselow, M.S. (1994). Neural organization of the defensive behavior system responsible for fear. Psychon. Bull. Rev. *1*, 429–438.

Fanselow, M.S., Sigmundi, R.A., and Williams, J.L. (1987). Response selection and the hierarchical organization of species-specific defense reactions: the relationship between freezing, flight, and defensive burying. Psychol. Rec. *37*, 381–386.

Fenno, L.E., Mattis, J., Ramakrishnan, C., Hyun, M., Lee, S.Y., He, M., Tucciarone, J., Selimbeyoglu, A., Berndt, A., Grosenick, L., et al. (2014). Targeting cells with single vectors using multiple-feature Boolean logic. Nat. Methods *11*, 763–772.

Flandreau, E.I., and Toth, M. (2018). Animal models of PTSD: A critical review. In Current Topics in Behavioral Neurosciences, (Springer Verlag), pp. 47–68.

Garcia, Kimeldorf, D.J., and Koelling, R.A. (1955). Conditioned aversion to saccharin resulting from exposure to gamma radiation. Science *122*, 157–158.

Garcia, J., McGowan, B.K., Ervin, F.R., and Koelling, R.A. (1968). Cues: their relative effectiveness as a function of the reinforcer. Science (80-.). *160*, 794–795.

Gauriau, C., and Bernard, J.-F. (2002). Pain pathways and parabrachial circuits in the rat. Pain *87*, 251–258.

Ghosh, K.K., Burns, L.D., Cocker, E.D., Nimmerjahn, A., Ziv, Y., Gamal, A. El, and Schnitzer, M.J. (2011). Miniaturized integration of a fluorescence microscope. Nat. Methods.

Govorunova, E.G., Sineshchekov, O.A., Janz, R., Liu, X., and Spudich, J.L. (2015). Natural light-gated anion channels: A family of microbial rhodopsins for advanced optogenetics. Science (80-.). *349*, 647–650.

Gozzi, A., Jain, A., Giovannelli, A., Giovanelli, A., Bertollini, C., Crestan, V., Schwarz, A.J., Tsetsenis, T., Ragozzino, D., Gross, C.T., et al. (2010). A neural switch for active and passive fear. Neuron *67*, 656–666.

Gross, C.T., and Canteras, N.S. (2012). The many paths to fear. Nat. Rev. Neurosci. *13*, 651–658.

Grupe, D.W., and Nitschke, J.B. (2013). Uncertainty and anticipation in anxiety: An integrated neurobiological and psychological perspective. Nat. Rev. Neurosci. *14*, 488–501.

Han, J.S., Li, W., and Neugebauer, V. (2005). Critical role of calcitonin gene-related peptide 1 receptors in the amygdala in synaptic plasticity and pain behavior. J. Neurosci. *25*, 10717–10728.

Han, S., Soleiman, M., Soden, M., Zweifel, L., and Palmiter, R.D. (2015). Elucidating an Affective Pain Circuit that Creates a Threat Memory. Cell *162*, 363–374.

Haubensak, W., Kunwar, P.S., Cai, H., Ciocchi, S., Wall, N.R., Ponnusamy, R., Biag, J., Dong, H.-W., Deisseroth, K., Callaway, E.M., et al. (2010). Genetic dissection of an amygdala microcircuit that gates conditioned fear. Nature *468*, 270–276.

Herry, C., Ciocchi, S., Senn, V., Demmou, L., Müller, C., and Lüthi, A. (2008). Switching on and off fear by distinct neuronal circuits. Nature *454*, 600–606.

Hua, T., Chen, B., Lu, D., Sakurai, K., Zhao, S., Han, B.X., Kim, J., Yin, L., Chen, Y., Lu, J., et al. (2020). General anesthetics activate a potent central pain-suppression circuit in the amygdala. Nat. Neurosci. *23*, 854–868.

Isosaka, T., Matsuo, T., Yamaguchi, T., Funabiki, K., Nakanishi, S., Kobayakawa, R., and Kobayakawa, K. (2015). Htr2a-Expressing Cells in the Central Amygdala Control the Hierarchy between Innate and Learned Fear. Cell *163*.

Iwata, J., and LeDoux, J.E. (1988). Dissociation of associative and nonassociative concomitants of classical fear conditioning in the freely behaving rat. Behav. Neurosci. *102*, 66–76.

Janak, P.H., and Tye, K.M. (2015). From circuits to behaviour in the amygdala. Nature *517*, 284–292.

Jo, Y.S., Heymann, G., and Zweifel, L.S. (2018). Dopamine Neurons Reflect the Uncertainty in Fear Generalization. Neuron *100*.

Jolkkonen, E., Miettinen, R., Pikkarainen, M., and Pitkänen, A. (2002). Projections from the amygdaloid

complex to the magnocellular cholinergic basal forebrain in rat. Neuroscience *111*, 133–149.
Kaur, S., Wang, J.L., Ferrari, L., Thankachan, S., Kroeger, D., Venner, A., Lazarus, M., Wellman, A., Arrigoni, E., Fuller, P.M., et al. (2017). A Genetically Defined Circuit for Arousal from Sleep during Hypercapnia. Neuron *96*, 1153-1167.e5.
Killcross, S., Robbins, T.W., and Everitt, B.J. (1997). Different types of fear-conditioned behaviour mediated by separate nuclei within amygdala. Nature.
Kim, J., Pignatelli, M., Xu, S., Itohara, S., and Tonegawa, S. (2016). Antagonistic negative and positive neurons of the basolateral amygdala. Nat. Neurosci. *19*, 1636–1646.
Kim, J., Zhang, X., Muralidhar, S., LeBlanc, S.A., and Tonegawa, S. (2017). Basolateral to central amygdala neural circuits for appetitive behaviors. Neuron *93*, 1464--1479.e5.
Landeira-Fernandez, J., DeCola, J.P., Kim, J.J., and Fanselow, M.S. (2006). Immediate shock deficit in fear conditioning: Effects of shock manipulations. Behav. Neurosci. *120*, 873–879.
Lanuza, E., Nader, K., and Ledoux, J.E. (2004). Unconditioned stimulus pathways to the amygdala: Effects of posterior thalamic and cortical lesions on fear conditioning. Neuroscience *125*, 305–315.
Lanuza, E., Moncho-Bogani, J., and LeDoux, J.E. (2008). Unconditioned stimulus pathways to the amygdala: Effects of lesions of the posterior intralaminar thalamus on foot-shock-induced c-Fos expression in the subdivisions of the lateral amygdala. Neuroscience *155*, 959–968.
Ledoux, J.E., Ruggiero, D.A., Forest, R., Stornetta, R., and Reis, D.J. (1987). Topographic organization of convergent projections to the thalamus from the inferior colliculus and spinal cord in the rat. J. Comp. Neurol. *264*, 123–146.
LeDoux, J.E. (2000). Emotion circuits in the brain. Annu. Rev. Neurosci. *23*, 155–184.
LeDoux, J.E., Iwata, J., Cicchetti, P., and Reis, D.J. (1988). Different projections of the central amygdaloid nucleus mediate autonomic and behavioral correlates of conditioned fear. J. Neurosci. *8*, 2517–2529.
Leibold, N.K., van den Hove, D.L.A., Viechtbauer, W., Buchanan, G.F., Goossens, L., Lange, I., Knuts, I., Lesch, K.P., Steinbusch, H.W.M., and Schruers, K.R.J. (2016). {CO}2 exposure as translational cross-species experimental model for panic. Transl. Psychiatry *6*, e885.
Letzkus, J.J., Wolff, S.B.E., and Lüthi, A. (2015). Disinhibition, a Circuit Mechanism for Associative Learning and Memory. Neuron.
Liberzon, I., and Sripada, C.S. (2007). The functional neuroanatomy of PTSD: a critical review. Prog. Brain Res. *167*, 151–169.
Linke, R., Braune, G., and Schwegler, H. (2000). Differential projection of the posterior paralaminar thalamic nuclei to the amygdaloid complex in the rat. Exp. Brain Res. *134*, 520–532.
Lissek, S., Kaczkurkin, A.N., Rabin, S., Geraci, M., Pine, D.S., and Grillon, C. (2014). Generalized anxiety disorder is associated with overgeneralization of classically conditioned fear. Biol. Psychiatry *75*, 909–915.
Liu, H., and Fontanini, A. (2015). State dependency of chemosensory coding in the gustatory thalamus (VPMpc) of alert rats. J. Neurosci. *35*, 15479–15491.
Livneh, Y., Ramesh, R.N., Burgess, C.R., Levandowski, K.M., Madara, J.C., Fenselau, H., Goldey, G.J., Diaz, V.E., Jikomes, N., Resch, J.M., et al. (2017). Homeostatic circuits selectively gate food cue responses in insular cortex. Nature *546*, 611–616.
Lu, J., Li, C., Singh-Alvarado, J., Zhou, Z.C., Fröhlich, F., Mooney, R., and Wang, F. (2018). MIN1PIPE: A Miniscope 1-Photon-Based Calcium Imaging Signal Extraction Pipeline. Cell Rep. *23*, 3673–3684.
Mahn, M., Prigge, M., Ron, S., Levy, R., and Yizhar, O. (2016). Biophysical constraints of optogenetic inhibition at presynaptic terminals. Nat. Neurosci. *19*, 554–556.
Maren, S. (2001). Neurobiology of Pavlovian Fear Conditioning. Annu. Rev. Neurosci. *24*, 897–931.
Maren, S. (2005). Synaptic mechanisms of associative memory in the amygdala. Neuron *47*, 783–786.
Martin, B. (1961). The assessment of anxiety by physiological behavioral measures. Psychol. Bull. *58*,

234–255.
Mestanik, M., Mestanikova, A., Visnovcova, Z., Calkovska, A., and Tonhajzerova, I. (2015). Cardiovascular sympathetic arousal in response to different mental stressors. Psychol. Bull. *64 Suppl 5*, S585--594.
Mikics, É., Tóth, M., Varjú, P., Gereben, B., Liposits, Z., Ashaber, M., Halász, J., Barna, I., Farkas, I., and Haller, J. (2008). Lasting changes in social behavior and amygdala function following traumatic experience induced by a single series of foot-shocks. Psychoneuroendocrinology *33*, 1198–1210.
Mogenson, G.J., Swanson, L.W., and Wu, M. (1985). Evidence that projections from substantia innominata to zona incerta and mesencephalic locomotor region contribute to locomotor activity. Brain Res. *334*, 65–76.
Namburi, P., Beyeler, A., Yorozu, S., Calhoon, G.G., Halbert, S.A., Wichmann, R., Holden, S.S., Mertens, K.L., Anahtar, M., Felix-Ortiz, A.C., et al. (2015). A circuit mechanism for differentiating positive and negative associations. Nature *520*, 675–678.
Neugebauer, V., Galhardo, V., Maione, S., and Mackey, S.C. (2009). Forebrain pain mechanisms. Brain Res. Rev. *60*, 226–242.
Okutsu, Y., Takahashi, Y., Nagase, M., Shinohara, K., Ikeda, R., and Kato, F. (2017). Potentiation of NMDA receptor-mediated synaptic transmission at the parabrachial-central amygdala synapses by CGRP in mice. Mol. Pain *13*, 1744806917709201.
Ozawa, T., Ycu, E.A., Kumar, A., Yeh, L.-F., Ahmed, T., Koivumaa, J., and Johansen, J.P. (2017). A feedback neural circuit for calibrating aversive memory strength. Nat. Neurosci. *20*, 90–97.
Pellow, S., Chopin, P., File, S.E., and Briley, M. (1985). Validation of open:closed arm entries in an elevated plus-maze as a measure of anxiety in the rat. J. Neurosci. Methods *14*, 149–167.
Petrovich, G.D., and Swanson, L.W. (1997). Projections from the lateral part of the central amygdalar nucleus to the postulated fear conditioning circuit. Brain Res. *763*, 247–254.
Rescorla, R.A. (1972). Informational Variables in Pavlovian Conditioning. In Psychology of Learning and Motivation, G.H. Bower, ed. (Academic Press), pp. 1–46.
Rizvi, T.A., Ennis, M., Behbehani, M.M., and Shipley, M.T. (1991). Connections between the central nucleus of the amygdala and the midbrain periaqueductal gray: topography and reciprocity. J. Comp. Neurol. *303*, 121–131.
Roelofs, K. (2017). Freeze for action: neurobiological mechanisms in animal and human freezing. Philos. Trans. R. Soc. Lond. B. Biol. Sci. *372*.
Roman, C.W., Derkach, V.A., and Palmiter, R.D. (2016). Genetically and functionally defined NTS to PBN brain circuits mediating anorexia. Nat. Commun. *7*.
Romanski, L.M., Clugnet, M.C., Bordi, F., and LeDoux, J.E. (1993). Somatosensory and Auditory Convergence in the Lateral Nucleus of the Amygdala. Behav. Neurosci. *107*, 444–450.
Sanford, C.A., Soden, M.E., Baird, M.A., Miller, S.M., Schulkin, J., Palmiter, R.D., Clark, M., and Zweifel, L.S. (2017). A Central Amygdala {CRF} Circuit Facilitates Learning about Weak Threats. Neuron *93*, 164–178.
Saper, C.B. (2002). The Central Autonomic Nervous System: Conscious Visceral Perception and Autonomic Pattern Generation. Annu. Rev. Neurosci. *25*, 433–469.
Saper, C.B., Romanovsky, A.A., and Scammell, T.E. (2012). Neural circuitry engaged by prostaglandins during the sickness syndrome. Nat. Neurosci. *15*, 1088–1095.
Sarhan, M., Freund-Mercier, M.-J., and Veinante, P. (2005). Branching patterns of parabrachial neurons projecting to the central extended amgydala: single axonal reconstructions. Eur. J. Neurosci. *491*, 418–442.
Sato, M., Ito, M., Nagase, M., Sugimura, Y.K., Takahashi, Y., Watabe, A.M., and Kato, F. (2015). The lateral parabrachial nucleus is actively involved in the acquisition of fear memory in mice. Mol. Brain *8*, 22.

Shadmehr, R., Reppert, T.R., Summerside, E.M., Yoon, T., and Ahmed, A.A. (2019). Movement Vigor as a Reflection of Subjective Economic Utility. Trends Neurosci. *42*, 323–336.

Shi, C., and Davis, M. (1999). Pain pathways involved in fear conditioning measured with fear-potentiated startle: Lesion studies. J. Neurosci. *19*, 420–430.

Shinohara, K., Watabe, A.M., Nagase, M., Okutsu, Y., Takahashi, Y., Kurihara, H., and Kato, F. (2017). Essential role of endogenous calcitonin gene-related peptide in pain-associated plasticity in the central amygdala. Eur. J. Neurosci. *46*, 2149–2160.

Sigmundi, R.A., Bouton, M.E., and Bolles, R.C. (1980). Conditioned freezing in the rat as a function of shock intensity and CS modality. Bull. Psychon. Soc. *15*, 254–256.

Silva, B.A., Mattucci, C., Krzywkowski, P., Murana, E., Illarionova, A., Grinevich, V., Canteras, N.S., Ragozzino, D., and Gross, C.T. (2013). Independent hypothalamic circuits for social and predator fear. Nat. Neurosci. *16*, 1731–1733.

Sutherland, M.R., and Mather, M. (2018). Arousal (but not valence) amplifies the impact of salience. Cogn. Emot. *32*, 616–622.

Swerdlow, N.R., Swanson, L.W., and Koob, G.F. (1984). Substantia innominata: critical link in the behavioral expression of mesolimbic dopamine stimulation in the rat. Neurosci. Lett. *50*, 19–24.

Tokita, K., Inoue, T., and Boughter, J.D. (2010). Subnuclear organization of parabrachial efferents to the thalamus, amygdala and lateral hypothalamus in C57BL/6J mice: A quantitative retrograde double labeling study. Neuroscience *171*, 351–365.

Tovote, P., Esposito, M.S., Botta, P., Chaudun, F., Fadok, J.P., Markovic, M., Wolff, S.B.E., Ramakrishnan, C., Fenno, L., Deisseroth, K., et al. (2016). Midbrain circuits for defensive behaviour. Nature *534*, 206–212.

Tye, K.M., Prakash, R., Kim, S.Y., Fenno, L.E., Grosenick, L., Zarabi, H., Thompson, K.R., Gradinaru, V., Ramakrishnan, C., and Deisseroth, K. (2011). Amygdala circuitry mediating reversible and bidirectional control of anxiety. Nature.

Unal, C.T., Pare, D., and Zaborszky, L. (2015). Impact of basal forebrain cholinergic inputs on basolateral amygdala neurons. J. Neurosci. *35*, 853–863.

Veening, J.G., Swanson, L.W., and Sawchenko, P.E. (1984). The organization of projections from the central nucleus of the amygdala to brainstem sites involved in central autonomic regulation: A combined retrograde transport-immunohistochemical study. Brain Res. *303*, 337–357.

Vianna, D.M.L., and Carrive, P. (2005). Changes in cutaneous and body temperature during and after conditioned fear to context in the rat. Eur. J. Neurosci. *21*, 2505–2512.

Wenk, G.L. (1997). The nucleus basalis magnocellularis cholinergic system: One hundred years of progress. Neurobiol. Learn. Mem.

Wilson, T.D., Valdivia, S., Khan, A., Ahn, H.S., Adke, A.P., Gonzalez, S.M., Sugimura, Y.K., and Carrasquillo, Y. (2019). Dual and Opposing Functions of the Central Amygdala in the Modulation of Pain. Cell Rep. *29*, 332-346.e5.

Yizhar, O., Fenno, L.E., Davidson, T.J., Mogri, M., and Deisseroth, K. (2011). Optogenetics in Neural Systems. Neuron *71*, 9–34.

Yu, K., Ahrens, S., Zhang, X., Schiff, H., Ramakrishnan, C., Fenno, L., Deisseroth, K., Zhao, F., Luo, M.-H., Gong, L., et al. (2017). The central amygdala controls learning in the lateral amygdala. Nat. Neurosci. *20*, 1680–1685.

Ziemann, A.E., Allen, J.E., Dahdaleh, N.S., Drebot, I.I., Coryell, M., Wunsch, A.M., Lynch, C.M., Faraci, F.M., Howard, M.A., Welsh, M.J., et al. (2009). The Amygdala is a Chemosensor that Detects Carbon Dioxide and Acidosis to Elicit Fear Behavior. Cell *139*, 1012–1021.

Zweifel, L.S., Fadok, J.P., Argilli, E., Garelick, M.G., Jones, G.L., Dickerson, T.M.K., Allen, J.M., Mizumori, S.J.Y., Bonci, A., and Palmiter, R.D. (2011). Activation of dopamine neurons is critical for aversive conditioning and prevention of generalized anxiety. Nat. Neurosci. *14*, 620–628.